DISSERTATION

Fractional Diffusion by Random Walks on Hierarchical and Fractal Topological Structures

Ausgeführt zum Zwecke der Erlangung des akademischen Grades
eines Doktors der technischen Wissenschaften
unter der Leitung von

Ao.Univ.Prof. Dipl.-Ing. Dr.techn. Felix Breitenecker
Institut für Analysis und Scientific Computing

eingereicht an der Technischen Universität Wien
Fakultät für Mathematik und Geoinformation
von

Dipl.-Ing. Günter Schneckenreither

Wien, am 2. Februar 2020

Kurzfassung

Heterogene dynamische Systeme können eine Vielzahl interessanter und komplexer Phänomene hervorbringen. Topologische Strukturen, die im Zusammenhang mit lokaler und nicht-lokaler Interaktion auftreten, können als Ansatzpunkt für die Analyse und Charakterisierung dienen. Hier wird ein mathematischer Ansatz präsentiert, um gewisse topologische Konfigurationen in heterogenen Systemen für anomalen Transport und Diffusion verantwortlich zu zeichnen. Die untersuchten Strukturen sind hierarchische und fraktale Anordnungen von räumlichen Clustern aggregierter Dichte mit ausgezeichneter lokaler Interaktion. Eine stochastische Interpretation dieser Modelle liefert eine mathematische Verbindung zu Continuous Time Random Walks und einer fraktionalen Diffusionsgleichung.

Die fraktionale Diffusionsgleichung im Caputo und Riesz-Feller Sinn sowie Continuous Time Random Walks sind zwei gängige Formalisierungen anomaler Diffusion. In beiden Betrachtungsweisen werden exponentielle Formen und Differentialoperatoren, die für die Beschreibung gewöhnlicher Diffusion verwendet werden, durch nichtgeschlossene Ausdrücke ersetzt. Der erste Teil dieser Arbeit fasst die zugrundeliegende mathematische Theorie für den zweidimensionalen Fall zusammen und präsentiert die Verbindung zwischen beiden Formulierungen. Die notwendigen numerischen Algorithmen und Funktionsauswertungen um letzterer Aussage in stochastischen Simulationen zu reproduzieren sind nicht in den gängigen Programmierumgebungen enthalten. Daher wurde eine entsprechende Programmbibliothek für die Simulation der fraktionalen Diffusionsgleichung in zwei Dimensionen durch Continuous Time Random Walks erstellt. Die Bibliothek beinhaltet Wahrscheinlichkeitsverteilungen wie die Mittag-Leffler und die Lévy-stabile Verteilung, Routinen zur Laplace und Fourier Transformation, Umrechnungen für die Parametrisierung der Inkrement-Verteilungen und Implementierungen von statistischen Maßen wie lokale Zeit, Zeit-gemittelte fraktionale Abweichung und Geschwindigkeits-Autokorrelation.

Der zweite Teil dieser Arbeit behandelt heterogene Block-Strukturen, die in den zweidimensionalen Euklidischen Raum eingebettet werden können. Räumlich begrenz-

te Blöcke repräsentieren dabei stark interagierende Cluster und werden als Gaußsche Dichten modelliert. In einer hierarchischen und einer weiteren fraktalen Entwicklung dieses Modells werden aus den hervorgehenden persistenten und stochastischen Strukturen Interaktions-Wahrscheinlichkeiten abgeleitet. Diese topologischen Interaktions-Wahrscheinlichkeiten werden mit stabilen räumlichen Inkrementen identifiziert, welche auch in Continuous Time Random Walks auftreten. Die resultierende mathematische Verbindung zwischen Block-Modellen und der fraktionalen Diffusionsgleichung wird empirisch untermauert indem erzeugte topologische Random Walk Trajektorien anhand der implementierten Maße quantifiziert und analysiert werden.

Hier wird, in Übereinstimmung mit ähnlichen Ansätzen aus der Literatur, eine stochastische topologische Struktur als intermediäres Modell verwendet, um Systeme mit persistenten strukturellen Anordnungen und fraktionale Diffusion in Beziehung zu bringen. Die topologische Perspektive dieses Ansatzes reflektiert das Auftreten lokaler Cluster aufeinanderfolgender Partikel-Positionen in Continuous Time Random Walks. Weiters wird das Zusammenspiel von Verweildauern und der Konfiguration lokaler Cluster mit erhöhter Interaktion im Hinblick auf dynamische Transport- und Interaktionsprozesse beleuchtet. Diese Untersuchungen wurden durch frühere Arbeiten zu Transportprozessen in dynamischen Modellen strukturierter und interagierender Populationen motiviert. Die resultierende mathematische Verbindung zwischen strukturellen Eigenschaften und anomaler Diffusion könnte neue Einblicke und technische Zugänge für die Forschung in diesem Bereich liefern.

Abstract

Heterogeneous dynamical systems can expose a variety of complex and interesting phenomena. Topological structures on the heterogeneity space that emerge in conjunction with local and non-local interaction can be a leverage point for characterization and analysis. Here, a mathematical framework is presented for identifying certain topological configurations of heterogeneous systems as drivers for anomalous transport and diffusion. The structures investigated are hierarchical and fractal arrangements of spatial clusters of aggregated density with distinguished local interaction. A stochastic interpretation of these models yields a mathematical connection to continuous time random walks and a fractional diffusion equation.

The fractional diffusion equation in the Caputo and Riesz-Feller sense and continuous time random walks are two related formalizations of anomalous diffusion. In either case, non-closed form expressions replace the exponential shapes and differential operators encountered in usual diffusion. The first part of this thesis compiles the mathematical theory for the two-dimensional setting and reviews the connection between both formulations. The numerical algorithms and function implementations required for reproducing the latter statement in stochastic simulations are not included in standard programming environments. Therefore, a proof-of-concept programming library for simulating the fractional diffusion equation in two dimensions by continuous time random walks was created. The library contains a collection of probability distributions, including Mittag-Leffler and bivariate Lévy-stable distributions, Laplace and Fourier transform routines, formulas for the exact parameterization of the increment distributions and implementations of statistical measures such as local time, time average fractional displacement and velocity autocorrelation.

The second part of this work introduces heterogeneous block structures that can be embedded in the two-dimensional Euclidean space. Spatially confined blocks represent strongly interconnected clusters and are modeled as overlapping Gaussian densities. In a hierarchical and a further fractal progression of this model, stochastic interaction likelihoods are constructed from the implied persistent and latent structures. These

topological interaction likelihoods are then identified with the stable spatial increments occurring in continuous time random walks. The obtained mathematical connection between topological block models and fractional diffusion is reinforced by quantifying and analyzing generated topological random walk trajectories using the implemented empirical methods.

In alignment with similar geometric approaches in literature, here, a stochastic topological structure is used as an intermediate model to relate systems with persistent structural layout to fractional diffusion. The topological perspective of this approach reflects the emergence of local clusters of consecutive particle positions in continuous time random walks. Furthermore, the interplay of dwelling times and the configuration of local clusters with elevated interaction is discussed in the context of dynamic transport and interaction processes. This investigation was largely motivated by previous research on transport precesses in models of structured and interacting populations. The resulting mathematical connection between structural features and anomalous diffusion could provide new insight and technical approaches for the research in this domain and in more general settings.

Contents

1 Introduction

The notion of anomalous diffusion subsumes the breakage of hypotheses and conditions that characterize usual diffusion such as locality, Markovianity and ergodicity. The intention of the present work is to investigate whether a certain topological feature of spatial heterogeneous dynamical systems is responsible for anomalous characteristics in transport and diffusion processes. For instance, in populations where interaction is driven by a community structure and infrequent non-local outliers, effects typical for anomalous diffusion can be observed. Here, a link is established between systems with certain block structures and continuous time random walks simulating a fractional diffusion equation. The term topology is used to refer to the encounter of local clusters or aggregations of density, that are characterized by elevated interaction.

1.1 Background

The results and methods presented in this work originate from past research on dynamical systems with heterogeneous topological structures in terms of networks, stochastic processes and differential equations. The author of this thesis is also the main author of the according publications cited within this section; he developed the research topics and is responsible for the scientific results in these publications and in this thesis. The perspectives and techniques are influenced by a record in modeling and simulation, in scientific computing, in applied medical and health systems research and by university lectures and the research of a greater ambient scientific community.

A prototypical model that can expose heterogeneous structuring and non-local interaction is a population of interacting individuals that transmit information or infectious diseases. Qualities that render this particular model a good practical example include the unambiguous underlying conception, a strong presence in literature and education and the possibility of systematic derivations based on abstracted interaction-transmission models. It is known that by distributing populations on spatial domains [91] and introducing topological structures [94], increasingly complex dynamic phenomena can be simulated. The research presented in this thesis delivers tools and

approaches that are useful for increasing the tractability of certain observations and hypotheses in connection with heterogeneous structuring and non-local interaction based on the mathematical theory on anomalous diffusion.

A key aspect of heterogeneous dynamical systems is the synergy of (spatial) alignment and interaction. In the context of epidemic spread in spatially distributed populations, system formulations by partial differential equations and stochastic lattice models were compared in earlier research [91]. It was shown that the characteristics of reaction-diffusion systems (based on lattice gas cellular automata) can be reproduced in stochastic systems with non-diffusing populations and Gaussian interaction kernels (stochastic cellular automata) by using an intermediate mean-field description (partial differential equations). In further investigations, more general systems with stochastic states were regarded and a distinction between persistent spatial alignment and topological features induced by local and non-local interaction was formalized [89, 90].

An important effect of spatial alignment and local interaction is the delayed transport of information into different spatial regions. In [93] the stochastic and distributed representation of infection states in heterogeneous spatial systems led to formalizations by stochastic and partial differential equations. From the stochastic and distributed interpretation of states, a connection to systems with delayed reaction terms was established, and formalizations of the epidemiologic reproduction number for the distributed and the stochastic case were developed.

A data-driven model for simulating the transmission of infectious diseases in structured heterogeneous populations was developed in [94]. Large populations were sampled from demographic and sociol-economic data and individuals were grouped into social communities like households and workplaces according to geographic residence, commuting distances, income and further social attributes. In combination with additional survey data, networks of persistent social relations and temporal close proximity interaction patterns were inferred. The resulting networks were used to simulate the temporal instantiation of close proximity contacts and the derived transport dynamics served as a basis for simulating disease transmission. A prototypical infectious disease

with the basic characteristics of measles was used to investigate dynamical effects of the topological structuring on the incidence and prevalence in sampled statistical populations. The interplay of strong intra-community links and weak ties corresponding to non-local interaction was found to result in dynamical patterns also encountered in epidemic outbreaks. It was further shown that heterogeneous immunization taking into account the topological layout can severely impact the velocity and percolation properties of epidemics (quantified by the epidemiologic reproduction number and the number of secondary infections).

The transport mechanics produced by this model display some typical characteristics of anomalous diffusion, which indicates that anomalous behavior in heterogeneous dynamical systems might be attributable to topological structuring. As a consequence, this thesis aims at identifying stochastic transport or interaction processes in topologically structured models with continuous time random walks and the associated fractional diffusion equation. This investigation contributes to existing research on topological structures and anomalous patterns in heterogeneous dynamical systems and could also help to approximate the dynamics of large individual-based models with heterogeneous structuring by macroscopic descriptions (fractional transport-reaction differential equations).

Anomalous diffusion is also encountered in microbiology, for instance in molecular transport and cell migration. In the latter context, an agent-based model for simulating melanocytic skin lesions was developed in an interdisciplinary effort [95]. In this model, the physiological habitat of simulated cells is characterized by a periodically distorted geometric surface which was formalized as a differentiable manifold. The geometric shape implies a certain topology on the simulation domain and is responsible for trapping effects and inhomogeneous movement and distribution of cells. Hence, in combination with cellular proliferation and migration, the topology of the spatial simulation domain is a key driver for emerging macroscopic patterns relevant for clinical diagnosis. It might be possible to approximate the macroscopic dynamical patterns of this agent-based simulation model by fractional and stochastic diffusion-reaction equa-

tions in future research. Furthermore, malignant transformation and spread seem to be predestined for a description in terms of anomalous dynamics.

1.2 Discourse

The preliminaries of this thesis (Section 2) prepare the relevant mathematical foundations of fractional calculus and anomalous diffusion. This includes the Fourier, Laplace and Mellin transform as well as certain special functions and heavy-tailed probability distributions such as Mittag-Leffler and Lévy-stable distributions. Then the basics of the mathematical theory are collected without aiming for a complete discourse of the topic (Section 3). This chapter introduces the time-space fractional diffusion equation in the Caputo and Riesz-Feller sense and presents a formalization of corresponding continuous time random walks in two dimensions. In literature, the mathematical connection between both models (for space-time fractional diffusion) is most often treated in the one-dimensional setting, but it is known that certain effects only emerge in higher dimensions. A coherent derivation of the connection between the fractional diffusion equation in two dimensions and equivalent random walks was composed. This concerns in particular the parameterization of the spatial and temporal increment distributions in the random walk model and the transition to the fractional diffusion equation in the continuum limit.

In parallel to the mathematical formalization, a library for the Python programming language was created with the capabilities to simulate and quantify continuous time random walk trajectories [92]. Algorithmic implementations of the aforementioned integral transforms and probability distributions are a necessary prerequisite. The majority of the required components is available in existing software libraries or repositories. The presented framework collects those implementations, complements missing parts – for the two-dimensional scenario – and demonstrates a coherent implementation for simulating continuous time random walks with a special focus on the combined scaling of the increment distributions. Consecutive development of the formal theory and implementation permitted to validate both tracks against each other. The

identification of simulated continuous time random walks with the fractional diffusion equation is based on the evaluation and comparison of the fundamental solution and measures such as the mean fractional displacement, time average fractional displacement, local time and velocity autocorrelation. Corresponding numerical algorithms were implemented and occasionally the mathematical formalizations were extended in order to work in the space and time fractional setting (Section 3.3).

The preceding discussion of the mathematical theory on anomalous diffusion and continuous time random walks provides the tools and perspectives required in the following construction and analysis of topologically structured heterogeneous systems. In a first step towards the initially proposed problem, a topological block model for generating populations with heterogeneous densities on two-dimensional domains was developed (Section 4.1). In this model, blocks are formalized as surroundings with finite spatial extent that additively contribute to the total population density. The mathematical formalization is by bivariate Gaussian probability densities with their centers distributed evenly on a bounded domain. In addition to the resulting heterogeneous population density, a spatial interaction kernel can be used to describe non-local transport and interaction processes.

The model was then extended to hierarchical layouts by positioning blocks according to the distribution of larger blocks (Section 4.2). A new interaction mechanism, entirely based on the topological layout, was constructed. This topological interaction concept is driven by a stochastic selection of a layer in the hierarchy that in turn determines a particular pool of neighboring sub-blocks qualifying for interaction. A stochastic formalization of the topological layout allowed to condense the interaction concept into stochastic spatial increments. The resulting probabilistic formulation of spatial jumps can be separated into a bivariate normal displacement and a multiplicative scale determined by the random level.

In a generalization of the hierarchical model, fractional levels were introduced on unbounded domains. The resulting topological layout consists of an infinite number of blocks arranged in a fractal configuration and only exists in a latent sense. The

corresponding stochastic formalization of jumps was easier to treat analytically and was identified with the stable spatial increments encountered in Lévy flights and continuous time random walks (Section 4.3). In a certain sense, the fractal block model serves as an intermediate mathematical model to relate interaction dynamics on hierarchical block structures with continuous time random walks and fractional diffusion. The theoretical results were validated empirically by using the implemented quantification methods and demonstrating that trajectories generated from the hierarchical and fractal block model share the characteristics of continuous time random walks and simulate the fractional diffusion equation (Section 4.4).

1.3 Discussion and outlook

The mathematical connection between topological block models on two-dimensional domains and continuous time random walks is the central result of this thesis. As a consequence, anomalous transport and diffusion can be regarded as the result of topological structuring and interaction – at least under certain conditions. This topological interpretation aligns with the observation of anomalous diffusion on fractal geometries in existing research and provides new perspectives on the topic. In Section 5.1.4 the techniques developed in this work are put into context with existing geometric formalizations of anomalous diffusion. In Section 5.1.3 the spatial distribution of ensembles of random walk particles generated from the topological block models as well as classical continuous time random walks are compared to the fundamental solution of the fractional diffusion equation.

An important aspect of the presented connection concerns the persistence of spatial alignment and topological layout. Heterogeneous systems, characterized by an inherent and persistent hierarchical block structure, are linked to fractional diffusion processes by an intermediate description in terms of fractal block models with volatile and stochastic topologies. A similar observation was already made in heterogeneous systems with local interaction and also applies to stochastic fractal geometries as drivers for anomalous diffusion. A further but related theoretical result concerns the observation of volatile

or latent clusters emerging in the trajectories of continuous time random walks. In this context, clusters are understood as local areas that confine a number of consecutive particle positions and that are separated by larger jumps in the trajectory. In simulated trajectories, clusters exist in all orders of magnitude and the presented block models turn out to reproduce these latent structures in a more explicit fashion. A discussion of the presented work with respect to the aforementioned and further geometric and topological observations can be found in Section 5.2.

In Section 5.3 the thesis is concluded with an outlook and review on the application of fractional differential equations for simulating complex interaction processes in structured populations. The topological perspective on fractional diffusion provides additional insight in the construction of macroscopic models in this domain.

2 Preliminaries

The aim of this section is to prepare the necessary mathematical tools. Some terminologies and conventions on special functions, integral transforms and probability distributions are declared. Occasionally, numerical approximation techniques are discussed. The most relevant topics in this section concern the Mittag-Leffler function (Section 2.1.3), the associated Mittag-Leffler distribution (Section 2.4.2), univariate skew Lévy-stable distributions (Section 2.5.3) and bivariate isotropic Lévy-stable distributions (Section 2.5.4).

2.1 Special functions

The functions presented here are encountered in many occasions during the discourse of fractional diffusion and continuous time random walks. For the sake of conciseness the mathematical statements are reduced to their bare minimum.

2.1.1 Gamma function

The Gamma function is defined as

$$\Gamma(z) = \int_0^\infty t^{z-1} \exp(-t)\, \mathrm{d}t \tag{2.1}$$

for complex z with positive real part. Analytic continuation allows all complex arguments except for the poles at negative integers. The identities

$$z\,\Gamma(z) = \Gamma(z+1) \qquad z \notin -\mathbb{N}, \tag{2.2}$$

$$\Gamma(1-z)\,\Gamma(z)\,\sin(\pi z) = \pi \qquad z \notin \mathbb{Z} \tag{2.3}$$

will be encountered occasionally.

2.1.2 Bessel functions

The Bessel function of first kind is defined as

$$J_0(z) = \frac{1}{2\pi} \int_{-\pi}^{\pi} \exp(iz \sin t)\, \mathrm{d}t \tag{2.4}$$

and the modified Bessel function of second kind is defined as

$$K_0(z) = \frac{1}{2} \int_{-\infty}^{\infty} \frac{\exp(izt)}{\sqrt{t^2+1}}\, \mathrm{d}t \tag{2.5}$$

with a pole at $z = 0$.

2.1.3 Mittag-Leffler function

The one- and two-parameter Mittag-Leffler functions are defined as

$$E_\beta(z) = \sum_{n=0}^{\infty} \frac{z^n}{\Gamma(\beta n + 1)}, \qquad E_{\beta,\delta}(z) = \sum_{n=0}^{\infty} \frac{z^n}{\Gamma(\beta n + \delta)} \tag{2.6}$$

for $\beta > 0$ and $\delta \in \mathbb{R}$. A generalization to complex parameters is possible. Clearly $E_{\beta,1}(z) = E_\beta(z)$, and a simple calculation shows that

$$-\frac{\mathrm{d}}{\mathrm{d}z} E_\beta\big(-z^\beta\big) = z^{\beta-1} E_{\beta,\beta}\big(-z^\beta\big). \tag{2.7}$$

An important property of the (one-parameter) Mittag-Leffler function is that it interpolates between a stretched exponential function for small arguments and a power-law for large arguments [42, 60]. For different parameterizations various exponential and trigonometric functions can be expressed with the Mittag-Leffler function. For instance $E_1(z) = \exp(z)$.

The Mittag-Leffler function is usually not implemented in standard programming libraries. Numerical evaluation [30, 31, 34] is commonly based on integral representations and the separation of oscillatory and monotonic integrands. In this work, existing

Python implementations, which additionally rely on precalculated look-up tables are used [29, 46].

2.1.4 Fox-H function

Fox-H functions are defined by a Mellin-Barnes integral [26, 51, 59, 85]

$$\mathrm{H}_{p,q}^{m,n}(z) := \mathrm{H}_{p,q}^{m,n}\left[z\middle|\begin{matrix}(a_1,A_1) & (a_2,A_2) & \dots & (a_p,A_p)\\ (b_1,B_1) & (b_2,B_2) & \dots & (b_q,B_q)\end{matrix}\right] \tag{2.8}$$

$$:= \frac{1}{2\pi i}\int_L \frac{\prod_{k=1}^{m}\Gamma(b_k+B_k s)\prod_{k=1}^{n}\Gamma(1-a_k-A_k s)}{\prod_{k=n+1}^{p}\Gamma(a_k+A_k s)\prod_{k=m+1}^{q}\Gamma(1-b_k-B_k s)}\, z^{-s}\,\mathrm{d}s \tag{2.9}$$

where the integration path L separates the poles of the integrand. The specialties of the Fox-H function are vast and out of the scope of this introduction. The Mittag-Leffler functions are special cases of Fox-H functions. Due to the arbitrarily large number of parameters, general numerical routines are not available.

2.2 Integral transforms

In connection with calculus and fractional calculus in particular, integral transforms are a powerful tool for transforming differential into algebraic equations. Here, a short introduction is given on some transforms and certain specialties. A more thorough examination in the context of fractional calculus can be found in the cited literature. The short notations $\tilde{f}$ and $\hat{f}$ are used for the Laplace and Fourier or Hankel transform of a function f.

2.2.1 Laplace transform

The Laplace transform of a function $f(t)$ is defined as

$$\mathcal{L}_t\big\{f(t)\big\}(s) = \int_0^\infty \exp(-st)\, f(t)\,\mathrm{d}t \qquad s\in\mathbb{C}, \tag{2.10}$$

where the integral can be understood in different senses. For power laws with a singularity at the origin, the Laplace transform is a convergent integral only for $\mathrm{Re}(s) > \sigma_a$, where σ_a is called abscissa of convergence. The inverse Laplace transform is defined as

$$\mathcal{L}_s^{-1}\{g(s)\}(t) = \frac{1}{2\pi i}\int_{\sigma-i\infty}^{\sigma+i\infty} \exp(st)\, g(s)\, \mathrm{d}s \qquad Re(s) = \sigma > \sigma_a \qquad t > 0, \tag{2.11}$$

where the constant σ ensures that g is analytic on the integration path.

Numerical approximation of the improper integral in (2.10) can be accomplished with standard numerical quadrature routines available in standard programming libraries [96]. The numerical inverse Laplace transform requires more elaborate routines, often implemented in high-precision arithmetic [69].

The following scaling property holds

$$\mathcal{L}_t\{f(\varepsilon\, t)\}(s) = \varepsilon^{-1}\mathcal{L}_t\{f(t)\}(\varepsilon^{-1}\, s). \tag{2.12}$$

2.2.2 Fourier and Hankel transform

The Fourier transform (of integrable functions with convergent integral) can be defined in correspondence with the definition of the characteristic function of probability distributions

$$\varphi_X(k) = \mathbb{E}\big[\exp(ikX)\big] = \mathcal{F}_x\{f_X(x)\}(k). \tag{2.13}$$

Hence,

$$\mathcal{F}_x\{f(x)\}(k) = \int_{-\infty}^{\infty} \exp(ikx)\, f(x)\, \mathrm{d}x \tag{2.14}$$

$$\mathcal{F}_k^{-1}\{g(k)\}(x) = \frac{1}{2\pi}\int_{-\infty}^{\infty} \exp(-ikx)\, g(k)\, \mathrm{d}k \tag{2.15}$$

and in two dimensions

$$\mathcal{F}_{\boldsymbol{x}}\{f(\boldsymbol{x})\}(\boldsymbol{k}) = \int_{\mathbb{R}^2} \exp(i\boldsymbol{k}\cdot\boldsymbol{x})\, f(\boldsymbol{x})\,\mathrm{d}\boldsymbol{x} \tag{2.16}$$

$$\mathcal{F}^{-1}_{\boldsymbol{k}}\{g(\boldsymbol{k})\}(\boldsymbol{x}) = \frac{1}{(2\pi)^2}\int_{\mathbb{R}^2} \exp(-i\boldsymbol{k}\cdot\boldsymbol{x})\, g(\boldsymbol{k})\,\mathrm{d}\boldsymbol{k}. \tag{2.17}$$

Radial symmetry $f(\boldsymbol{x}) = f(r,\theta) = f(r)$ is preserved in two-dimensional Fourier transform. For functions with this property the two-dimensional Fourier transform corresponds to the Hankel transform of the radial function representation,

$$\mathcal{F}_{\boldsymbol{x}}\{f(\boldsymbol{x})\}(\boldsymbol{k}) = \int_{\mathbb{R}^2} \exp(i\boldsymbol{k}\cdot\boldsymbol{x})\, f(\boldsymbol{x})\,\mathrm{d}\boldsymbol{x} \tag{2.18}$$

$$= \int_0^\infty \int_0^{2\pi} \exp(i|\boldsymbol{k}|r\,\cos\theta)\, f(r,\theta)\,\mathrm{d}\theta\,\mathrm{d}r \tag{2.19}$$

$$= 2\pi \int_0^\infty J_0(kr)\, r\, f(r)\,\mathrm{d}r \tag{2.20}$$

$$= 2\pi\,\mathcal{H}_r\{f(r)\}(k), \tag{2.21}$$

where θ reduces to the angle between $\boldsymbol{x}$ and $\boldsymbol{k}$ and J_0 is the 0-order Bessel function and $k = |\boldsymbol{k}|$. The inverse Hankel transform is defined as

$$\mathcal{H}^{-1}_k\{g(k)\}(r) = \int_0^\infty J_0(kr)\, k\, g(k)\,\mathrm{d}k \tag{2.22}$$

$$= 2\pi\,\mathcal{F}^{-1}_{\boldsymbol{k}}\{g(\boldsymbol{k})\}(\boldsymbol{x}) \tag{2.23}$$

and corresponds to the two-dimensional inverse Fourier transform if $g(k)$ is the radial representation of a symmetric function $g(\boldsymbol{k})$.

As an alternative to numerical integration [70], efficient discrete Fourier transform methods (FFT) can be used if a regularly spaced grid of sample points is available or can be calculated.

The formulas in the following example must be interpreted in a distributional sense [84]. For simple power laws,

$$\mathcal{F}_{\boldsymbol{x}}\Big\{|\boldsymbol{x}|^{-(2+\alpha)}\Big\}(\boldsymbol{k}) = c(\alpha)\,|\boldsymbol{k}|^{\alpha} \tag{2.24}$$

where $0 < \alpha < 2$. The factor

$$c(\alpha) = \frac{\pi}{2^{\alpha}} \frac{\Gamma\big(-\frac{\alpha}{2}\big)}{\Gamma\big(1+\frac{\alpha}{2}\big)} = -\frac{2^{1-\alpha}\pi}{\alpha} \frac{\Gamma\big(1-\frac{\alpha}{2}\big)}{\Gamma\big(1+\frac{\alpha}{2}\big)} \tag{2.25}$$

can also be found in the formulation of Riesz potentials, which are related to the inversion of certain Laplace operators (compare Section 3.1.1).

For two-dimensional Fourier transform,

$$\mathcal{F}_{\boldsymbol{x}}\big\{f(\varepsilon\,\boldsymbol{x})\big\}(\boldsymbol{k}) = |\varepsilon|^{-2}\,\mathcal{F}_{\boldsymbol{x}}\big\{f(\boldsymbol{x})\big\}(\varepsilon^{-1}\,\boldsymbol{k}). \tag{2.26}$$

2.2.3 Mellin transform

Another transform often encountered in fractional calculus is the Mellin integral transform

$$\mathcal{M}_x\big\{f(x)\big\}(s) = \int_0^{\infty} x^{s-1}\,f(x)\,\mathrm{d}x \tag{2.27}$$

or its inverse

$$\mathcal{M}_s^{-1}\big\{g(s)\big\}(x) = \frac{1}{2\pi i}\int_{\sigma-i\infty}^{\sigma+i\infty} x^{-s}\,g(s)\,\mathrm{d}s \tag{2.28}$$

which is related to the inverse Laplace transform. A more detailed discussion is not relevant to the presented work.

2.3 Univariate distributions with finite first moment

Some exponential-type distributions with finite expectations are introduced.

2.3.1 Exponential distribution

The exponential distribution $\mathrm{Exp}(\delta)$ on $[0, \infty)$ is parameterized with the scale parameter δ. The expected value is equal to δ and the probability density function is

$$f_\delta(t) = \frac{1}{\delta} \exp\left(-\frac{t}{\delta}\right). \tag{2.29}$$

2.3.2 Laplace distributions

The centered (expectation value 0) Laplace distribution $\mathrm{Laplace}(\delta)$ with scale δ and domain $\mathbb{R}$ is defined by the probability density and characteristic functions

$$f_\delta(t) = \frac{1}{2\delta} \exp\left(-\frac{|t|}{\delta}\right), \qquad \varphi_\delta(s) = \frac{1}{1+\delta^2 s^2}. \tag{2.30}$$

The Laplace distribution is sometimes referred to as bilateral exponential distribution. A skew version of the Laplace distribution [53] can be obtained by modifying the characteristic function with an additional parameter κ_1

$$\varphi_{\delta,\kappa_1}(s) = \frac{1}{1+\delta^2 s^2 - i\kappa_1 s}. \tag{2.31}$$

Introducing a second parameterization

$$\kappa_2 = \frac{\delta}{\kappa_1 + \sqrt{\delta^2 + \kappa_1}}, \qquad \kappa_1 = -\frac{\delta\,(\kappa_2 - 1)}{2\kappa_2}, \tag{2.32}$$

the density of the skew Laplace distribution can be written as

$$f_{\delta,\kappa_2}(t) = \frac{1}{\delta}\,\frac{\kappa_2}{1+\kappa_2^2} \begin{cases} \exp\left(-\dfrac{1}{\kappa_2}\dfrac{|t|}{\delta}\right) & t < 0 \\ \exp\left(-\kappa_2\dfrac{|t|}{\delta}\right) & t \geq 0 \end{cases}. \tag{2.33}$$

Skew Laplacian random variables $X \sim \text{Laplace}(\delta, \kappa_2)$ can be sampled using the formula

$$X \overset{d}{=} \delta \left(\kappa_2^{-1} E_1 - \kappa_2 E_2\right) \tag{2.34}$$

where $E_{1,2} \sim \text{Exp}(1)$ independently [53]. We note that

$$P(X < 0) = \int_{-\infty}^{0} f_{\delta,\kappa_2}(t)\,\mathrm{d}t = \frac{\kappa_2^2}{1+\kappa_2^2} \tag{2.35}$$

$$P(X \geq 0) = \int_{0}^{\infty} f_{\delta,\kappa_2}(t)\,\mathrm{d}t = \frac{1}{1+\kappa_2^2}. \tag{2.36}$$

For $\kappa_1 = 0$ and $\kappa_2 = 1$ the symmetric Laplace distribution is recovered.

2.3.3 Discrete distributions

Geometrically distributed random variables $X \sim \text{Geom}(p)$, have the probability mass function

$$f_p(t) = p\,(1-p)^t \tag{2.37}$$

with domain $\mathbb{N}$. The geometric distribution is related to the exponential distribution by $X = \lfloor Y \rfloor$ if $Y \sim \mathbb{E}(\delta)$ with scale $\delta = -\ln(1-p)^{-1}$. Hence, for $t \in \mathbb{N}$,

$$P(X = t) = f_p(t) = \int_{t}^{t+1} f_\delta(\tau)\,\mathrm{d}\tau = P\big(Y \in [t, t+1)\big). \tag{2.38}$$

A truncated geometric distribution $\text{Geom}(p, n)$ can be defined on $\{0, 1, \ldots, n\}$ by

$$f_{p,n}(t) = \frac{1}{1-(1-p)^{n+1}}\, p\,(1-p)^t. \tag{2.39}$$

A similar distribution is the truncated discrete exponential distribution, sometimes referred to as Boltzmann distribution,

$$f_{p,n}(t) = \frac{1-\exp(-1/\delta)}{1-\exp\big(-(n+1)/\delta\big)}\, \exp(-t/\delta). \tag{2.40}$$

2.4 Univariate distributions with infinite first moment

The distributions presented in this section are asymptotic Pareto or power laws with undefined and infinite moments.

2.4.1 Lomax distribution

The Lomax distribution $\mathrm{Lomax}(\beta, \tau)$ with shape β and scale τ has the probability density function

$$f_{\beta,\tau}(t) = \frac{\beta}{\tau}\left(1 + \frac{t}{\tau}\right)^{-(1+\beta)} = \beta\,\tau^{\beta}\,(\tau + t)^{-(1+\beta)} \tag{2.41}$$

on $[0, \infty)$. The expected value is undefined (infinite) for $\beta \leq 1$. For $\beta > 1$, the mean is $\tau/(\beta - 1)$.

2.4.2 Mittag-Leffler distribution

The Mittag-Leffler distribution $\mathrm{MiLeff}(\beta, \tau)$ on $[0, \infty)$ with shape parameter $0 < \beta \leq 1$ and scale $\tau > 0$ is defined by the probability density and cumulative distribution functions

$$f_{\beta,\tau}(t) = \frac{1}{\tau}\Big(\frac{t}{\tau}\Big)^{\beta-1} E_{\beta,\beta}\Big(-\Big(\frac{t}{\tau}\Big)^{\beta}\Big), \qquad F_{\beta,\tau}(t) = E_{\beta}\Big(-\Big(\frac{t}{\tau}\Big)^{\beta}\Big). \tag{2.42}$$

Usually neither the Mittag-Leffler function (2.6) nor the associated probability distribution is implemented in standard programming libraries. Elaborate numerical techniques are required for evaluating the probability density function. They are based on the approximation of the inverse Laplace transform of the characteristic function

$$\mathcal{L}_s\big\{f_{\beta,\tau}(t)\big\}(s) = \frac{1}{1 + (\tau s)^{\beta}} \tag{2.43}$$

or other improper integral representations (compare Section 2.1.3). The asymptotic behavior of the probability density function for $t \to \infty$ is given by [60]

$$f_{\beta,\tau}(t) \sim \tau^{\beta}\,\Gamma(\beta+1)\,\frac{\sin(\beta\pi)}{\pi}\,t^{-(1+\beta)} \tag{2.44}$$

$$\sim -\tau^{\beta}\,\Gamma(-\beta)^{-1}\,t^{-(1+\beta)}. \tag{2.45}$$

The Mittag-Leffler distribution belongs to the class of geometric stable distributions and allows to represent random variables as mixtures of uniform, exponential and skew Lévy-stable distributions (introduced in Section 2.5). For sampling, the following identities are useful [27]

$$\left.\begin{array}{l} -\tau \ln u \left(\dfrac{\sin(\beta\pi)}{\tan(\beta\pi v)} - \cos(\beta\pi)\right)^{1/\beta} \\ w^{1/\beta}\, s \end{array}\right\} \sim \mathrm{MiLeff}(\beta,\tau), \tag{2.46}$$

where $u, v \sim U(0,1)$ are standard uniform random variables, $w \sim \mathrm{Exp}(\tau)$ and $s \sim \mathrm{Stable}(\beta, 1, 1/8)$.

To assert the numerical accuracy of implementations for evaluating the probability density function (and Mittag-Leffler function), results were compared with the (more expensive) direct numerical inverse Laplace transform of (2.43) and sample histograms.

In accordance to the properties of the Mittag-Leffler function, the Mittag-Leffler distribution scales between the exponential distribution ($\beta = 1$) and a clear power law ($\beta \to 0$). For $\beta \to 1$ a Mittag-Leffler distributed random variable converges in distribution to the exponential distribution. The expectation of the Mittag-Leffler distribution is finite only for $\beta = 1$. In Figure 1 a comparison with the exponential and Lomax distribution is shown.

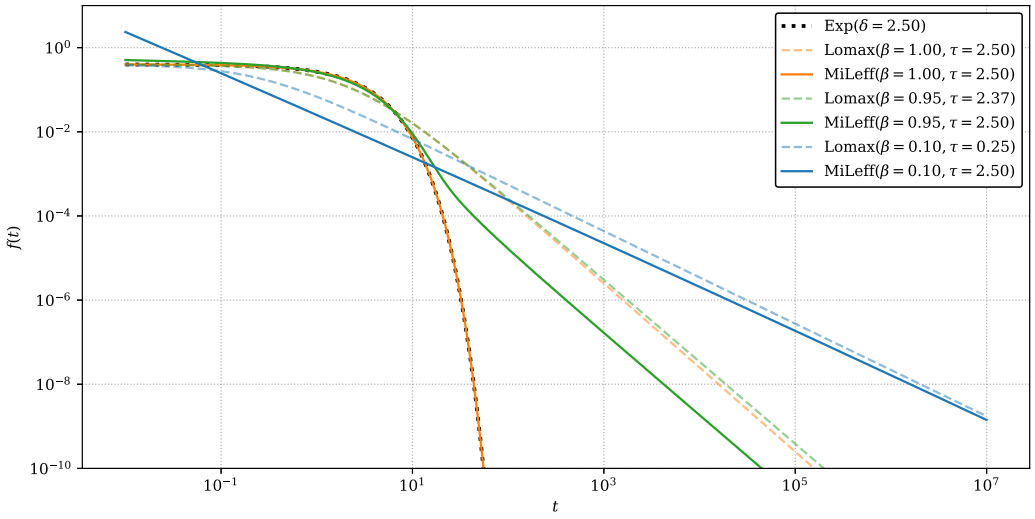

Figure 1: Probability density functions of the Mittag-Leffler distribution with different shape parameters. The Mittag-Leffler distribution scales between a power law and the exponential distribution. The Lomax distribution is a power law distribution with partially similar features as the Mittag-Leffler distribution and a closed-form density. The following parameterizations were used $\mathrm{MiLeff}\big(\beta = \beta, \tau = \tau_0\big)$, $\mathrm{Exp}(\delta = \tau_0)$, $\mathrm{Lomax}(\beta = \beta, \tau = \tau_0\beta)$.

2.5 Stable distributions

An important class of probability distributions with power-law tails is the family of Lévy- or α-stable distributions. The parameter $\alpha \in (0, 2]$ is called stability. The Normal and Cauchy distributions are special cases of Lévy-stable distributions with $\alpha = 2$ and $\alpha = 1$ respectively.

In general literature and in the field of fractional calculus commonly univariate Lévy-stable distributions are encountered. The extension to two or more dimensions does not come without some challenges, which is also true for the isotropic case, on which this introduction is limited. However, for isotropic bivariate stable distributions, the shape (or covariance matrix) can be reduced to a scalar parameter γ. The following scaling property holds for the probability density functions

$$\varepsilon^{-2} f_\gamma\big(\varepsilon^{-1}\boldsymbol{x}\big) = f_{\varepsilon\gamma}(\boldsymbol{x}). \tag{2.47}$$

2.5.1 Normal distribution

The density and characteristic function of the normal distribution with scale σ are given by

$$f_\sigma(x) = \frac{1}{\sqrt{2\pi}\sigma} \exp\Big(-\frac{1}{2}\frac{x^2}{\sigma^2}\Big), \qquad \varphi_\sigma(k) = \exp\Big(-\frac{1}{2}\sigma^2 k^2\Big). \tag{2.48}$$

Throughout this thesis normal distributions are parameterized with their scale and hence the notation Normal(σ) is used. The density and characteristic functions of the isotropic bivariate normal distribution $\text{Normal}_2(\sigma)$ are given by

$$f_\sigma(\boldsymbol{x}) = \frac{1}{2\pi\sigma^2} \exp\Big(-\frac{1}{2}\frac{|\boldsymbol{x}|^2}{\sigma^2}\Big), \qquad \varphi_\sigma(\boldsymbol{k}) = \exp\Big(-\frac{1}{2}\sigma^2|\boldsymbol{k}|^2\Big). \tag{2.49}$$

The distance from the origin (or location) of a isotropic bivariate normally distributed random variable is distributed with the Rayleigh distribution Rayleigh(σ) with density

$$f_\sigma(r) = \frac{r}{\sigma^2} \exp\Big(-\frac{1}{2}\frac{r^2}{\sigma^2}\Big) \tag{2.50}$$

and a non-closed-form characteristic function. Let $\boldsymbol{X} \sim \text{Normal}_2(\sigma)$, then $R := |\boldsymbol{X}| \sim$ Rayleigh(σ).

The normal distribution (in any dimensions) provides the following important properties. Let X_1, X_2, X_3 be independent identically distributed normal random variables. For given real a and b there exist real c and d such that $aX_1 + bX_2 \overset{d}{=} cX_3 + d$ (equal in distribution). In particular, if $X_1, X_2 \sim \text{Normal}_2(\sigma)$, then $X_1 + X_2 \sim \text{Normal}_2(\sqrt{2}\sigma)$. Secondly, the central limit theorem states that with growing n the distribution of the sum of n independent identically distributed (not necessarily normal) random variables with centered expectation and finite variance σ^2 approximates a normal distribution with variance $n\sigma^2$ and scale $\sqrt{n}\sigma$.

2.5.2 Cauchy distribution

The Cauchy distribution Cauchy(γ) with scale γ is defined by the density and characteristic functions

$$f_\gamma(x) = \frac{1}{\pi}\frac{\gamma}{x^2+\gamma^2}, \qquad \varphi_\gamma(k) = \exp(-\gamma|k|) \tag{2.51}$$

with infinite moments. The bivariate Cauchy distribution Cauchy$_2(\gamma)$ has the density and characteristic functions

$$f_\gamma(\boldsymbol{x}) = \frac{1}{2\pi}\frac{\gamma}{\left(|\boldsymbol{x}|^2+\gamma^2\right)^{3/2}}, \qquad \varphi_\gamma(\boldsymbol{k}) = \exp(-\gamma|\boldsymbol{k}|). \tag{2.52}$$

If $\boldsymbol{X} \sim$ Cauchy$_2(\gamma)$, then the distance from the origin $R := |\boldsymbol{X}|$ follows a distribution with density

$$f_\gamma(r) = \frac{\gamma r}{\left(r^2+\gamma^2\right)^{3/2}} \tag{2.53}$$

and without a closed-form characteristic function. By transformation of variables we find that $R \overset{d}{=} \sqrt{Z^2-\gamma^2}$ for a Pareto distributed random variable Z with scale γ and shape 1.

2.5.3 Univariate Lévy-stable distributions

The family of Lévy- or α-stable distributions has special properties similar to the Normal distribution and beyond. Stable random variables with common stability α are closed under linear combinations. In other words, the sum of n independent identically distributed stable random variables with stability parameter α and scale γ has a stable law with the same stability α and scale $n^{1/\alpha}\gamma$.

Moreover, a generalized central limit theorem [72] states that, with growing number, the distribution of the sum of independent (not necessarily Lévy-stable) random variables with power-law tailed densities $\sim |x|^{-(\alpha+1)}$ converges in distribution to a Lévy-stable law with stability α.

Lévy-stable distributions do not have a closed-form probability density function in general. Strictly stable distributions (i.e. with their location at the origin) in one dimension Stable(α, β, γ) are defined by their characteristic function

$$\varphi_{\alpha,\beta,\gamma}(k) = \exp\big(-\gamma^\alpha |k|^\alpha (1 - i\beta \operatorname{sgn}(k)\, \Phi)\big), \qquad \Phi = \begin{cases} \tan\left(\frac{\pi\alpha}{2}\right) & \alpha \neq 1 \\ -\frac{2}{\pi} \log|k| & \alpha = 1 \end{cases} \tag{2.54}$$

where α is called stability parameter, β is the skewness parameter and γ is the scale. Normal and Cauchy distributions are special cases of symmetric ($\beta = 0$) stable distributions with $\alpha = 2, \sigma = \sqrt{2}\gamma$ and $\alpha = 1$ respectively. Sampling usually relies on the fact that a stable random variable is equivalent in distribution to a certain (trigonometric) combination of an uniform and an exponential random variable [18].

Numerical approximation of the probability density is usually based on the inverse Fourier transform of the characteristic function and similar improper integral representations and implemented as elaborate algorithms using a combination or selection of FFT, specialized numerical quadrature methods and look-up tables [5, 68, 74, 82, 96]. For $\alpha < 2$, the asymptotic behavior of the probability density, however, is known to be Paretian of the form [72]

$$f_{\alpha,\beta,\gamma}(x) \sim \gamma^\alpha \left(1 + \operatorname{sgn}(x)\beta\right) \sin\left(\frac{\pi\alpha}{2}\right) \frac{\Gamma(1+\alpha)}{\pi} |x|^{-(1+\alpha)}. \tag{2.55}$$

2.5.4 Bivariate Lévy-stable distributions

Important resources for multivariate stable distributions are [73, 101]. Here only isotropic ($\beta = 0$) centered bivariate stable distributions are discussed. The bivariate isotropic and centered stable distribution Stable$_2(\alpha, \gamma)$ is defined by the characteristic function

$$\varphi_{\alpha,\gamma}(\boldsymbol{k}) = \exp\big(-\gamma^\alpha |\boldsymbol{k}|^\alpha\big). \tag{2.56}$$

If $\mathbf{X} \sim \text{Stable}_2(\alpha, \gamma)$ and $\alpha < 2$ then $\mathbf{X}$ can be represented as the product of a bivariate normal random variable and the square root of a univariate stable random variable [73], $\mathbf{X} \overset{d}{=} \mathbf{N}\sqrt{A}$ where

$$\mathbf{N} \sim \text{Normal}_2(1), \tag{2.57}$$

$$A \sim \text{Stable}\left(\overline{\alpha} = \frac{\alpha}{2}, \overline{\beta} = 1, \overline{\gamma} = 2\gamma^2 \cos\left(\frac{\pi\alpha}{4}\right)^{2/\alpha}\right). \tag{2.58}$$

The distribution of A is fully skewed ($\overline{\beta} = 1$) with the stability and scale parameter as functions of the parameters of $\mathbf{X}$. The probability density $f_{\sqrt{A}}$ can be written as a transformation of f_A,

$$f_{\sqrt{A}}(\sigma) = 2\sigma\, f_A(\sigma^2). \tag{2.59}$$

While $\sqrt{A}$ can be interpreted as the distributed scaling of $\mathbf{N}$ (compare prior or mixing distribution), A corresponds to a distributed variance. Ultimately, multivariate isotropic stable random variables can be sampled using implementations of univariate stable distributions and their distribution functions can be represented as transformations of distribution functions of univariate skew stable random variables.

$$f_{\alpha,\gamma}(\boldsymbol{x}) = \int_0^\infty f_{\mathbf{N}}(\boldsymbol{x}\sigma^{-1})\, \sigma^{-2}\, f_{\sqrt{A}}(\sigma)\, \mathrm{d}\sigma \tag{2.60}$$

$$= \int_0^\infty f_{\mathbf{N}}(\boldsymbol{x}\sigma^{-1})\, 2\sigma^{-1}\, f_A(\sigma^2)\, \mathrm{d}\sigma \tag{2.61}$$

The distance or absolute value of a bivariate isotropic stable random variable with $\alpha < 2$ can be written as $R := |\mathbf{X}| \overset{d}{=} \sqrt{A\mathbf{N}^2} \overset{d}{=} \sqrt{AT}$ where T reduces to a special case of the chi-squared distribution, the exponential distribution with scale $\delta = 2$, $T \sim \text{Exp}(2)$. In [73] the distance R is called amplitude. The bivariate variable $\mathbf{X}$ can be recovered from R by $\mathbf{X} \overset{d}{=} R\mathbf{U} \overset{d}{=} \sqrt{AT}\mathbf{U}$ where $\mathbf{U}$ is uniformly distributed on the unit circle. The density of R can be obtained from a transformation of (2.61) and the Rayleigh

distribution or from the product distribution of AT and a square-root transform

$$f_R(r) = 2r \int_0^\infty f_T(t)\, t^{-1}\, f_A(r^2 t^{-1})\, \mathrm{d}t. \tag{2.62}$$

This form of the density of the amplitude allows additional tweaks for increased performance when evaluated numerically [73]. Since the probability density function is the inverse Fourier transform of the characteristic function, the amplitude distribution can also be written using the Hankel transform as [110]

$$f_R(r) = \frac{1}{2\pi} \int_0^\infty J_0(kr)\, kr \exp\bigl(-\gamma^\alpha k^\alpha\bigr)\, \mathrm{d}k. \tag{2.63}$$

The integrands in both representations (2.62) and (2.63) are improper integrals in the first place. Although sophisticated numerical algorithms exist for calculating both integrands, we can expect a certain amplification of errors and computation time in the evaluation of the density function of bivariate Lévy-stable distributions especially when using direct numerical integration. Figure 2 shows densities calculated from a tweaked version of (2.62) using direct numerical integration. Without a proper numerical analysis we find that (2.63) is faster but has issues with small α. The formulation (2.62) on the other hand is slower but less prone to numerical errors (see also Section 2.5.5). A sophisticated algorithm or implementation for directly approximating multivariate stable densities is not available.

For validating or comparing sample histograms or empirical distributions with the distribution of isotropic bivariate Lévy-stable random variables different avenues are possible. Statistical fitting and inference methods for multivariate stable (anisotropic) distributions are not very common in standard programming libraries (compare [14, 15]). In the isotropic case the problem can be reduced to the amplitude distribution or the distribution of A. For univariate stable distributions implementations of statistical and fitting methods are readily available [82, 96]. In literature often the Fourier transform (FFT) of (radial) sample histograms is compared with the characteristic function

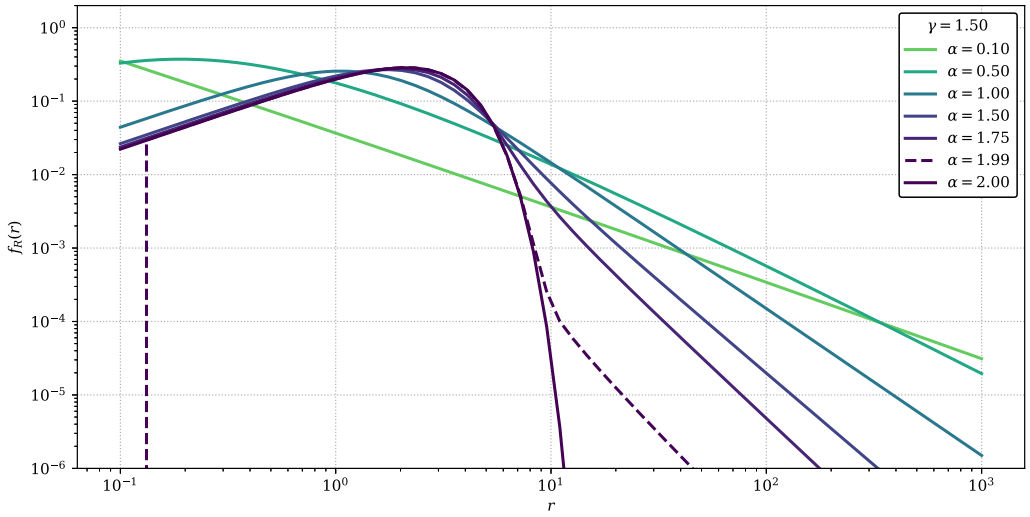

Figure 2: Numerical approximation of the density of the amplitude of isotropic bivariate Lévy-stable distributions $\text{Stable}_2(\alpha, \gamma)$. For $\alpha = 1$ and $\alpha = 2$ the density functions of the amplitudes of $\text{Cauchy}_2(\gamma)$ and $\text{Normal}_2(\sqrt{2}\gamma)$ are shown. The amplitude distribution scales between a clear power law and the Rayleigh distribution with the stability parameter α. Numerical and convergence issues are visible at $\alpha = 1.99$.

as shown in Figure 3. Sometimes it is sufficient to assert the asymptotic behavior of empirical distributions.

2.5.5 Asymptotic behavior and transitions

The asymptotic behavior for $r \to \infty$ of the amplitude density for $\alpha < 2$ is given by [73]

$$f_R(r) \sim (2\gamma)^\alpha \, \alpha \, \frac{\Gamma(1+\alpha/2)}{\Gamma(1-\alpha/2)} \, r^{-(1+\alpha)}. \tag{2.64}$$

And the following representation of the bivariate density is known [73]

$$f_{\alpha,\gamma}(\boldsymbol{x}) = \begin{cases} \dfrac{\Gamma(2/\alpha)}{2\pi\alpha\gamma^2} & \boldsymbol{x} = 0 \\ \dfrac{1}{2\pi} |\boldsymbol{x}|^{-1} f_R(|\boldsymbol{x}|) & \boldsymbol{x} \neq 0 \end{cases}. \tag{2.65}$$

Together, the following asymptotic behavior for $|\boldsymbol{x}| \to \infty$ of isotropic bivariate stable densities with $\alpha < 2$ can be calculated,

$$f_{\alpha,\gamma}(\boldsymbol{x}) \sim \frac{1}{2\pi} (2\gamma)^\alpha \, \alpha \, \frac{\Gamma(1+\alpha/2)}{\Gamma(1-\alpha/2)} \, |\boldsymbol{x}|^{-(2+\alpha)} \tag{2.66}$$

$$\sim \gamma^\alpha \, \frac{1}{-c(\alpha)} \, |\boldsymbol{x}|^{-(2+\alpha)}. \tag{2.67}$$

The factor $c(\alpha)$ was introduced in (2.25) and occurs in the Fourier transform $|\boldsymbol{x}|^{-(2+\alpha)} \longleftrightarrow c(\alpha) \, |\boldsymbol{k}|^\alpha$ (2.24). Note that the characteristic function has the asymptotic expansion $\exp(-\gamma^\alpha |\boldsymbol{k}|^\alpha) \sim 1 - \gamma^\alpha |\boldsymbol{k}|^\alpha$ for small $|\boldsymbol{k}|$.

For $\alpha \to 2$ an α-stable random variable converges in distribution to a normal random variable. This follows from the pointwise convergence of the characteristic function and Lévy's continuity theorem. However, this does not imply or require the respective (pointwise) transition of the probability density functions. Analogously, we can expect that the amplitude of an isotropic bivariate stable random variable converges in distribution to a Rayleigh random variable. Again, this does not necessarily mean that the density of the amplitude converges pointwise to the density function of the Rayleigh distribution (compare Figure 2 and the approximation errors for large α).

Regard the decomposition $\boldsymbol{X} = \boldsymbol{N}\sqrt{A}$ of a bivariate isotropic stable random variable $\boldsymbol{X} \sim \text{Stable}_2(\alpha, 1)$, where $\boldsymbol{N}$ is a standard bivariate normal random variable and

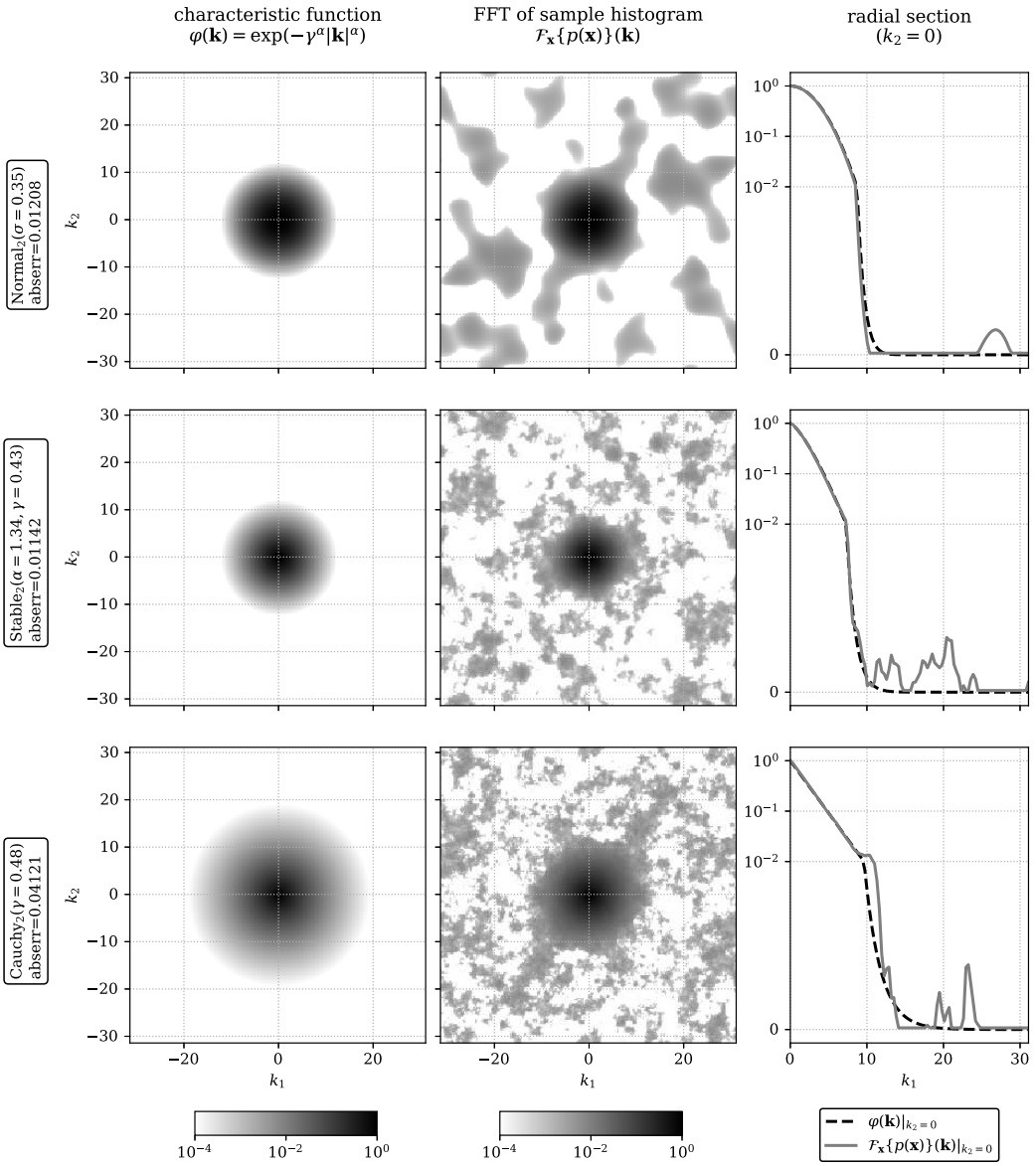

Figure 3: Comparison of the Fourier transform of two-dimensional sample histograms $p(\boldsymbol{x})$ (10^5 samples) with the characteristic function $\varphi(\boldsymbol{k})$ of isotropic bivariate Lévy-stable distributions $\text{Stable}_2(\alpha, \gamma)$. The pointwise maximum absolute error is printed on the left. On the right, a section along the first axis ($\boldsymbol{k} = (k_1, k_2)$) is shown in a mixed linear-logarithmic scale.

$A \sim \text{Stable}\big(\alpha/2, 1, 2\cos(\pi\alpha/4)^{2/\alpha}\big)$. For $\alpha \to 2$ we have $\boldsymbol{X} = \boldsymbol{N}\sqrt{A} \xrightarrow{d} \sqrt{2}\boldsymbol{N}$. Hence we expect that $\sqrt{A}$ approaches a degenerate distribution with the constant value $\sqrt{2}$ as $\alpha \to 2$. A degenerate random variable, however, cannot be modeled with Lévy-stable distributions. This aligns with the exclusive validity of the decomposition for $\alpha < 2$. Also note that with $\alpha = 2$ the stability parameter of A is 1 and accordingly the support is the whole real line, which is not the case for $\alpha < 2$.

For $\alpha < 2$ the characteristic function of A is (2.54)

$$\varphi_A(z) = \exp\left(-2^{\alpha/2}\cos\left(\frac{\pi\alpha}{4}\right)|z|^{\alpha/2}\left(1 - i\,\text{sgn}(z)\tan\left(\frac{\pi\alpha}{4}\right)\right)\right) \tag{2.68}$$

$$= \exp\left(-|2z|^{\alpha/2}\cos\left(\frac{\pi\alpha}{4}\right) + |2z|^{\alpha/2}\,i\,\text{sgn}(z)\sin\left(\frac{\pi\alpha}{4}\right)\right) \tag{2.69}$$

with the pointwise limit $\exp(2zi)$ for $\alpha \to 2$, which is the characteristic function of a degenerate distribution with location 2. The inverse Fourier transform $\mathcal{F}_z^{-1}\{\exp(2zi)\}(x) = \delta_0(x-2)$ must be understood in a distributional sense.

As a consequence, the predicted result $A \xrightarrow{d} 2$ is true. For $\alpha = 2$, the decomposition $\boldsymbol{X} = \boldsymbol{N}\sqrt{A}$ requires a degenerate random variable A.

3 Fractional diffusion

Anomalous diffusion comprehends certain phenomena not covered by the usual formalization of diffusion processes. This concerns in particular sub- and super-diffusive systems, in which the ratio between spatial dispersion and time is no longer linear. The former case occurs for instance when a liquid is subject to local trapping as it is in porous media. The latter describes systems where spatial displacement can occur in all orders of magnitude.

Formalizations of anomalous diffusion are for instance via fractional calculus and the fractional diffusion equation (Section 3.1) or by the observation of ensembles of certain random walks (Section 3.2). For analyzing and quantifying the emerging memory, clustering and long-range interaction effects, special statistical measures and techniques are required (Section 3.3). The results of this chapter were implemented in a Python programming library (Section 3.4) for simulating and analyzing continuous time random walks that reproduce the fractional diffusion equation in the Caputo and Riesz-Feller sense.

3.1 Short introduction to fractional calculus

An introduction to fractional calculus can be found, for instance, in [26, 67, 108]. Here, a selection of topics, some special cases and occasional reductions or extensions to two dimensions are presented. If not explicitly separated or otherwise mentioned, equations with vector notation $\boldsymbol{x}$ refer to the two-dimensional ($d = 2$) and the one-dimensional ($d = 1$) case. A straight-forward generalization to dimensions $d > 2$ is however not necessarily valid in the following presentation.

3.1.1 Fractional differential operators

Fractional differential operators are often defined in the Fourier-Laplace domain. Let ${}_{\mathrm{R}}D_x^{\alpha}$ and ${}_{\mathrm{C}}D_t^{\beta}$ be defined by [27, 35, 37, 66, 88]

$$\mathcal{L}_t\{{}_{\mathrm{C}}D_t^{\beta} f(t)\}(s) = s^{\beta}\tilde{f}(s) - s^{\beta-1}f(0) \tag{3.1}$$

$$\mathcal{F}_x\{{}_{\mathrm{R}}D_x^{\alpha} f(x)\}(k) = |k|^{\alpha}\hat{f}(k) \qquad x \in \mathbb{R} \tag{3.2}$$

$$\mathcal{F}_{\boldsymbol{x}}\{{}_{\mathrm{R}}D_{\boldsymbol{x}}^{\alpha} f(\boldsymbol{x})\}(\boldsymbol{k}) = |\boldsymbol{k}|^{\alpha}\hat{f}(\boldsymbol{k}) \qquad \boldsymbol{x} \in \mathbb{R}^2 \tag{3.3}$$

for $0 < \beta \leq 1$ and $0 < \alpha \leq 2$ and functions f that suffice the requirements of the respective transforms. In the two-dimensional case, it is required that f is a Schwartz function [16, 25].

There, however, also exist integral representations of the fractional differential operators introduced above. The generalized Caputo fractional derivative (3.1) can be defined as [88, 100]

$${}_{\mathrm{C}}\mathcal{D}_t^{\eta} f(t) = \int_0^t \eta(t-\tau)\frac{\mathrm{d}}{\mathrm{d}\tau}f(\tau)\,\mathrm{d}\tau \tag{3.4}$$

and with a memory kernel $\eta(t) = t^{-\beta}/\Gamma(1-\beta)$ reduces for $0 < \beta < 1$ to the usual Caputo fractional derivative [35, 58, 85, 88]

$${}_{\mathrm{C}}D_t^{\beta} f(t) = \frac{1}{\Gamma(1-\beta)}\int_0^t (t-\tau)^{-\beta}\frac{\mathrm{d}}{\mathrm{d}\tau}f(\tau)\,\mathrm{d}\tau \tag{3.5}$$

which is linked to (3.1) by the Laplace transform and a convolution. Note that also the Riemann-Liouville fractional derivative delivers the same results in connection with the fractional diffusion equation as long as the initial conditions are taken into consideration [27, 88]. We skip the details and rely on the above definition throughout this presentation.

Following the definition in (3.2), the fractional space derivative is the inverse of the Riesz potential operator and known as the Riesz derivative (or symmetric Riesz-Feller

derivative) [58]

$$ {}_{\mathrm{R}}D_x^{\alpha} f(x) = \frac{\Gamma(1+\alpha)}{\pi} \sin\Big(\frac{\alpha\pi}{2}\Big) \int_0^{\infty} \frac{f(x-\xi) - 2f(x) + f(x+\xi)}{\xi^{1+\alpha}} \,\mathrm{d}\xi \tag{3.6} $$

for $0 < \alpha < 2$. In two dimensions the (hyper singular) integral expressions [25, 83, 84]

$$ {}_{\mathrm{R}}D_{\boldsymbol{x}}^{\alpha} f(\boldsymbol{x}) = \frac{1}{|c(\alpha)|} \lim_{\varepsilon\to 0} \int_{\mathbb{R}^2\setminus B_\varepsilon(0)} \frac{f(\boldsymbol{x}) - f(\boldsymbol{x}-\boldsymbol{\xi})}{|\boldsymbol{\xi}|^{2+\alpha}} \,\mathrm{d}\boldsymbol{\xi} \tag{3.7} $$

$$ {}_{\mathrm{R}}D_{\boldsymbol{x}}^{\alpha} f(\boldsymbol{x}) = \frac{1}{d_k(\alpha)} \lim_{\varepsilon\to 0} \int_{\mathbb{R}^2\setminus B_\varepsilon(0)} \frac{\Delta_{\boldsymbol{\xi}}^k f(\boldsymbol{x})}{|\boldsymbol{\xi}|^{2+\alpha}} \,\mathrm{d}\boldsymbol{\xi} \tag{3.8} $$

are valid for $0 < \alpha < 2$ and $0 < \alpha$ respectively. However, the second form requires that $(1 + |\boldsymbol{x}|)^{-(2+\alpha)} f(\boldsymbol{x})$ is integrable [25]. The factor $c(\alpha)$ was defined in (2.25). The remaining constants and the finite difference (finite Laplace operator) in above equations are defined as

$$ d_k(\alpha) = -c(\alpha) \sum_{j=0}^{k} (-1)^j \binom{k}{j} \Big|\frac{k}{2} - j\Big|^2 \tag{3.9} $$

$$ \Delta_{\boldsymbol{\xi}}^k f(\boldsymbol{x}) = \sum_{j=1}^{k} (-1)^j \binom{k}{j} f\Big(\boldsymbol{x} + \Big(\frac{k}{2} - j\Big)\boldsymbol{\xi}\Big). \tag{3.10} $$

The well known result for $\alpha = 2$,

$$ \mathcal{F}_{\boldsymbol{x}}\big\{-\Delta_{\boldsymbol{x}} f(\boldsymbol{x})\big\}(\boldsymbol{k}) = |\boldsymbol{k}|^2 \hat{f}(\boldsymbol{k}) \tag{3.11} $$

implies that the Riesz fractional derivative can be interpreted as a fractional Laplacian and motivates the notation $(-\Delta_{\boldsymbol{x}})^{\alpha/2} = {}_{\mathrm{R}}D_{\boldsymbol{x}}^{\alpha}$.

3.1.2 Fractional diffusion equation

With above construction of fractional differential operators, the fractional diffusion equation can be written as

$$ {}_{\mathrm{C}}D_t^{\beta}\, u(t,\boldsymbol{x}) = C_{\alpha,\beta}\ {}_{\mathrm{R}}D_{\boldsymbol{x}}^{\alpha}\, u(t,\boldsymbol{x}) \qquad t \geq 0, \boldsymbol{x} \in \mathbb{R}^d \tag{3.12} $$

where $0 < \beta \leq 1$, $0 < \alpha \leq 2$ and $d = 1, 2$. The generalized diffusion coefficient

$$ C_{\alpha,\beta} = \frac{C_D^{\alpha/d}}{C_T^{\beta}}, \tag{3.13} $$

can be interpreted as a a scaling between time and space where C_D corresponds to a contraction of space and C_T to a stretching of time.

In the Fourier-Laplace domain the fractional diffusion equation reads as

$$ s^{\beta}\, \hat{\tilde{u}}(s,\boldsymbol{k}) - s^{\beta-1} = -C_{\alpha,\beta}\, |\boldsymbol{k}|^{\alpha}\, \hat{\tilde{u}}(s,\boldsymbol{k}). \tag{3.14} $$

The algebraic solution of this equation with initial condition $u(0,\boldsymbol{x}) = \delta(\boldsymbol{x})$ is the Fourier-Laplace transform of the fundamental solution or Green's function [58, 66]

$$ \hat{\tilde{G}}_{\alpha,\beta}(s,\boldsymbol{k}) = \frac{s^{\beta-1}}{s^{\beta} + C_{\alpha,\beta}\, |\boldsymbol{k}|^{\alpha}}. \tag{3.15} $$

3.1.3 Fundamental solutions

From the Fourier and Laplace transform the following scaling property (see (2.12) and (2.26)) can be concluded

$$ G_{\alpha,\beta}(\varepsilon t, \boldsymbol{x}) = \varepsilon^{-d\beta/\alpha} G_{\alpha,\beta}(t, \varepsilon^{-\beta/\alpha}\boldsymbol{x}), \tag{3.16} $$

which allows to treat the fundamental solution as a single argument function by writing [27, 58]

$$G_{\alpha,\beta}(t,\boldsymbol{x}) = t^{-d\beta/\alpha} K_{\alpha,\beta}(\boldsymbol{x} t^{-\beta/\alpha}). \tag{3.17}$$

From the Laplace transform of the Mittag-Leffler function (2.43) and (3.15) we find that

$$\hat{G}_{\alpha,\beta}(t,\boldsymbol{k}) = E_\beta\big(-C_{\alpha,\beta}\,|\boldsymbol{k}|^\alpha\, t^\beta\big) \tag{3.18}$$

and by factorizing the generalized diffusion constant,

$$\hat{G}_{\alpha,\beta}(t,\boldsymbol{k}) = E_\beta\Big(-\big(C_D^{1/d}\,|\boldsymbol{k}|\big)^\alpha\,\big(C_T^{-1}\,t\big)^\beta\Big). \tag{3.19}$$

The detailed requirements for the inverse Fourier transform and the normalization of $G_{\alpha,\beta}$ as well as a discussion of special cases of the fundamental solution for particular α and β in one dimension can be found in [58, 59]. A reference for fundamental solutions in higher dimensions and their asymptotic behavior is [51]. For $\alpha = 2$ and $\beta = 1$ (the Mittag-Leffler function corresponds to the exponential function) the usual Gaussian shape is recovered

$$G_{2,1}(t,\boldsymbol{x}) = t^{-d/2} f(\boldsymbol{x} t^{-1/2}) \qquad f(\boldsymbol{x}) \sim \mathrm{Normal}_d\Big(\sqrt{2}\,C_D^{1/d}\,C_T^{-1/2}\Big) \tag{3.20}$$

$$= g(\boldsymbol{x}) \qquad g(\boldsymbol{x}) \sim \mathrm{Normal}_d\Big(\sqrt{2}\,C_D^{1/d}\,C_T^{-1/2}\,t^{1/2}\Big). \tag{3.21}$$

For $\alpha < 2$ and $\beta = 1$ the fundamental solution is the density of a Lévy-stable distribution with stability α,

$$G_{\alpha,1}(t,\boldsymbol{x}) = t^{-d/\alpha} f(\boldsymbol{x} t^{-1/\alpha}) \qquad f(\boldsymbol{x}) \sim \mathrm{Stable}_d\Big(\alpha, C_D^{1/d}\,C_T^{-1/\alpha}\Big) \tag{3.22}$$

$$= g(\boldsymbol{x}) \qquad g(\boldsymbol{x}) \sim \mathrm{Stable}_d\Big(\alpha, C_D^{1/d}\,C_T^{-1/\alpha}\,t^{1/\alpha}\Big). \tag{3.23}$$

The diffusion process is called strictly space fractional. For strictly time fractional diffusion ($\alpha = 2$ and $\beta < 1$), Fourier and Hankel transformation rules deliver for $d = 1$ and $d = 2$ respectively

$$G_{2,\beta}(t,x) = \frac{C_T}{2C_D}\,\mathcal{L}_s^{-1}\left\{(C_T s)^{\beta/2-1}\,\exp\Big(-|x|\,C_D^{-1}\,(C_T s)^{\beta/2}\Big)\right\}(t), \tag{3.24}$$

$$G_{2,\beta}(t,\boldsymbol{x}) = \frac{C_T}{2\pi C_D}\,\mathcal{L}_s^{-1}\left\{(C_T s)^{\beta-1}\,K_0\Big(|\boldsymbol{x}|\,C_D^{-1/2}\,(C_T s)^{\beta/2}\Big)\right\}(t), \tag{3.25}$$

where $K_0(s)$ denotes the modified Bessel function of second kind (2.5). Note that $K_0(s)$ decays exponentially like $\exp(-s)$ but has a logarithmic singularity at 0. Accordingly, for $|\boldsymbol{x}| \ll 1$ and in particular for $|\boldsymbol{x}| = 0$, the numerical inverse Laplace transform $\mathcal{L}_s^{-1}\big(\ldots K_0(\ldots |\boldsymbol{x}|\,s^{\beta/2})\big)$ fails. The analytical result can however be interpreted as a limit $|\boldsymbol{x}| \to 0$.

In the general space and time fractional case ($\alpha < 2$ and $\beta < 1$), the fundamental solution can be expressed in terms of Fox-H functions (Section 2.1.4). A discussion of this representation in one dimension can be found in [9, 26, 48, 59, 66, 85], the higher dimensional case – not very common in literature – can be found in [51],

$$G_{\alpha,\beta}(t,x) = \frac{1}{\alpha\,|x|}\,\mathrm{H}_{3,3}^{2,1}\left[\frac{|x|}{C_{\alpha,\beta}^{1/\alpha}\,t^{\beta/\alpha}}\middle|\begin{matrix}(1,1/\alpha) & (1,\beta/\alpha) & (1,1/2)\\ (1,1) & (1,1/\alpha) & (1,1/2)\end{matrix}\right], \tag{3.26}$$

$$G_{\alpha,\beta}(t,\boldsymbol{x}) = \frac{1}{\alpha\,|\boldsymbol{x}|^d\,\pi^{d/2}}\,\mathrm{H}_{2,3}^{2,1}\left[\frac{|\boldsymbol{x}|}{2\,C_{\alpha,\beta}^{1/\alpha}\,t^{\beta/\alpha}}\middle|\begin{matrix}(1,1/\alpha) & (1,\beta/\alpha) & \\ (d/2,1/2) & (1,1/\alpha) & (1,1/2)\end{matrix}\right]. \tag{3.27}$$

Note that also in the general form, the fundamental solution is singular at the origin.

3.2 Continuous time random walks

Here, the term *continuous time random walk* (CTRW) is mainly used to refer to random walks that simulate fractional diffusion (the fractional diffusion equation) and not to stochastic processes that just operate on continuous time scales. However, to simplify the nomenclature, also random walks with discrete time increments and heavy-tailed spatial increments (Lévy flights) are occasionally referred to as continuous time random walks. Furthermore, fractional Brownian motion (power-law time-correlated Gaussian spatial increments) is not discussed in this thesis.

A recent overview on continuous time random walks can be found in [54], the mathematical details are laid out extensively in [9, 35, 66, 88]. This section contains an extension to two dimensions, which in particular concerns parameterization, identification with the fractional diffusion equation and quantification of random walk trajectories.

3.2.1 Definition

We trace particles in $\mathbb{R}^2$ performing jumps $d\boldsymbol{x}$ with waiting, resting or travel times dt. Occasionally continuous time random walks in $\mathbb{R}$ will be discussed, the notation is analogous. The increments are assumed to be independently distributed random variables. The trajectory of a particle is given by interpolation points $(t_i, \boldsymbol{x}_i)$ where

$$t_i = \sum_{k=0}^{i-1} dt_k \qquad\qquad \boldsymbol{x}_i = \sum_{k=0}^{i-1} d\boldsymbol{x}_k \tag{3.28}$$

for $i \in \{1, 2, \dots\}$ and $t_0 = 0$ and $\boldsymbol{x}_0 = \mathbf{0}$. A càdlàg (not continuous) formulation of the trajectory is

$$\boldsymbol{x}(t) := \sum_i d\boldsymbol{x}_i \, \mathbb{I}_{(0,t]}(t_{i+1}) = \sum_i d\boldsymbol{x}_i \, \mathbb{I}_{[t_{i+1},\infty)}(t) = \boldsymbol{x}_{I(t)} \tag{3.29}$$

and an analogous averaged formulation of the increments is

$$d\boldsymbol{x}(t,\Delta) := \sum_i d\boldsymbol{x}_i \, \mathbb{I}_{(t,t+\Delta]}(t_{i+1}) \quad = \quad \boldsymbol{x}(t+\Delta) - \boldsymbol{x}(t) \quad = \quad \boldsymbol{x}_{I(t+\Delta)} - \boldsymbol{x}_{I(t)} \tag{3.30}$$

$$dt(t,\Delta) := \sum_i dt_i \, \mathbb{I}_{(t,t+\Delta]}(t_{i+1}) \quad = \quad t_{I(t+\Delta)} - t_{I(t)} \tag{3.31}$$

where

$$I(t) := i : t_i \leq t < t_{i+1} \qquad \text{and} \qquad I(t_a, t_b) := \{i : t_a < t_i \leq t_b\}. \tag{3.32}$$

Figure 4 is a visualization of this formulation.

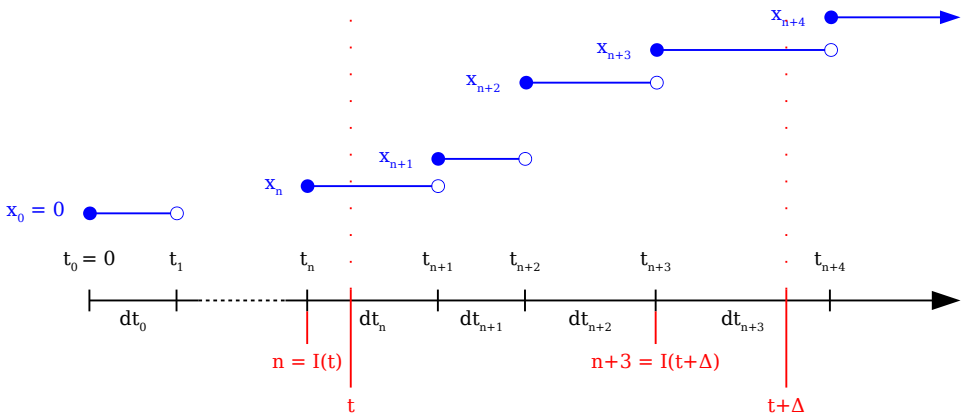

Figure 4: Schematic construction of continuous time random walks.

The velocity of a particle can be defined as the stochastic process $\boldsymbol{v}_i = d\boldsymbol{x}_i/dt_i$ with the càdlàg interpolation

$$\boldsymbol{v}(t) := \boldsymbol{v}_{I(t)} = \frac{d\boldsymbol{x}_{I(t)}}{dt_{I(t)}}. \tag{3.33}$$

A further (moving average) form of velocity is

$$\boldsymbol{v}(t,\Delta) := \frac{1}{\Delta}\int_t^{t+\Delta} \boldsymbol{v}(\tau)\,\mathrm{d}\tau. \tag{3.34}$$

Note that this definition does not correspond to the definition of $d\boldsymbol{x}(t,\Delta)$ and $dt(t,\Delta)$, rather

$$\boldsymbol{v}(t,\Delta) = \frac{1}{\Delta}\left(\left(t_{I(t)+1} - t\right)\boldsymbol{v}_{I(t)} + \sum_{j=I(t)+1}^{I(t+\Delta)} dt_j\,\boldsymbol{v}_j - \left(t_{I(t+\Delta)+1} - t - \Delta\right)\boldsymbol{v}_{I(t+\Delta)}\right). \tag{3.35}$$

3.2.2 Link to fractional diffusion

A simple master equation approach [35, 60, 66] delivers the probability for a particle to be at position $\boldsymbol{x}$ at time t. Let $\lambda(\boldsymbol{x})$ and $\psi(t)$ be the densities of the jump vectors and waiting times, then

$$p(t,\boldsymbol{x}) = \delta(\boldsymbol{x})\Psi(t) + \int_0^t \int_{\mathbb{R}^2} \psi(t-\eta)\,\lambda(\boldsymbol{x}-\boldsymbol{\xi})\,p(\eta,\boldsymbol{\xi})\,\mathrm{d}\boldsymbol{\xi}\,\mathrm{d}\eta \tag{3.36}$$

where $\Psi(t) = 1 - \int_0^t \psi(\eta)\,\mathrm{d}\eta$ is the survival probability associated with the waiting time distribution. The expression above separates into a resting and into a jumping part and the initial condition of the process is given by $p(0,\boldsymbol{x}) = \delta(\boldsymbol{x})$. In the Fourier-Laplace domain the master equation reads

$$\hat{\tilde{p}}(s,\boldsymbol{k}) = \tilde{\Psi}(s) + \tilde{\psi}(s)\,\hat{\lambda}(\boldsymbol{k})\,\hat{\tilde{p}}(s,\boldsymbol{k}) = \frac{1-\tilde{\psi}(s)}{s} + \tilde{\psi}(s)\,\hat{\lambda}(\boldsymbol{k})\,\hat{\tilde{p}}(s,\boldsymbol{k}) \tag{3.37}$$

with algebraic solution (Montroll-Weiss equation)

$$\hat{\tilde{p}}(s,\boldsymbol{k}) = \frac{\tilde{\Psi}(s)}{1-\tilde{\psi}(s)\,\hat{\lambda}(\boldsymbol{k})} = \frac{1-\tilde{\psi}(s)}{s}\frac{1}{1-\tilde{\psi}(s)\,\hat{\lambda}(\boldsymbol{k})}. \tag{3.38}$$

In [60, 100] a memory kernel $\Phi(t)$ was introduced such that

$$\Psi(t) = \int_0^t \Phi(t-\eta)\,\psi(\eta)\,\mathrm{d}\eta. \tag{3.39}$$

This allows to distinguish Markovian and long-memory processes by $\Phi(t) = \delta(t)$ and $\Phi(t) = t^{-\beta}/\Gamma(1-\beta)$ respectively with a transition as $\beta \to 1$. It follows that $\tilde{\Phi}(s) = 1/s^{1-\beta}$, $\tilde{\Psi}(s) = s^{\beta-1}/(1+s^{\beta})$ and $\tilde{\psi}(s) = (1+s^{\beta})^{-1}$, which means that by (2.43) $\psi(t)$ is the density of the Mittag-Leffler distribution MiLeff(β, τ). The same transition can be recognized by the fact that the Mittag-Leffler distribution converges to the exponential distribution as $\beta \to 1$.

The following statement is a generalization of two Lemmata in [35]. Let $\lambda(x)$, $\lambda(\boldsymbol{x})$ and $\psi(t)$ be (symmetric) probability density functions on $\mathbb{R}$, $\mathbb{R}^2$ and $\mathbb{R}_+$, then

$$\lambda(x) \sim A_\alpha\,|x|^{-(1+\alpha)} \quad \Longrightarrow \quad \hat{\lambda}(k) \sim 1 - A_\alpha\,\frac{\pi}{\Gamma(1+\alpha)\,\sin(\pi\alpha/2)}\,|k|^\alpha \tag{3.40}$$

$$\lambda(\boldsymbol{x}) \sim A_\alpha\,|\boldsymbol{x}|^{-(2+\alpha)} \quad \Longrightarrow \quad \hat{\lambda}(\boldsymbol{k}) \sim 1 - A_\alpha\,\big(-c(\alpha)\big)\,|\boldsymbol{k}|^\alpha \tag{3.41}$$

$$\psi(t) \sim A_\beta\,t^{-(1+\beta)} \quad \Longrightarrow \quad \tilde{\psi}(s) \sim 1 - A_\beta\,\frac{\Gamma(1-\beta)}{\beta}\,s^\beta \tag{3.42}$$

for $|x|, |\boldsymbol{x}|, t \to \infty$ and $|k|, |\boldsymbol{k}|, s \to 0$. A thorough proof requires some theorems from functional analysis. Here, numerical computations were used to validate the statement. The inverted logical implication is not true.

One way to obtain the fractional diffusion equation (3.14) from the Montroll-Weiss equation (3.38) is by explicitly defining the jump and waiting time probability distributions ($d = 1, 2$) as

$$dt \sim \text{MiLeff}(\beta, \tau) \quad \Longrightarrow \quad \begin{cases} \psi(t) \sim \tau^\beta \, \dfrac{\beta}{\Gamma(1-\beta)} \, t^{-(\beta+1)} \\ \tilde{\psi}(s) = \dfrac{1}{1+\tau^\beta s^\beta} \end{cases} \tag{3.43}$$

$$d\boldsymbol{x} \sim \text{Stable}_2(\alpha, \gamma) \quad \Longrightarrow \quad \begin{cases} \lambda(\boldsymbol{x}) \sim \gamma^\alpha \, \dfrac{1}{-c(\alpha)} \, |\boldsymbol{x}|^{-(\alpha+2)} \\ \hat{\lambda}(\boldsymbol{k}) = \exp(-\gamma^\alpha |\boldsymbol{k}|^\alpha) \end{cases} \tag{3.44}$$

$$dx \sim \text{Stable}_1(\alpha, \gamma) \quad \Longrightarrow \quad \begin{cases} \lambda(x) \sim \gamma^\alpha \, \dfrac{\Gamma(1+\alpha)\,\sin(\pi\alpha/2)}{\pi} \, |x|^{-(\alpha+1)} \\ \hat{\lambda}(k) = \exp(-\gamma^\alpha |k|^\alpha) \end{cases} . \tag{3.45}$$

The asymptotic relations from above are not violated. The factors A_* correspond to the respective constant factor in the asymptotic expansion of the density (not including the scale factors τ^β or γ^α) and are reciprocal to the constant factors in the transformed asymptotic densities from above.

An alternative route to the fractional diffusion equation is by more general probability densities with only the asymptotic behavior prescribed by

$$\psi(t) \sim C_T^\beta \, \Delta t \, A_\beta \, t^{-(1+\beta)} \qquad \tilde{\psi}(s) \sim 1 - C_T^\beta \, \Delta t \, s^\beta \tag{3.46}$$

$$\lambda(\boldsymbol{x}) \sim C_D^{\alpha/d} \, \Delta t \, A_\alpha \, |\boldsymbol{x}|^{-(d+\alpha)} \qquad \hat{\lambda}(\boldsymbol{k}) \sim 1 - C_D^{\alpha/d} \, \Delta t \, |\boldsymbol{k}|^\alpha \tag{3.47}$$

for $t, |\boldsymbol{x}| \to \infty$ and $s, |\boldsymbol{k}| \to 0$, or – for the usual case – with finite mean and variance presumed. The common scale factor Δt is a practical means for investigating the continuum limit ($\Delta t \to 0$) of both increment distributions. Analogous to Mittag-Leffler and stable densities, the factors A_* shall eliminate the coefficients in the asymptotic expansions of the transformed densities (characteristic functions). We can anticipate that this weaker approach is owed to the properties of Lévy-stable and normal distributions and the generalized and usual central limit theorem in particular.

However, not every continuous time random walk with uncoupled power-law increments simulates a solution of the fractional diffusion equation. It is necessary to impose

the scaling relation [35, 45, 54]

$$C_T^\beta \, \Delta t = C_D^{\alpha/d} \, \Delta t \tag{3.48}$$

such that in the continuum limit of the Fourier-Laplace domain, the master equation (3.38) actually converges to the fundamental solution of the fractional diffusion equation (3.15). For Mittag-Leffler and stable increments, this implies that $\tau = C_T \, \Delta t^{1/\beta}$ and $\gamma = C_D^{1/d} \, \Delta t^{1/\alpha}$.

By identifying the continuum limit of the master equation with the fundamental solution of the fractional diffusion equation, the generalized diffusion constant can be directly linked to the time and space scaling of the increment distributions by

$$C_{\alpha,\beta} = \frac{C_D^{\alpha/d}}{C_T^\beta} = \frac{\gamma^\alpha}{\tau^\beta}. \tag{3.49}$$

A basic example with the scaling relation violated and a vanishing diffusion constant is discussed in [45]. Hence, "a power-law tail in the waiting time [and jump vector] density is not sufficient to guarantee the emergence of the propagator of fractional diffusion in the continuum limit" [45].

3.2.3 Parameterization

For the configuration of a continuous time random walk with Mittag-Leffler type waiting times and Lévy-stable jumps, the parameters α and β as well as the scaling parameters C_D and C_T are required. An additional variable Δt for scaling both scaling parameters simultaneously while leaving their ratio constant was introduced (compare scaling relation). As a consequence Δt allows to control the resolution of sampled trajectories of a continuous time random walk while retaining the analytical properties. It is a logical consequence that in any code that calculates analytical or theoretical results of the continuous time random walk model, the parameter Δt is not required. The scale Δt can be compared with the step size in iterative numerical schemes.

This setup results in the following parameterization of probability distributions in the one and two dimensional case.

$$\psi(t) \sim \begin{cases} \text{MiLeff}(\beta, C_T\,\Delta t^{1/\beta}) & 0 < \beta < 1 \\ \text{Exp}(C_T\,\Delta t) & \beta = 1 \\ C_T\,\Delta t & (*) \end{cases} \tag{3.50}$$

$$\lambda(x) \sim \begin{cases} \text{Normal}(\sqrt{2}\,C_D\,\sqrt{\Delta t}) & \alpha = 2 \\ \text{Cauchy}(C_D\,\Delta t) & \alpha = 1 \\ \text{Stable}(\alpha, C_D\,\Delta t^{1/\alpha}) & \text{else} \end{cases} \tag{3.51}$$

$$\lambda(\boldsymbol{x}) \sim \begin{cases} \text{Normal}_2(\sqrt{2}\,\sqrt{C_D}\,\sqrt{\Delta t}) & \alpha = 2 \\ \text{Cauchy}_2(\sqrt{C_D}\,\Delta t) & \alpha = 1 \\ \text{Stable}_2(\alpha, \sqrt{C_D}\,\Delta t^{1/\alpha}) & \text{else} \end{cases} \tag{3.52}$$

A constant waiting time $(*)$ corresponds to the classical discrete time random walk model. This scenario is compatible (in the sample average) with the exponential case ($\beta = 1$) because the first moment of the exponential waiting time distribution is finite (Poisson process) and corresponds to a constant value waiting time. In Figure 5 simulated trajectories with different configurations of the stable and Mittag-Leffler distribution are shown. A comparison of different waiting time configurations (in terms of the lag between operational and physical time) can be found in Figure 6.

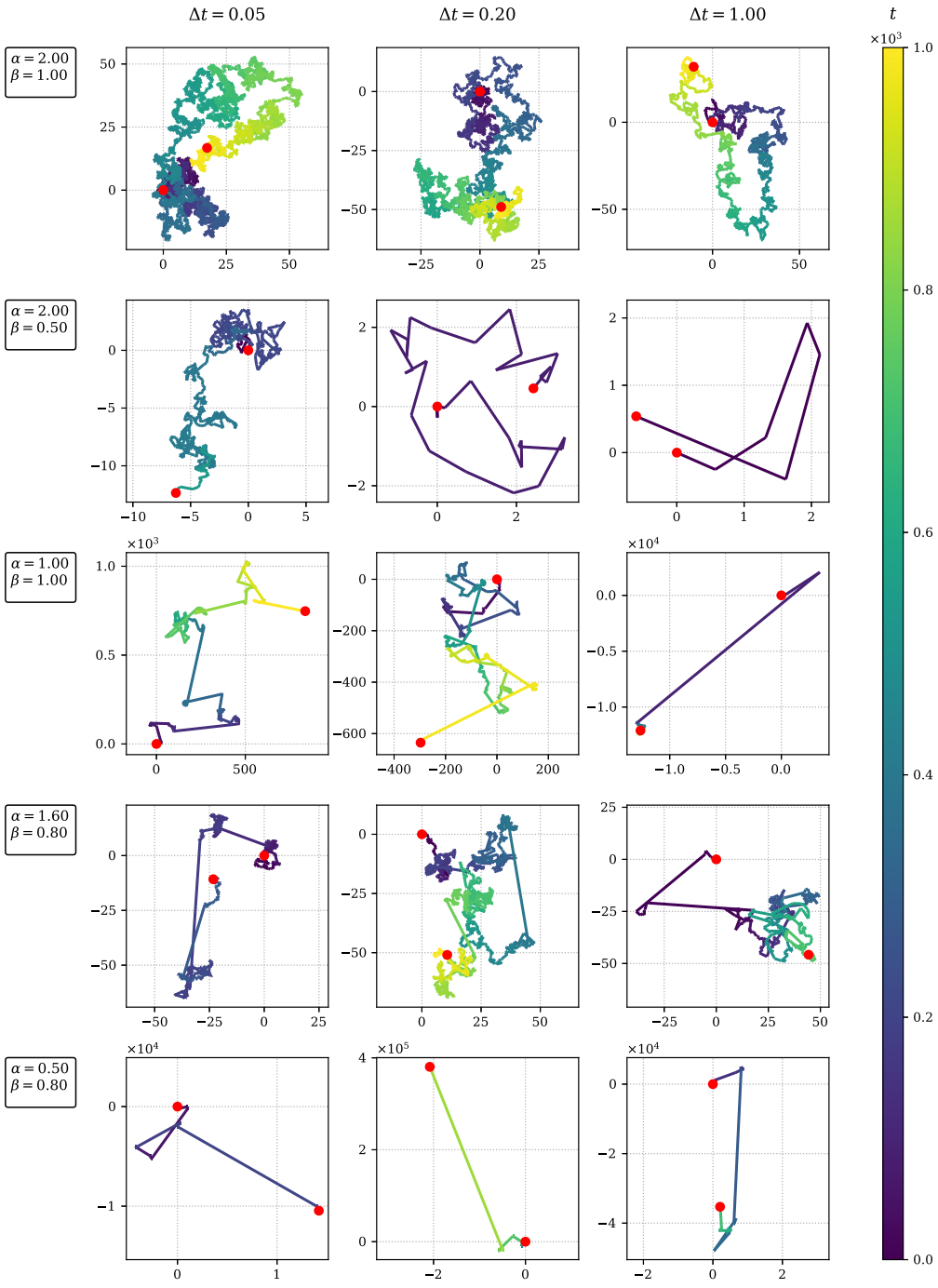

Figure 5: Trajectories of simulated continuous time random walks with different step sizes or scaling Δt and different α and β combinations. The base scaling constants were set to $C_D = C_T = 1$.

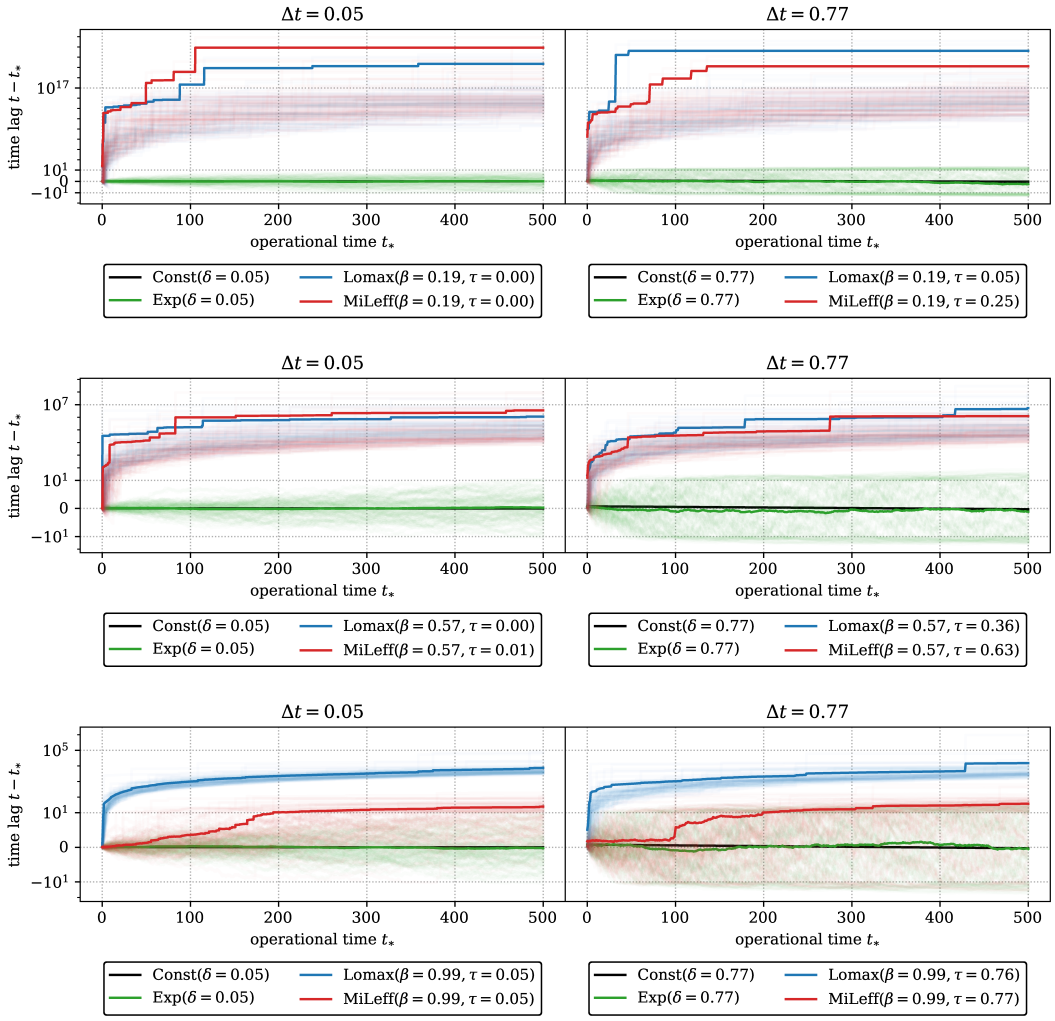

Figure 6: Cumulative sum of sampled waiting times dt (physical time) relative to operational time t_*, which corresponds to the index of a jump in continuous time random walks. The scale of the vertical axis is linear for small values and logarithmic for large values. For each case 100 samples were drawn of which 50 are displayed as transparent lines, the mean is displayed as a thicker solid line. For usual diffusion with constant time steps, physical time and operational time coincide. For small β the Mittag-Leffler distribution has power-law behavior and is thus (asymptotically) similar to the Lomax distribution. For large β the Mittag-Leffler distribution approximates the exponential distribution. The obtained (average) time lag is independent of the step size Δt. In all cases $C_T = 1$.

3.2.4 Subordination and stochastic resetting

If the time and space processes are regarded as separate random walks, the index i implies an additional linear time scale, often referred to as operational time t_*. By setting $t_{*,i} := i\,dt_*$, where usually $dt_* = 1$, the two uncoupled random walks in operational time can be written as

$$t(t_*) = t_{\lfloor t_* \rfloor}, \qquad t(t_{*,i}) = t_i \tag{3.53}$$

$$\boldsymbol{y}(t_*) = \boldsymbol{x}_{\lfloor t_* \rfloor}, \qquad \boldsymbol{y}(t_{*,i}) = \boldsymbol{x}_i. \tag{3.54}$$

In general, from a (space fractional) Markovian random walk $\boldsymbol{y}(t_*)$, a continuous time random walk with memory can be constructed by subordination [37, 64, 88]. Subordinating the random walk to a non-decreasing process $t_*(t)$ yields a new stochastic process

$$\boldsymbol{x}(t) = \boldsymbol{y}\big(t_*(t)\big), \tag{3.55}$$

which is no longer Markovian if the processes $t(t_*)$ and $t_*(t)$ have increments in varying orders of magnitude. The inverse time transformation $t(t_*)$ to physical time, corresponds to the process t_i in the construction of continuous time random walks in Section 3.2.1. Operational time t_* is thus a continuous form of the index i.

The inverse approach to subordination can be understood as the simulation of a continuous time random walk with a discrete time random walk. The number of constant time steps $C_T\,\Delta t$ required for simulating one time increment dt in the continuous time process follows a discrete version of the waiting time distribution. During this random integer number of discrete time increments only one spatial jump is performed. In theory, this approximation requires that $\Delta t \to 0$. An equivalent technical implementation is by stochastic resetting [36], which means that instead of omitting spatial jumps, every step a simulated particle is randomly reset to a certain position from its past trajectory. The number of backward jumps is again determined by a discretization of the waiting time distribution.

3.3 Special properties and quantification

> One can say that there are two essential interrelated problems of the CTRW: (i) the initial preparation of the system, important for all random walk models, and (ii) the weak ergodicity breaking, which is of great interest both from theoretical and empirical points of view. [54]

In contrast to usual diffusion, fractional diffusion allows a much wider range of configurations and exhibits additional phenomena as mentioned above. As a consequence, in addition to the well known mean-square deviation, new measures are required to unambiguously identify or characterize continuous time random walks. In this section a couple of measures for particle trajectories are presented and some special properties of continuous time random walks are discussed.

3.3.1 Memory and initial conditions

The initial condition in the master equation $\Psi(t)\delta(\boldsymbol{x})$ is a spike with mass $\Psi(t) = P(t_1 > t)$ at the origin. In contrast to usual discrete time random walks and especially for power-law waiting times, a particle can remain at the origin for a relatively long period of time depending on the parameter β and the scale τ. This effect can be seen in spatially resolved sample histograms for small times and is demonstrated in [27]. Figure 7 is a reproduction of this demonstration. Figure 8 extends the demonstration to two dimensions. By decreasing the step size Δt, or equivalently by rescaling both distributions, the mass of the spike can be reduced. If the particles of an observed ensemble are not *synchronized* at $t_0 = 0$ but we start our observation of particles already in flight at an arbitrary point in time (and reset their locations to $\boldsymbol{x}_0 = 0$), we also can assume a reduced spike mass. This scenario of non-synchronized or *equilibrated* initial conditions is discussed and formalized in [23]. In general, due to long-memory and infinite-distance effects, the initial conditions in fractional diffusion are more crucial when compared to usual diffusion.

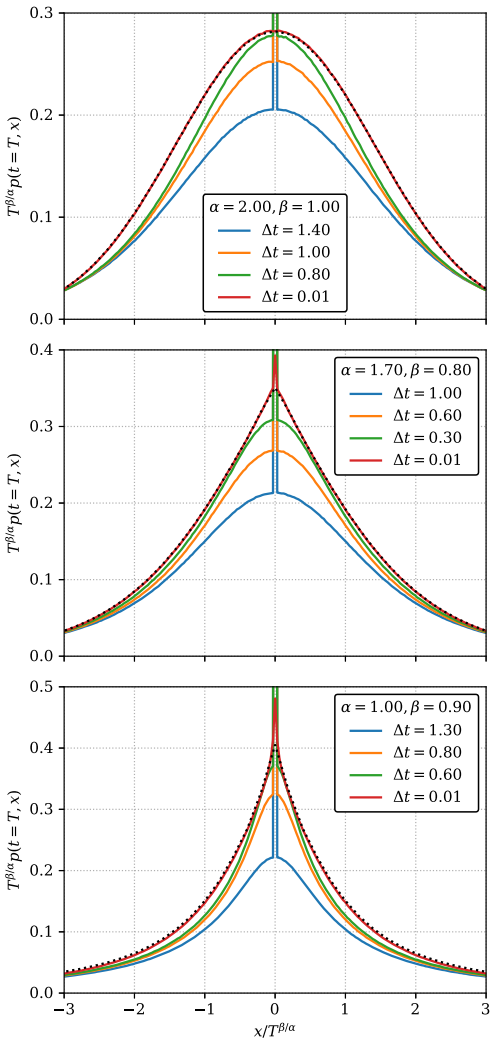

Figure 7: Reproduced results from [27]. Comparison of the one-dimensional scaled fundamental solution $K_{\alpha,\beta}(x\,T^{-\beta/\alpha})$ (dotted line, approximated using FFT) with sample histograms $p(t = T, x)$ of 10^8 particle trajectories at $T = 2.0$. For decreasing time step Δt the central spikes become less pronounced and the histogram approaches the fundamental solution.

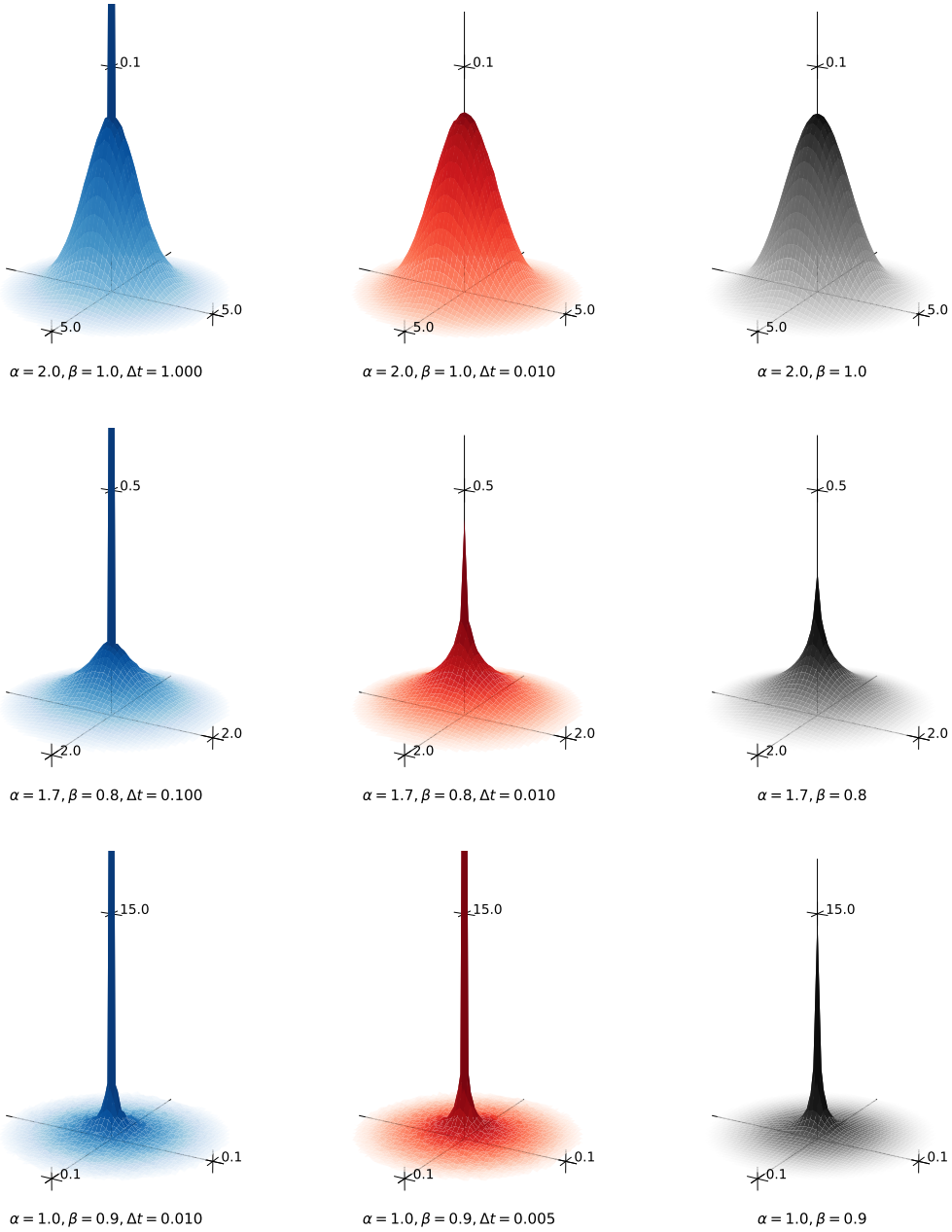

Figure 8: Comparison of the (unscaled) fundamental solution at time $T = 2.0$ (right column, black, calculated as the inverse Fourier transform of the Mittag-Leffler function using FFT) with sample histograms of 10^7 simulated continuous time random walk trajectories at $T = 2.0$ with different step sizes Δt (left and center columns). With smaller step size, the sample histogram approximates the fundamental solution, that is, the spike at the origin diminishes. Note that for a small sample range and large spacing in the FFT, the height of the fundamental solution at the origin can be distorted. Also for the two-dimensional histograms, the bin sizes can influence the height of the center spike.

3.3.2 Ensemble average fractional displacement

From the identification with fractional diffusion we conclude that the fundamental solution represents the sample mean spatial configuration of continuous time random walk particles for a given point in time. A derived feature of continuous time random walk trajectories is the *sample average fractional displacement* measure

$$\left\langle |\boldsymbol{x}(t)|^m \right\rangle = \frac{1}{N} \sum_{n=1}^{N} |\boldsymbol{x}_n(t)|^m = \frac{1}{N} \sum_{n=1}^{N} |\boldsymbol{x}_{n,i(t)}|^m \tag{3.56}$$

where N is the number of observed particles and for $m = 2$ the usual mean square displacement is restored. For large N the m-th fractional central moment of the fundamental solution is approximated, with existence ensured for $m < \alpha/\beta$.

The asymptotic behavior of the fractional moments of the fundamental solution is [66, 85]

$$\mathbb{E}\left[|\boldsymbol{x}(t)|^m\right] = \int_{\mathbb{R}^2} |\boldsymbol{x}|^m \, G(t, \boldsymbol{x}) \, \mathrm{d}\boldsymbol{x} \sim B(\alpha, \beta, m, d) \, (C_{\alpha,\beta} t)^{m\beta/\alpha}. \tag{3.57}$$

Exact calculation of the factor $B(\alpha, \beta, m, d)$ is possible at least in some special cases (usually the one-dimensional case $d = 1$ is discussed in literature). Figure 9 compares the fractional displacement of simulated particles with different configurations and the above theoretical scaling property.

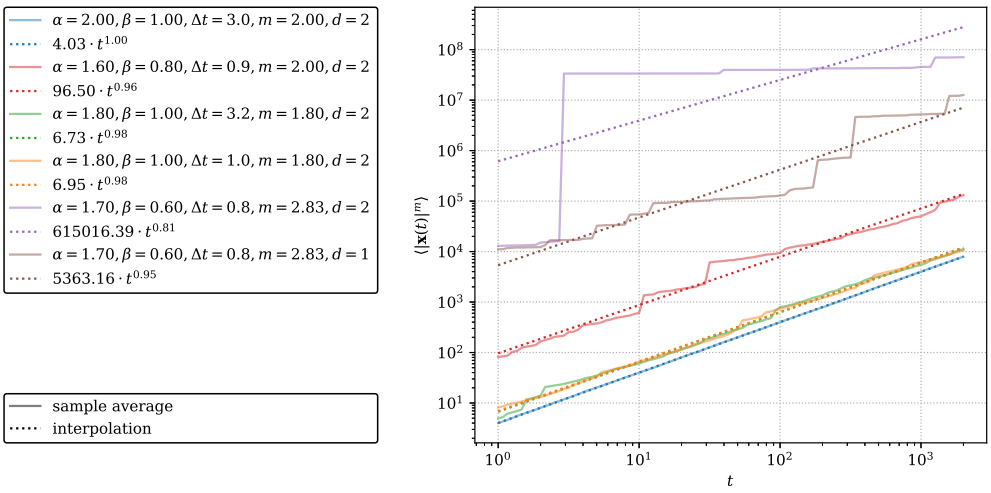

Figure 9: Sample average displacement in different continuous time random walk configurations. Despite the analytical result in (3.57) is valid for $m < \alpha/\beta$, the numerical results usually also hold for $m = \alpha/\beta$. With $m = \alpha/\beta$ the fractional displacement yields a linear slope in logarithmic plots.

3.3.3 Time average fractional displacement

For particles performing usual diffusion, the ergodic hypothesis states that the ensemble and time average configuration are identical given a large enough ensemble and a long enough observation period. The latter is problematic for heavy-tailed waiting times because the observation period is always smaller than the characteristic time scale of the particle dynamics. As a consequence, the time and ensemble average can not coincide and we speak of *weak ergodicity breaking*. For strictly space fractional diffusion this problem does not occur because for finite time scales, the time-average can be calculated on arbitrary spatial scales. To quantify the differences in the strictly time fractional setting, usually the ensemble average mean square displacement is compared with the *time average mean square displacement* [12, 44, 65]. We extend the definition to fractional moments m other than $m = 2$, in order to treat the case of space and time fractional diffusion, and use the term *time average fractional displacement*

$$\overline{\delta^m}(\Delta, T) = \frac{1}{T-\Delta}\int_0^{T-\Delta} \left|d\boldsymbol{x}(t,\Delta)\right|^m \mathrm{d}t \tag{3.58}$$

$$= \frac{1}{T-\Delta}\int_0^{T-\Delta} \left|\boldsymbol{x}(t+\Delta) - \boldsymbol{x}(t)\right|^m \mathrm{d}t \tag{3.59}$$

where Δ should not be confused with the step size parameter Δt.

The time average fractional displacement is some kind of moving average measure and its integrand captures the average spatial displacement during a certain time interval. The occurrence of events in non-synchronized intervals (the left limit of the time intervals does not coincide with event times) is related to the situation of equilibrated or aged initial conditions [23, 44, 65] as discussed above.

For $m = \alpha$ (actually m should be smaller than α but the numerical results usually hold) time-average fractional displacement is expected to behave linearly with the interval length Δ

$$\left\langle \overline{\delta^\alpha}(\Delta, T) \right\rangle \propto \frac{T^{1+\beta} - \Delta^{1+\beta} - (T-\Delta)^{1+\beta}}{T-\Delta} \sim \frac{\Delta}{T^{1-\beta}} \tag{3.60}$$

where the asymptotic behavior is valid for $\Delta \ll T$ or $T \to \infty$ [44, 65]. This result describes what is known as *ageing* effect: "the longer the process goes on the more likely we are to find long trapping times of the order of the measurement time ... T" [44] and with longer trapping times the instantaneous (fractional) diffusivity of the process decreases. The diffusivity must hence be treated as a random variable [12, 44, 65].

When comparing the time and sample average displacement, we let T constant and have

$$\left\langle \overline{\delta^\alpha}(t,T) \right\rangle \sim t\, T^{\beta-1} \tag{3.61}$$

$$\left\langle |\boldsymbol{x}(t)|^\alpha \right\rangle \sim t^\beta \tag{3.62}$$

for $\beta < 1 \wedge t \ll T$. In Figure 10 simulation results from [44, 65] are reproduced in two dimensions. From the vertical offset of the time average fractional displacement of individual trajectories, we can see that $\overline{\delta^\alpha}(\Delta, T)$ is a random variable. Calculation of the coefficient in the predicted sample-mean time average fractional displacement is omitted (compare the situation with sample average fractional displacement), but the linear behavior is reproduced correctly anyways. For comparison, the power-law behavior Δ^β of the sample average fractional displacement is shown in Figure 10.

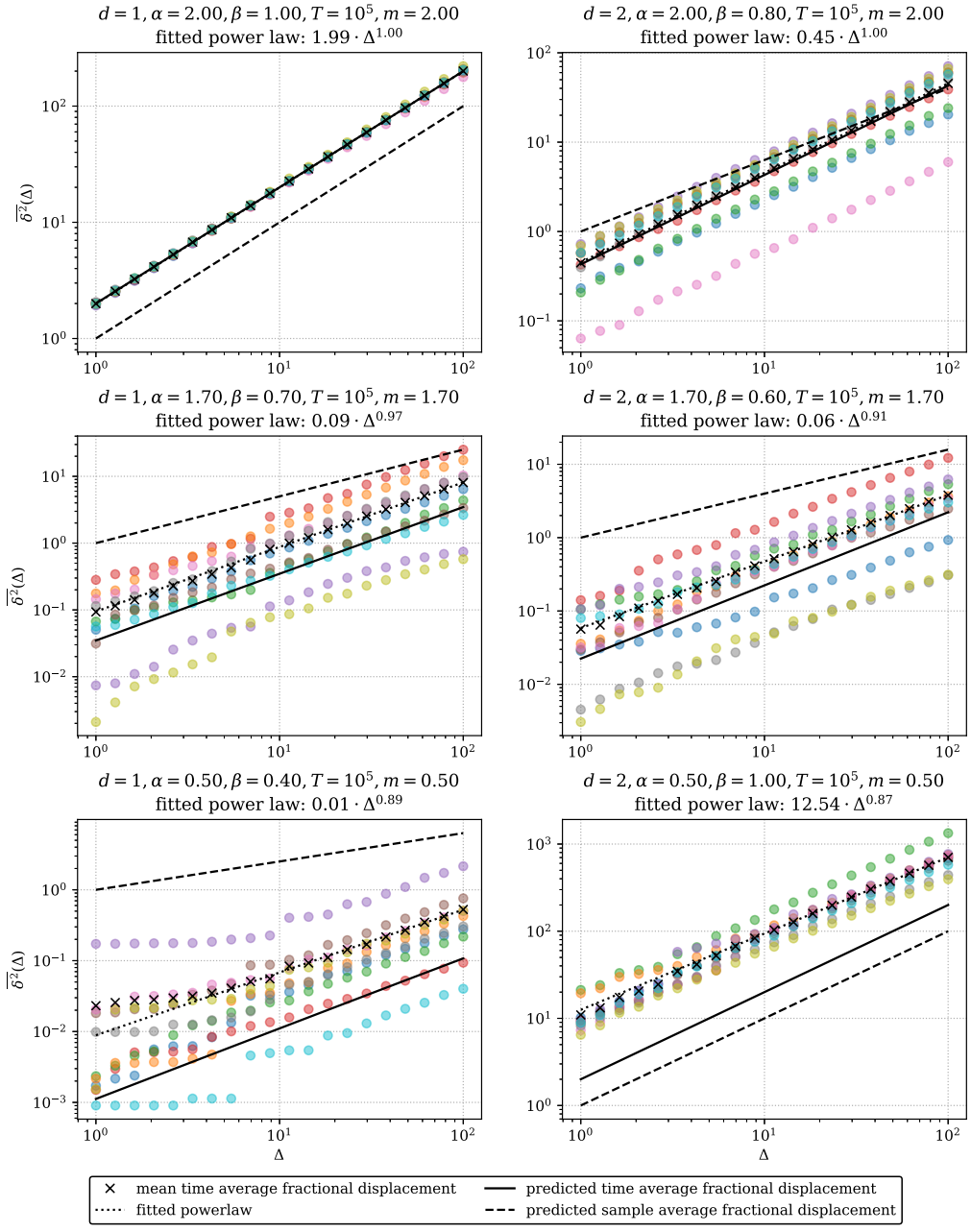

Figure 10: Time average fractional displacement for different continuous time random walk configurations. Similar plots can be found in [44, 65]. For each of the six configurations, where d is the dimension, 10 trajectories were sampled with final time $T = 10^5$. The pointwise mean time average fractional displacement is indicated by cross markers and fitted with a power law as a dotted line. For comparison, the sample average fractional displacement is shown as a dashed line.

3.3.4 Velocity autocorrelation

Another way to characterize continuous time random walks is by *velocity autocorrelation* [106], which quantifies the variation or persistence of the velocity vector in a trajectory over time. The following integral defines normalized velocity autocorrelation in a similar manner as time average fractional displacement,

$$\mathrm{VAC}_1(\Delta, T) = \frac{1}{T-\Delta} \int_0^{T-\Delta} \frac{\boldsymbol{v}(t+\Delta) \cdot \boldsymbol{v}(t)}{|\boldsymbol{v}(t+\Delta)|\,|\boldsymbol{v}(t)|}\,\mathrm{d}t \tag{3.63}$$

For numerical approximation of the velocity autocorrelation of simulated particles, let τ be the integration step such that $T/N = \tau$ for a reasonably large integer N, then

$$\mathrm{VAC}_1(\Delta, T) \approx \frac{\tau}{T-\Delta} \sum_{n=0}^{\lfloor N-\Delta/\tau \rfloor} \frac{\boldsymbol{v}(n\tau+\Delta) \cdot \boldsymbol{v}(n\tau)}{|\boldsymbol{v}(n\tau+\Delta)|\,|\boldsymbol{v}(n\tau)|} \tag{3.64}$$

$$= \frac{\tau}{T-\Delta} \sum_{n=0}^{\lfloor N-\Delta/\tau \rfloor} \frac{d\boldsymbol{x}_{I(n\tau+\Delta)} \cdot d\boldsymbol{x}_{I(n\tau)}}{|d\boldsymbol{x}_{I(n\tau+\Delta)}|\,|d\boldsymbol{x}_{I(n\tau)}|}. \tag{3.65}$$

A similar approximation was also used for calculating the time average displacement of simulated particles. From the moving average form of velocity, a second version of velocity autocorrelation can be constructed,

$$\mathrm{VAC}_2(\Delta, T) = \frac{1}{T-\Delta} \int_0^{T-\Delta} \frac{\boldsymbol{v}(t+\Delta, \Delta) \cdot \boldsymbol{v}(t, \Delta)}{|\boldsymbol{v}(t+\Delta, \Delta)|\,|\boldsymbol{v}(t, \Delta)|}\,\mathrm{d}t. \tag{3.66}$$

Some important features of normalized velocity autocorrelation of continuous time random walks can be recognized in Figure 11:

(i) The autocorrelation in Markovian random walks has a spike at $\Delta = 0$.

(ii) The memory effect of heavy-tailed waiting time distributions leads to more persistent (correlated) velocities. Because waiting times are likely to occur in the same order of magnitude as the observation time T, the velocity autocorrelation decays not before Δ approaches T, also for extremely large simulation times T.

(iii) Continuous time random walks with coupled time and space increments may be fully velocity autocorrelated.

(iv) Non-locality in the spatial jump process has no effect on normalized velocity autocorrelation. Hence, velocity autocorrelation qualifies as a means to determine the memory effect in simulated trajectories irrespective of the spatial jump process.

(v) Velocity autocorrelation is affected by rescaling of the jump and waiting time distributions. Let $\mathrm{VAC}_*^{\Delta t}$ be the velocity autocorrelation of a continuous time random walk with scaling parameter Δt, then

$$\mathrm{VAC}_*^{\Delta t}(\Delta \cdot \Delta t, T \cdot \Delta t) \equiv \mathrm{VAC}_*^{\Delta t=1}(\Delta, T). \tag{3.67}$$

The multiplication of the maximum observation time T is required if $\beta < 1$. An increase of Δt means that fewer jumps with larger distances occur and hence the velocity autocorrelation has a slower decay.

Whereas the first version VAC_1 is problematic if long rests are simulated with 0-length jumps, the second version VAC_2 can average out 0-jump resting states by increasing Δ in $\boldsymbol{v}(t, \Delta)$. As a drawback, the latter requires a larger sample size at large Δ to deliver a smooth curve. For small Δ the first version is sufficient.

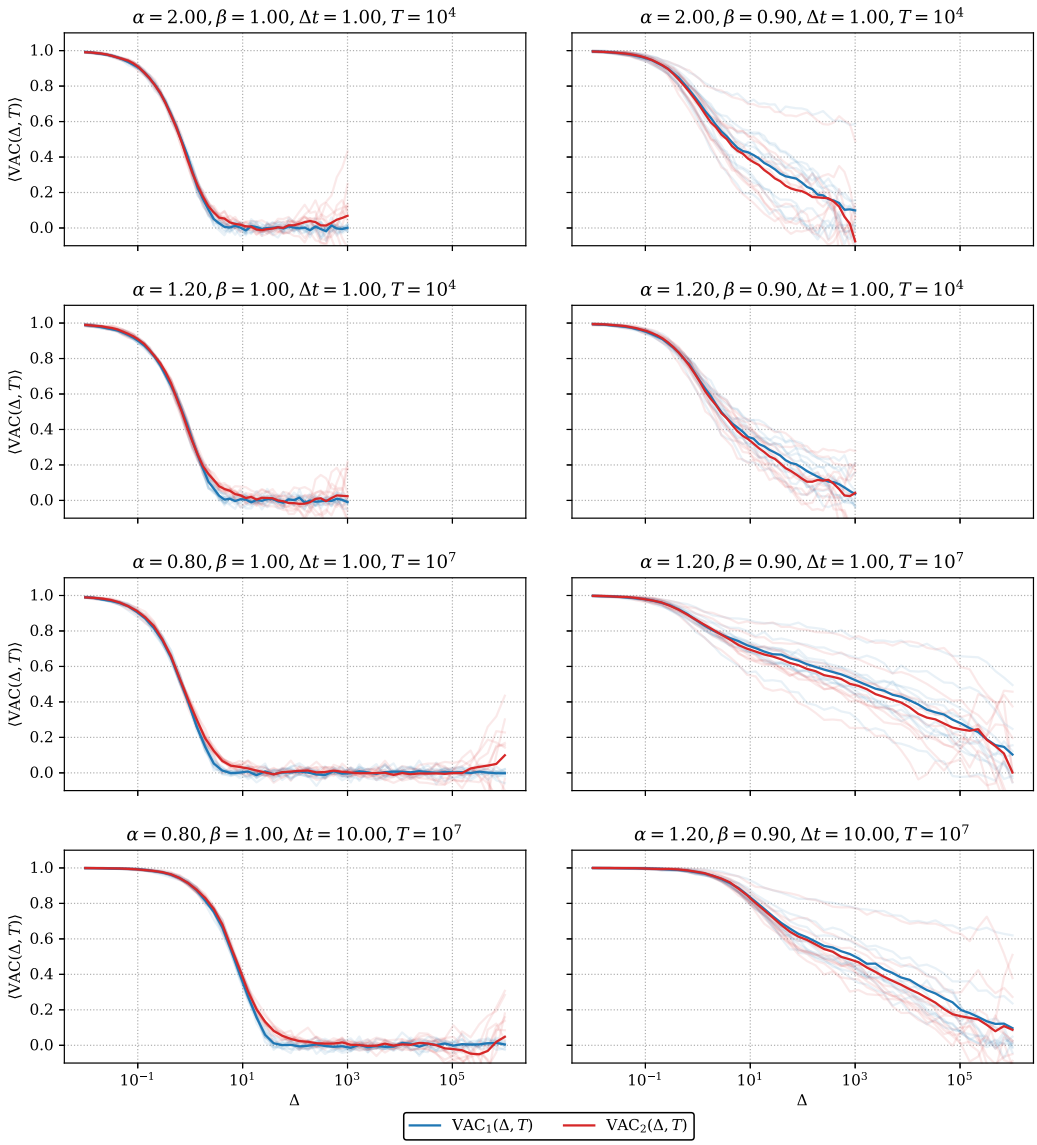

Figure 11: Velocity autocorrelation measured in different continuous time random walk configurations with 10 samples each. The maximum value for Δ is always set to $0.1\,T$. When the measurement distance Δ exceeds the characteristic scale of the memory effect (only possible if $\beta = 1$) or when Δ approaches T, the correlation of (normalized) velocities of a particle decays. The scaling effect can be recognized by comparing the third and fourth row.

3.3.5 Local time

Local time is a concept to capture the sojourn time of a random walk particle in a given location of the domain. The usual formulation of local time is

$$L(t, \boldsymbol{x}) = \int_0^t \delta\big(\boldsymbol{x} - \boldsymbol{x}(\tau)\big)\, \mathrm{d}\tau. \tag{3.68}$$

Because the spatial profile of local time is not smooth, for visualization spatial histograms of the local time are useful for visualization. A related approach for displaying the local time profile is by replacing the delta distribution with Gaussian kernels $\mu(\boldsymbol{x}) \sim \mathrm{Normal}_2(r)$,

$$L_\mu(t, \boldsymbol{x}) = \int_0^t \mu\big(\boldsymbol{x} - \boldsymbol{x}(\tau)\big)\, \mathrm{d}\tau = \sum_{i:t_i \le t} \mu(\boldsymbol{x} - \boldsymbol{x}_i)\, dt_i. \tag{3.69}$$

The scale or dispersion r of the kernel does not depend on the particle dynamics and the residence time dt_i linearly scales the weight of the stencil. For $r = 0$ and $\mu = \delta$, the usual local time is restored. For large t, if the characteristic spatial scale of the particle dynamics outranks the kernel scale r, the distributed measure approximates the usual definition.

The sample average local time $\langle L_\mu(t, \boldsymbol{x})\rangle$ is an approximation of the ensemble-time average spatial particle distribution in continuous time random walks,

$$\mathbb{E}\big[L_\mu(t, \boldsymbol{x})\big] = \int_0^t \int_{\mathbb{R}^2} \mu(\boldsymbol{x} - \boldsymbol{y})\, G(\tau, \boldsymbol{y})\, \mathrm{d}\boldsymbol{y}\, \mathrm{d}\tau \tag{3.70}$$

$$= \int_{\mathbb{R}^2} \mu(\boldsymbol{x} - \boldsymbol{y}) \int_0^t G(\tau, \boldsymbol{y})\, \mathrm{d}\tau\, \mathrm{d}\boldsymbol{y} \tag{3.71}$$

$$\mathbb{E}\big[L_\delta(t, \boldsymbol{x})\big] = \int_0^t G(\tau, \boldsymbol{x})\, \mathrm{d}\tau. \tag{3.72}$$

Hence, the kernel μ can be interpreted as an initial condition of the diffusion equation or as a spatial filter for the usual ensemble average local time.

Moments of the local time profile of a particle can be defined as

$$l_\mu^m(t) = \int_{\mathbb{R}^2} |\boldsymbol{x}|^m \, L_\mu(t, \boldsymbol{x}) \, \mathrm{d}\boldsymbol{x} \tag{3.73}$$

$$= \int_0^t \int_{\mathbb{R}^2} |\boldsymbol{x}|^m \, \mu\big(\boldsymbol{x} - \boldsymbol{x}(\tau)\big) \, \mathrm{d}\boldsymbol{x} \, \mathrm{d}\tau \tag{3.74}$$

$$= \sum_{i: t_i \le t} \int_{\mathbb{R}^2} |\boldsymbol{x}|^m \, \mu\big(\boldsymbol{x} - \boldsymbol{x}_i\big) \, \mathrm{d}\boldsymbol{x} \, dt_i, \tag{3.75}$$

and in the ensemble average correspond to

$$\mathbb{E}\big[l_\mu^m(t)\big] = \int_{\mathbb{R}^2} \underbrace{\int_{\mathbb{R}^2} |\boldsymbol{x}|^m \, \mu(\boldsymbol{x} - \boldsymbol{y}) \, \mathrm{d}\boldsymbol{x}}_{(*)} \int_0^t G(\tau, \boldsymbol{y}) \, \mathrm{d}\tau \, \mathrm{d}\boldsymbol{y}. \tag{3.76}$$

In the standard case ($\mu = \delta$) the integral $(*)$ reduces to $|\boldsymbol{y}|^m$ such that

$$\mathbb{E}\big[l_\delta^m(t)\big] = \int_0^t \int_{\mathbb{R}^2} |\boldsymbol{y}|^m \, G(t, \boldsymbol{y}) \, \mathrm{d}\boldsymbol{y} \, \mathrm{d}\tau = \int_0^t \mathbb{E}\big[|\boldsymbol{x}(\tau)|^m\big] \, \mathrm{d}\tau \tag{3.77}$$

$$\propto \int_0^t \tau^{m\beta/\alpha} \, \mathrm{d}\tau = t^{m\beta/\alpha + 1}. \tag{3.78}$$

If μ is the density of $\mathrm{Normal}_2(r)$, then $(*) = \mathbb{E}\big[|\boldsymbol{Z}|^m\big]$ for a random variable $\boldsymbol{Z} \sim \mathrm{Normal}_2(r)$ centered around the location $\boldsymbol{y}$, which leads to a formulation containing confluent hypergeometric functions.

In Figure 12 spatial profiles of the sample average local time $\big\langle L_\delta(t, \boldsymbol{x}) \big\rangle$ in different continuous time random walk configurations, a diametral section of the spatial profile, the radial profile and spatial moments $\big\langle l_\delta^m(t) \big\rangle$ are presented. To obtain the distributed local time profile (not shown in the figures), a Gaussian filter can be applied on the usual local time profile according to (3.71). The fractional moments of distributed local time can be obtained from a stochastic integration approach based on (3.75).

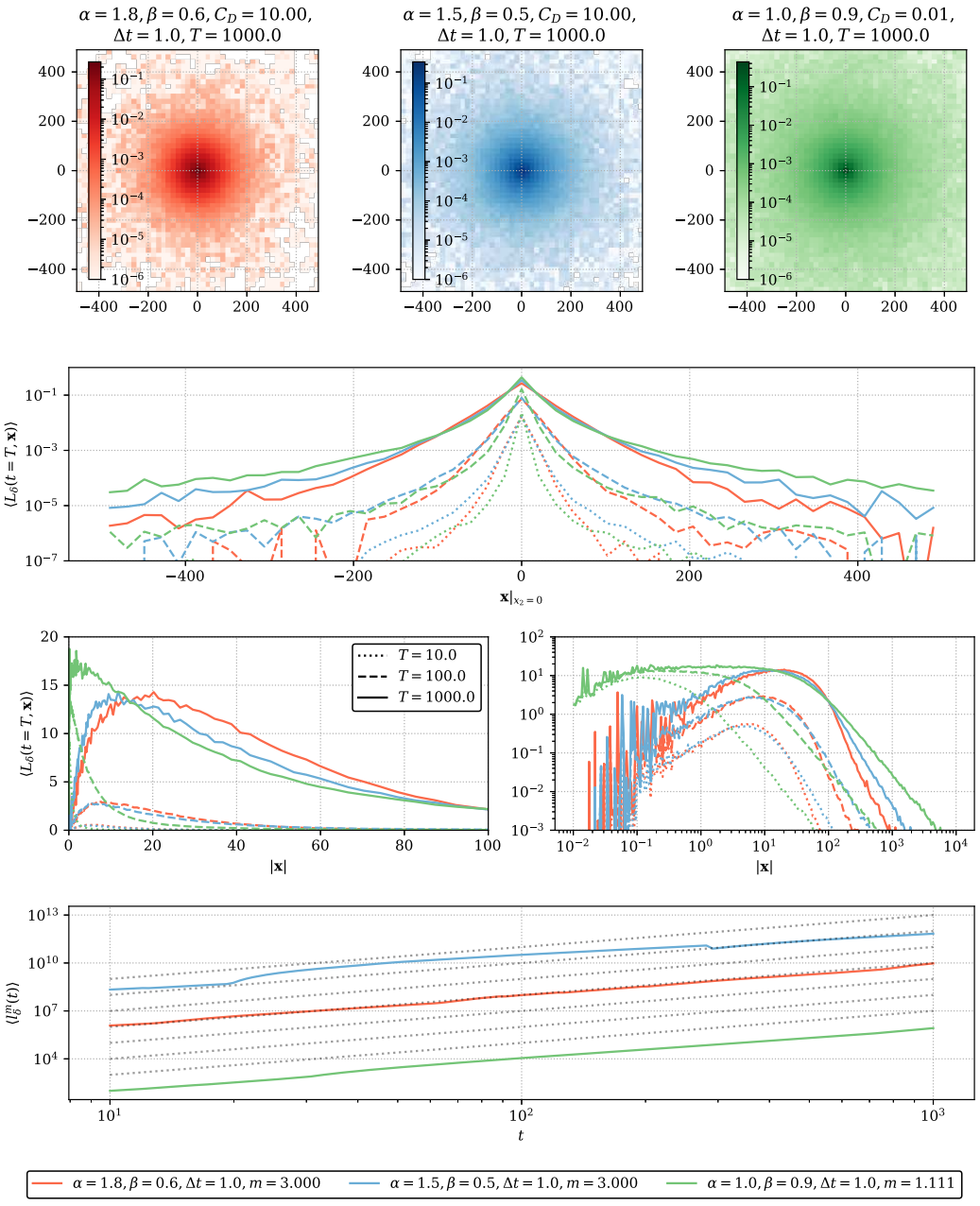

Figure 12: Top row: Spatial local time profiles $\langle L_\delta(t = 10^3, \boldsymbol{x}) \rangle$ of trajectory ensembles (10^5 samples) of different continuous time random walk configurations (color coded). Second and third row: Corresponding diametral sections of the spatial time profile $\langle L_\delta(t = T, \boldsymbol{x}) \rangle|_{x_2=0}$ and radial local time profile for $T = 10, 100, 1\,000$. Last row: Spatial moments $\langle l_\delta^m(t) \rangle$. The exponents in the spatial moments were set to $m = \alpha/\beta$ such that the result from (3.78) can be recognized. The dotted lines indicate the expected quadratic law t^2.

3.4 A proof-of-concept programming library

The construction and parameterization of continuous time random walks, the according probability distributions and function evaluations and the statistical methods presented in this chapter were implemented in an open-source Python programming library [92]. The library is structured into submodules that implement probability distributions, integral transforms and stochastic processes.

3.4.1 Probability distributions and integral transforms

The two central probability distributions are the Mittag-Leffler distributions (Section 2.4.2) for sampling power-law waiting times and bivariate isotropic Lévy-stable distributions (Section 2.5.4) for generating spatial increments with algebraic tails. Existing algorithms and implementations for the evaluation of the Mittag-Leffler function [29, 30, 31, 34, 46] and univariate Lévy-stable densities [5, 68, 74, 82, 96] were incorporated into the software. The definitions in [73, 101] were used to implement bivariate Lévy-stable probability distributions as transformations of the univariate case.

Different approaches for the Fourier transform of functions with two-dimensional domain were implemented. If equally spaced sample points of a function are available, highly optimized FFT algorithms can be used to calculate transformed function values on a discrete lattice. For pointwise or functional evaluation of the two-dimensional Fourier transform, direct calculation of the Hankel transform formula by specialized numerical quadrature routines [70] is provided. Included inverse Laplace transform routines rely on algorithms in high precision arithmetic [69].

3.4.2 Stochastic processes

Continuous time random walks are implemented according to the definition in Section 3.2.1. Program routines for the correct parameterization (Section 3.2.3) of the Mittag-Leffler and the Lévy-stable distribution are provided in the stochastic processes submodule. The input arguments are the stability parameter α, the memory parameter β, the time and diffusion constants C_T and C_D as well as a scaling parameter Δt

that can be used to determine the resolution of simulated trajectories by rescaling both constants simultaneously.

The module implements the statistical measures and approaches from Section 3.3 for analyzing and quantifying ensembles of generated particle trajectories. This includes velocity autocorrelation, sample average fractional displacement, time average fractional displacement, and the calculation of radial moments of the empirical distribution and the local time profile. If available, analytical results such as the coefficients of certain power laws are also included in the library. This allows to compare and validate ensembles of sampled trajectories with expected theoretical behavior.

For validating spatial sample histograms at given points in time against the fundamental solution in two dimensions, the following technical approaches were implemented for calculating function values of the fundamental solution (Section 3.1.3):

(i) From the solution of the fractional diffusion equation in the frequency domain (3.19), we can approximate the fundamental solution using two-dimensional inverse Fourier transform. A generous choice for the number of sample points and their range in the frequency domain ensures the accuracy of the result. Because of the symmetries in the Fourier transform, evaluation of the Mittag-Leffler function can be reduced to one half of a quadrant. This approach requires some parameter transformations and careful alignment of the sample points, but is very efficient if evaluations on a regular lattice are required.

(ii) For pointwise evaluation, the symmetry of the fundamental solution (in the frequency domain) allows to calculate the inverse two-dimensional Fourier transform using the numerical Hankel transform.

(iii) In case of strictly time fractional diffusion ($\alpha = 2$), the fundamental solution can be evaluated by numerical inverse Laplace transform according to (3.25).

(iv) In the strictly space fractional case ($\beta = 1$) the fundamental solution can be modeled with Lévy-stable densities.

(v) Direct numerical quadrature of the Mellin-Barnes integrals in Fox-H functions (Section 2.1.4) according to (3.27) was not implemented, but could be a future addition.

Visual demonstrations of the presented validation approaches are provided in testing routines, which also serve as code examples for the application of the library. The code, however, is not optimized and should be regarded as an accessible proof-of-concept implementation. Some of the figures in this thesis can be reproduced with the provided testing routines. The library allows to use user-provided temporal and spatial increment distributions aside from the Mittag-Leffler and Lévy-stable distributions for generating random walk trajectories. This functionality and the quantification methods were used in Section 4.4 for the construction of random walks on topological structures and for the numerical evaluation of the presented theory.

4 Fractional diffusion in topological models

This chapter starts with the formalization of heterogeneous structures on two-dimensional domains in terms of *block models* (Section 4.1). Blocks represent local clusters of entities or aggregations of density, such that their locations on the domain and their shape imply a heterogeneous density profile. In according heterogeneous dynamical systems, spatial interaction is assumed to be stronger within blocks (intra-block) than between different blocks (inter-block). Hence, the concept of blocks refers to two essentially distinct concepts; spatial proximity and elevated interaction.

In hierarchical and fractal progressions of the block model (Section 4.2) more complex forms of persistent and volatile topological structures are possible. Stochastic formulations of interaction processes, that are determined by the block structure, lead to topological random walks. The random walks induced by the block models are then linked to continuous time random walks and fractional diffusion by identifying the asymptotic spatial increment distributions in both models (Section 4.3). An empirical evaluation shows that simulated topological trajectories have the same characteristics as sampled continuous time random walks and approximate the corresponding fractional diffusion equation (Section 4.4).

4.1 A basic block model

Let $\Omega = [0, \omega) \times [0, \omega)$ be a bounded spatial domain with periodic boundary conditions. The area or size of the domain is $|\Omega| = \omega^2$. The classical distance metric translates to the distance measure

$$d_{\text{per}}(\boldsymbol{x}, \boldsymbol{y}) = \sqrt{\left(d_1 - \left[\frac{d_1}{\omega}\right] \omega\right)^2 + \left(d_2 - \left[\frac{d_2}{\omega}\right] \omega\right)^2} \leq d(\boldsymbol{x}, \boldsymbol{y}) \tag{4.1}$$

where $d_1 = |y_1 - x_1|$, $d_2 = |y_2 - x_2|$ and $[\,\cdot\,]$ denotes the nearest integer operation. For convenience we replace the standard notation and set $|\boldsymbol{y} - \boldsymbol{x}| = d_{\text{per}}(\boldsymbol{x}, \boldsymbol{y})$ without further notice. If $\Omega = \mathbb{R}^2$, the usual definitions apply.

4.1.1 Block structure

On a periodic domain Ω, define a finite set of blocks B where each block $b \in B$ has a center location $\boldsymbol{x}_b$, distributed uniformly in Ω, a weight w_b and a spatial (bivariate and usually isotropic) membership distribution. We introduce the term *membership likelihood* for the density function $m_b(\boldsymbol{x})$ of the membership distribution. The weighted membership likelihood $w_b\, m_b(\boldsymbol{x})$ associates a certain part of the (population) density on Ω with a block $b \in B$.

From the periodicity of Ω it follows that $\int_\Omega m_b(\boldsymbol{x})\,\mathrm{d}\boldsymbol{x} = 1$ and as a consequence the total population is quantified by $\sum_{b\in B} w_b$. If the membership likelihood is isotropic, $m_b(\boldsymbol{x}) = m_b(|\boldsymbol{x} - \boldsymbol{x}_b|)$, and if all blocks have the same membership distribution (i.e. geometric shape), $m_b(\boldsymbol{x}) = m(|\boldsymbol{x} - \boldsymbol{x}_b|)$. Since clusters or blocks are assumed to be finite locally confined aggregations of the population, it is necessary that the membership likelihoods have finite moments. Henceforth, let the membership distributions be bivariate normal distributions, or equivalently, let the membership likelihoods $m_b(\boldsymbol{x})$ be Gaussian densities. We refer to this topological configuration as the (single-layered) *block model*.

In a discrete instantiation of the block model, each block shall be associated with a finite number of members or entities. The number of members is determined by the block weight and their locations are distributed around the block center according to the membership distribution. As a consequence, the locations $\boldsymbol{x}$ of the members of block b can be formalized as random variables

$$\boldsymbol{x} \overset{d}{=} \boldsymbol{x}_b + \boldsymbol{X}_b, \tag{4.2}$$

where $\boldsymbol{X}_b \sim \mathrm{Normal}_2(\sigma_b)$ with σ_b being the *block dispersion*.

4.1.2 Population density

Define the population density on Ω as

$$\rho(\boldsymbol{x}) = \sum_{b \in B} w_b \, m_b(\boldsymbol{x}). \tag{4.3}$$

From the random positioning of the blocks, it follows that the population density is inhomogeneous. However, if the block dispersion is significantly greater than the domain size, or especially if $\sigma_b \to \infty$, the resulting population is distributed uniformly on Ω. Accordingly, the dispersion of blocks (scale of the membership likelihood) is always assumed to be smaller than the domain size $\sigma_b < \omega$. Also if the number of blocks $|B|$ is very large, a homogeneous population density is approached.

The following calculations establish a relation between the number of blocks, block weight and average population density. Assume that the number of blocks $|B|$ is a random variable controlled by the block density β in units of blocks per area such that $\mathbb{E}[|B|] = \beta \, |\Omega|$. The block weights w_b are also random variables and they represent the amount of population associated with each block. If $\overline{\rho}$ is the average population density, then

$$\mathbb{E}[w_b] \, \mathbb{E}[|B|] = \mathbb{E}[w_b] \, \beta \, |\Omega| = \overline{\rho} \, |\Omega| \qquad \Longrightarrow \qquad \mathbb{E}[w_b] = \frac{\overline{\rho}}{\beta}. \tag{4.4}$$

Even though the generative block model associates a fixed local fraction of the population (proportional to the block weight and distributed with the membership likelihood) with each block, the superposition of membership likelihoods can be used to retrospectively and stochastically associate a given location with a block. For a given location $\boldsymbol{x}$ the association to block b can be expressed as

$$P(b|\boldsymbol{x}) = \frac{w_b m_b(\boldsymbol{x})}{\sum_{b' \in B} w_{b'} m_{b'}(\boldsymbol{x})} = \frac{w_b m_b(\boldsymbol{x})}{\rho(\boldsymbol{x})}. \tag{4.5}$$

This association corresponds to the idea of Gaussian mixture models (GMM) which are used in Figure 13 to infer the (latent) block structure from a sampled discrete population.

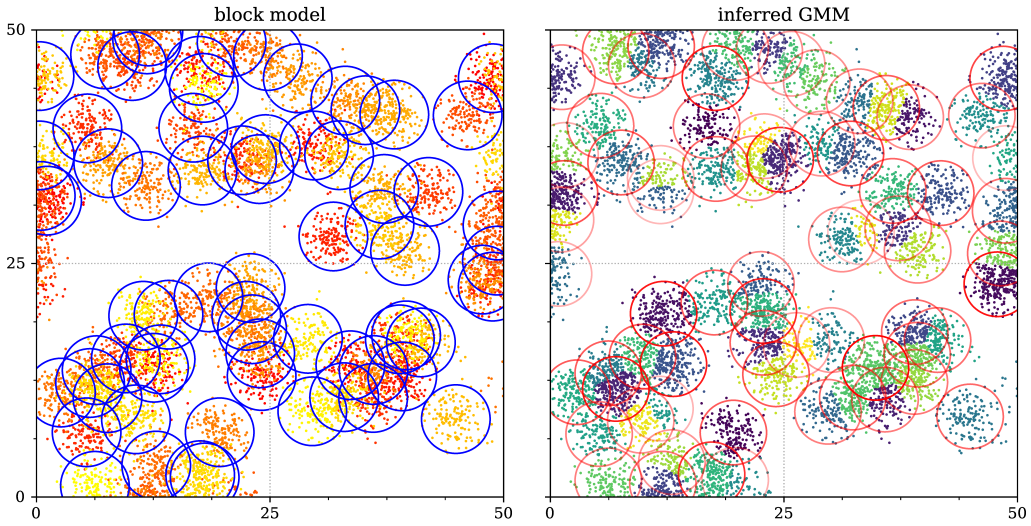

Figure 13: Inference of the topological structure of a previously sampled discrete population (70 blocks, 10.000 entities) with a Gaussian mixture model. The circles represent blocks with their area corresponding to the 95% confidence ellipse of the block membership distribution or the inferred components respectively. In the block model all blocks are weighted equally, the transparency of the red circles in the visualization of the GMM encodes the estimated relative component weight. The inferred block (center) locations and block weights can be reproduced rather accurately. Periodic boundary conditions are however not taken into account by the GMM.

4.1.3 Connectivity and interaction concepts

Independently of the topological block structure, a spatial *interaction likelihood* $\lambda(\boldsymbol{x}, \boldsymbol{y})$ can be introduced. These interaction kernels are assumed to be isotropic such that $\lambda(\boldsymbol{x}, \boldsymbol{y}) = \lambda(\boldsymbol{x}-\boldsymbol{y}) = \lambda(|\boldsymbol{x}-\boldsymbol{y}|)$. Again, bivariate isotropic probability density functions can be used to model the likelihood function. The characteristic length (scale) of interaction should however be significantly greater than the dispersion (scale) of blocks.

From the isotropic interaction likelihood we derive the *interaction potential* as

$$\kappa(\boldsymbol{x},\boldsymbol{y}) = \lambda(\boldsymbol{x},\boldsymbol{y})\,\rho(\boldsymbol{y}) \tag{4.6}$$

$$= \lambda(\boldsymbol{x},\boldsymbol{y}) \sum_{b\in B} w_b\, m_b(\boldsymbol{y}). \tag{4.7}$$

The aggregated or global interaction potential in $\boldsymbol{x}$ is given by

$$\kappa(\boldsymbol{x}) = \int_\Omega \lambda(\boldsymbol{x},\boldsymbol{y})\,\rho(\boldsymbol{y})\,\mathrm{d}\boldsymbol{y} \tag{4.8}$$

$$= \sum_{b\in B} w_b \int_\Omega \lambda(\boldsymbol{x},\boldsymbol{y})\, m_b(\boldsymbol{y})\,\mathrm{d}\boldsymbol{y}. \tag{4.9}$$

Because in both expressions, a potential left-hand factor $\rho(\boldsymbol{x})$ is absent, the interaction potential is independent of the population density in $\boldsymbol{x}$.

Above formulation of the interaction potential can be approximated by replacing the positions $\boldsymbol{x}$ and $\boldsymbol{y}$ with the centers of the nearest blocks or with a mixture of nearby block centers based on (4.5). The following variants of this approach are possible:

$$\kappa_L(\boldsymbol{x},\boldsymbol{y}) = \kappa(\boldsymbol{x},\boldsymbol{y}), \tag{4.10}$$

$$\kappa_{BL}(\boldsymbol{x},\boldsymbol{y}) = \sum_{b\in B} \frac{w_b m_b(\boldsymbol{x})}{\sum_{b'\in B} w_{b'} m_{b'}(\boldsymbol{x})} \lambda(\boldsymbol{x}_b,\boldsymbol{y})\rho(\boldsymbol{y}), \tag{4.11}$$

$$\kappa_{LB}(\boldsymbol{x},\boldsymbol{y}) = \sum_{b\in B} \lambda(\boldsymbol{x},\boldsymbol{x}_b) w_b m_b(\boldsymbol{y}), \tag{4.12}$$

$$\kappa_{BLB}(\boldsymbol{x},\boldsymbol{y}) = \sum_{b\in B}\sum_{b'\in B} \frac{w_b m_b(\boldsymbol{x})}{\sum_{b''\in B} w_{b''} m_{b''}(\boldsymbol{x})} \lambda(\boldsymbol{x}_b,\boldsymbol{x}_{b'}) w_{b'} m_{b'}(\boldsymbol{y}). \tag{4.13}$$

These approximations are valid because $m_b(\boldsymbol{x})$ is significantly greater than zero only if $\boldsymbol{x}$ is close to the block center $\boldsymbol{x}_b$. In this case $\lambda(\boldsymbol{x},\boldsymbol{y}) \approx \lambda(\boldsymbol{x}_b,\boldsymbol{y})$ because the characteristic scale of the interaction likelihood λ is significantly greater than the characteristic scale of the membership likelihood m. In (LB) and (BLB) the factor $\rho(\boldsymbol{y})$ is eliminated by the normalization of the block membership in $\boldsymbol{y}$.

4.1.4 Random walks

For simulating random jumps on the domain regard the normalized jump distributions of the form $P(\boldsymbol{x} \to \boldsymbol{y}) = \kappa(\boldsymbol{x}, \boldsymbol{y})/\kappa(\boldsymbol{x})$,

$$P_L(\boldsymbol{x} \to \boldsymbol{y}) = \frac{\lambda(\boldsymbol{x}, \boldsymbol{y})\rho(\boldsymbol{y})}{\int_\Omega \lambda(\boldsymbol{x}, \boldsymbol{y}')\rho(\boldsymbol{y}')\,\mathrm{d}\boldsymbol{y}'}, \tag{4.14}$$

$$P_{BL}(\boldsymbol{x} \to \boldsymbol{y}) = \sum_{b \in B} \underbrace{\frac{w_b m_b(\boldsymbol{x})}{\sum_{b' \in B} w_{b'} m_{b'}(\boldsymbol{x})}}_{P(b|\boldsymbol{x})} \underbrace{\frac{\lambda(\boldsymbol{x}_b, \boldsymbol{y})\rho(\boldsymbol{y})}{\int_\Omega \lambda(\boldsymbol{x}_b, \boldsymbol{y}')\rho(\boldsymbol{y}')\,\mathrm{d}\boldsymbol{y}'}}_{P(b \to \boldsymbol{y})}, \tag{4.15}$$

$$P_{LB}(\boldsymbol{x} \to \boldsymbol{y}) = \sum_{b \in B} \underbrace{\frac{\lambda(\boldsymbol{x}, \boldsymbol{x}_b) w_b}{\sum_{b' \in B} \lambda(\boldsymbol{x}, \boldsymbol{x}_{b'}) w_{b'}}}_{P(\boldsymbol{x} \to b)} \underbrace{\frac{m_b(\boldsymbol{y})}{1}}_{P(\boldsymbol{y}|b)}, \tag{4.16}$$

$$P_{BLB}(\boldsymbol{x} \to \boldsymbol{y}) = \sum_{b \in B} \sum_{b' \in B} \underbrace{\frac{w_b m_b(\boldsymbol{x})}{\sum_{b'' \in B} w_{b''} m_{b''}(\boldsymbol{x})}}_{P(b|\boldsymbol{x})} \underbrace{\frac{\lambda(\boldsymbol{x}_b, \boldsymbol{x}_{b'}) w_{b'}}{\sum_{b'' \in B} \lambda(\boldsymbol{x}_b, \boldsymbol{x}_{b''}) w_{b''}}}_{P(b \to b')} \underbrace{\frac{m_{b'}(\boldsymbol{y})}{1}}_{P(\boldsymbol{y}|b')}. \tag{4.17}$$

For sampling jumps, the approximations (LB) and (BLB) are useful because they are composed of discrete distributions and only contain the membership likelihood as a continuous distribution. The membership likelihood is however modeled as a normal distribution and random values can be generated easily. In particular the approximation (BLB) is an implementation of the block model. Note that a left-side factor $\rho(\boldsymbol{x})$ would be eliminated when normalizing the jump distributions.

4.2 Hierarchical and fractal block models

The flat block model from Section 4.1 can be extended by grouping blocks into higher level blocks such that a hierarchical block structure emerges and a single highest level block contains all other blocks. Also higher level blocks may be equipped with weights and membership likelihoods. We make the convention that the weight of a parent block is partitioned among child blocks. Consequently, the sum of all weights in each level is equal to the weight of the highest level block. In order to spatially integrate lower level blocks into higher level blocks, assume that child blocks are located according to the spatial membership likelihood of their parent and that their size or dispersion is smaller by a certain factor. This means that the dispersion of the membership likelihood scales with the block level. A similar scaling property applies to the block weights only if the number of children is a fixed constant and the weights are distributed equally among the child blocks of a parent block.

4.2.1 Indexing

Let B_0 be the set of all 0-level blocks. We make the assumption that only 0-level blocks may directly contain population entities. The blocks in the l-th level B_l only contain $(l-1)$-level blocks directly. If the number of block layers is $L+1$, the single upper most L-level block is the parent of all other blocks. To indicate the L-level proto block, we write $b_{(0)}$. If the proto block contains $n+1$ sub-blocks, we can indicate all level $L-1$ blocks by $b_{(0,0)}, b_{(0,1)}, \ldots, b_{(0,n)}$. The child blocks of $b_{(0,i)}$, where $0 \leq i \leq n$, are named $b_{(0,i,0)}, b_{(0,i,1)}, b_{(0,i,2)}, \ldots$ and belong to level $L-2$. For 0-level blocks this yields the notation $b_{(0,i_{L-1},i_{L-2},\ldots,i_0)}$. A l-level block can be written as $b_{(0,i_{L-1},\ldots,i_{l+1},i_l)}$. This notational convention implies the following semi-order on multiindices with varying

dimensions.

$$(0, i_{L-1}, \ldots, i_k, \ldots, i_l) \prec (0, i_{L-1}, \ldots, i_k) \qquad k > l \tag{4.18}$$

$$(0, i_{L-1}, \ldots, i_k, \ldots, i_l) \not\prec (0, i_{L-1}, \ldots, j_k) \qquad k > l, j_k \neq i_k \tag{4.19}$$

$$(0, i_{L-1}, \ldots, i_l) \simeq (0, i_{L-1}, \ldots, j_l) \qquad j_l \neq i_l \tag{4.20}$$

We also use the short notation $b_i = b_{(0,i_{L-1},\ldots,i_0)}$ and $b_j = b_{(0,j_{L-1},\ldots,j_0)}$. The same indexing can also be used for block weights $w_i = w_{(0,i_{L-1},\ldots,i_0)}$ and center locations $\boldsymbol{x}_i = \boldsymbol{x}_{(0,i_{L-1},\ldots,i_0)}$. Because block weights satisfy the partition property,

$$w_{(0,i_{L-1},\ldots,i_l)} = \sum_{k_{l+1}} w_{(0,i_{L-1},\ldots,i_l,k_{l+1})}. \tag{4.21}$$

4.2.2 Topological connectivity

The hierarchical layout permits to implement a connectivity measure without resorting to spatial interaction likelihoods. Let $P(l = 0)$ be the probability for intra-block interaction, that is the probability that a member of a certain 0-level block interacts with another member of the same 0-level block. Accordingly, $P(b_i \to b_i) = P(l = 0)$. In general, let $P(l)$ be the probability that interaction happens between entities with their lowest level common parent being of level l. We can write

$$P(b_i \to b_j) = \sum_{l=0}^{L} P(b_i \to b_j | l)\, P(l) \tag{4.22}$$

where $P(b_i \to b_j|l)$ is always 0 if the lowest level common parent of b_i and b_j is not a level l block. In other words, $P(b_i \to b_j|l) > 0$ if and only if

$$i = (i_L, i_{L-1}, \ldots, i_{l+1}, i_l, i_{l-1}, i_{l-2}, \ldots, i_0) \tag{4.23}$$

$$j = (i_L, i_{L-1}, \ldots, i_{l+1}, i_l, j_{l-1}, j_{l-2}, \ldots, j_0) \qquad j_{l-1} \neq i_{l-1}. \tag{4.24}$$

This also means that each pair of 0-level blocks (b_i, b_j) is connected in exactly one specific lowest level $l = \text{parent}(b_i, b_j)$. The common parent block level is also a distance measure in the widest sense.

In order to sample inter-block interactions, for a given block b_i and a given connection level l, a 0-level block b_j must be picked from the l-level parent of b_i excluding all sub-blocks of the $l-1$-level parent of b_i. The exclusion of $b_{(i_L,\dots,i_l,i_{l-1})}$ is necessary because the parameter l was defined to determine the *lowest* common level. Using the same indices as above and taking into account the hierarchical setup of weights, we find for $l > 0$

$$P(b_i \to b_j|l) = \frac{w_{(i_L,\dots,i_l,j_{l-1})}}{\sum_{k_{l-1}\neq i_{l-1}} w_{(i_L,\dots,i_l,k_{l-1})}} \cdot \frac{w_{(i_L,\dots,i_l,j_{l-1},j_{l-2})}}{\sum_{k_{l-2}} w_{(i_L,\dots,i_l,j_{l-1},k_{l-2})}} \cdots \tag{4.25}$$

$$\cdots \frac{w_{(i_L,\dots,i_l,j_{l-1},\dots,j_1,j_0)}}{\sum_{k_0} w_{(i_L,\dots,i_l,j_{l-1},\dots,j_1,k_0)}} \tag{4.26}$$

$$= \frac{w_{(j_L,\dots,j_l,j_{l-1})}}{w_{(j_L,\dots,j_l)} - w_{(i_L,\dots,i_l,i_{l-1})}} \cdot \prod_{k=0}^{l-2} \frac{w_{(j_L,\dots,j_{k+1},j_k)}}{w_{(j_L,\dots,j_{k+1})}} \tag{4.27}$$

$$= \frac{w_{(j_L,\dots,j_0)}}{w_{(j_L,\dots,j_l)} - w_{(i_L,\dots,i_l,i_{l-1})}}. \tag{4.28}$$

A possible choice for $P(l)$ is the geometric distribution $\text{Geom}(p)$ with probability mass function $p\,(1-p)^l$ such that p is the probability for intra-block connections and $1-p$ is the probability to step up one level in the connection process. Values above L must be clipped, such that effectively a truncated geometric distribution $\text{Geom}(p, L)$ is obtained. The resulting formula for $P(b_i \to b_j)$ in (4.22) can be used to replace the spatial block connectivity (based on the interaction likelihood) in the jump distribution P_{BLB} in (4.17) to obtain a new jump distribution $P_{BBB}(\boldsymbol{x} \to \boldsymbol{y})$. We call this model the *hierarchical block model* (HBM).

4.2.3 Structureless connectivity

For simplicity assume that all blocks have the same number of children N, that blocks of the same level have the same dispersion and that the dispersion of child blocks is a fraction of the dispersion of their parents. This yields

$$\sigma_l = \sigma_{l-1}\, c = \sigma_0\, c^l \qquad l = 1, \ldots, L \tag{4.29}$$

where $\sigma_0 > 0$ is the scale of 0-level blocks and $c > 1$ is a real scaling parameter that controls the fractional size ratio between parent and child blocks. Also assume that the weight of the parent is distributed equally among the children such that a similar scaling relation as above emerges and we can completely neglect block weights.

The center locations of child blocks of a parent block are distributed around the center location of the parent according to the parents dispersion,

$$\boldsymbol{x}_{(i_L,\ldots,i_l,i_{l-1})} \stackrel{d}{=} \boldsymbol{x}_{(i_L,\ldots,i_l)} + \boldsymbol{X}_l \tag{4.30}$$

where $\boldsymbol{X}_l \sim \text{Normal}_2(\sigma_l)$. Compare the construction of blocks in the flat block model in Section 4.1. The location $\boldsymbol{x}$ of a member of a 0-level block b_i satisfies

$$\boldsymbol{x} \stackrel{d}{=} \boldsymbol{x}_i + \boldsymbol{X}_0 \tag{4.31}$$

and we make the convention that $\boldsymbol{x}_L$ is either in the origin or in the center of the domain. Figure 14 shows different configurations of the described block model.

The difference between the center of a block and the center of one of its parent blocks can be formalized by

$$\boldsymbol{x}_{(i_L,\ldots,i_l,\ldots,i_k)} - \boldsymbol{x}_{(i_L,\ldots,i_l)} \stackrel{d}{=} \sum_{\lambda=k+1}^{l} \boldsymbol{X}_\lambda \sim \text{Normal}_2\left(\sqrt{\sum_{\lambda=k+1}^{l} \sigma_\lambda^2}\right) \tag{4.32}$$

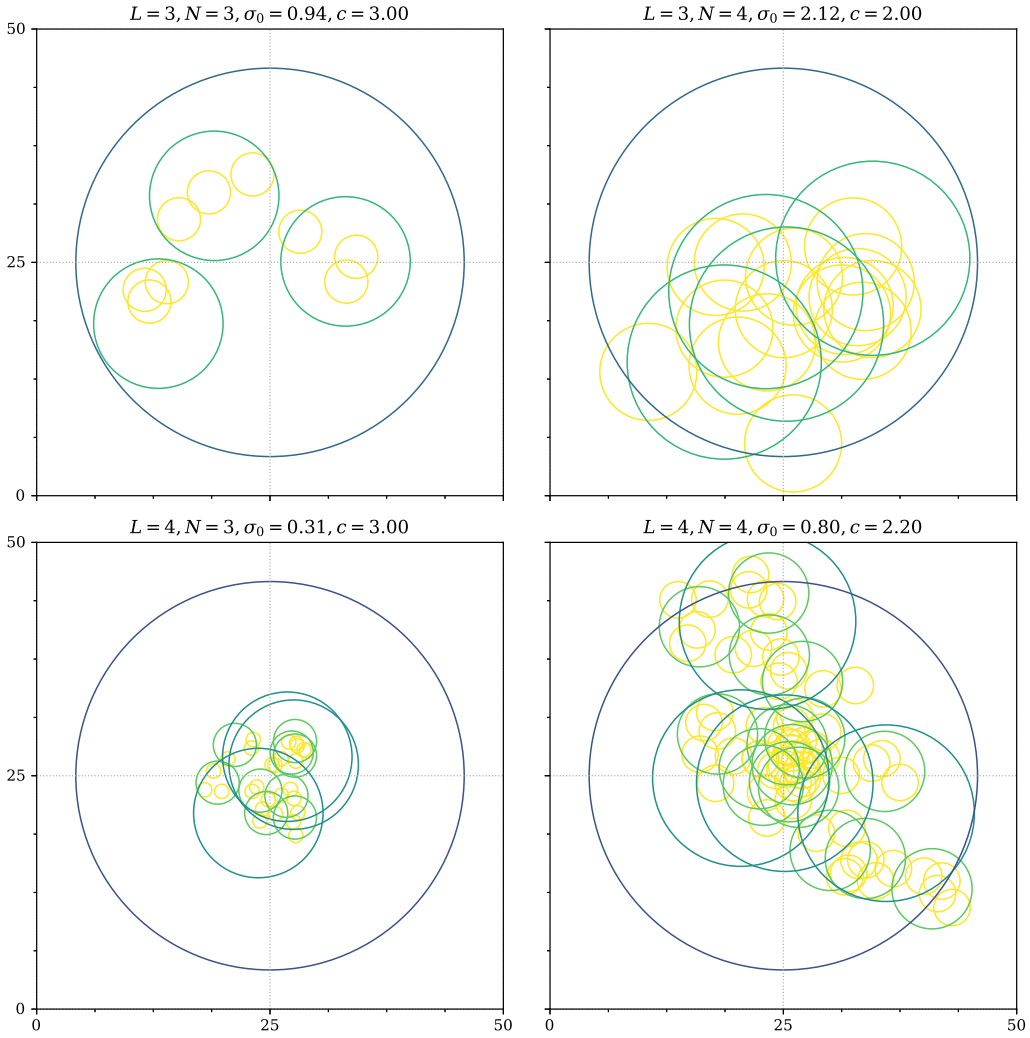

Figure 14: Comparison of different hierarchical block model configurations. The circles depict the 95% confidence ellipse of the membership likelihoods of all blocks with their level encoded in color. The number of children per block N is constant across all levels. The dispersion of 0-level blocks σ_0 was configured such that the L-level block fits the domain size.

which results from the normality – or from the finite moments – of the membership likelihoods. Since $\boldsymbol{x}_{(i_L,\ldots,i_l,\ldots,i_k)}$ is the center of a k-level block, the summation does not include $\boldsymbol{X}_k$.

For two arbitrary k-level blocks b_i and b_j with common parent level $l = \text{parent}(b_i, b_j)$, the location difference allows the following stochastic formulation

$$\boldsymbol{x}_{(i_L,\ldots,i_l,i_{l-1},\ldots,i_k)} - \boldsymbol{x}_{(i_L,\ldots,i_l,j_{l-1},\ldots,j_k)} \tag{4.33}$$

$$\stackrel{d}{=} \left(\boldsymbol{x}_{(i_L,\ldots,i_l)} + \sum_{\lambda=k+1}^{l} \boldsymbol{X}_\lambda^{(i)}\right) - \left(\boldsymbol{x}_{(i_L,\ldots,i_l)} + \sum_{\lambda=k+1}^{l} \boldsymbol{X}_\lambda^{(j)}\right) \tag{4.34}$$

$$\stackrel{d}{=} \sum_{\lambda=k+1}^{l} \boldsymbol{X}_\lambda^{(i)} + \sum_{\lambda=k+1}^{l} \boldsymbol{X}_\lambda^{(j)} \tag{4.35}$$

$$\sim \text{Normal}_2\left(\sqrt{2\sum_{\lambda=k+1}^{l} \sigma_\lambda^2}\right). \tag{4.36}$$

Note that $\boldsymbol{X}_\lambda^{(i)} \stackrel{d}{=} \boldsymbol{X}_\lambda^{(j)}$ but $\boldsymbol{X}_\lambda^{(i)} \neq \boldsymbol{X}_\lambda^{(j)}$ for $\lambda = k+1, \ldots, l$.

As a consequence, *structureless* jumps for a given interaction level l can be formalized using the bivariate normal distribution

$$\text{Normal}_2\left(\sqrt{2\sum_{\lambda=0}^{l} \sigma_\lambda^2}\right) \tag{4.37}$$

with the (isotropic) density denoted by $P(\boldsymbol{x} \to \boldsymbol{y}|l) = P(\boldsymbol{x} - \boldsymbol{y}|l)$. With a level distribution $P(l)$ (compare Section 4.2.2), the isotropic jump distribution

$$P_S(\boldsymbol{x} \to \boldsymbol{y}) = \sum_{l=0}^{L} P(\boldsymbol{x} \to \boldsymbol{y}|l)\, P(l) \tag{4.38}$$

can be defined in analogy to (4.22) and (4.17). The term structureless intends to indicate that the topological structure of the population is only present in a latent or stochastic sense.

4.2.4 Fractal connectivity

Recall that the scaling of block dispersion is based on the 0-level scale σ_0 and a scaling parameter $c > 1$,

$$\sigma_l = \sigma_0 \, c^l. \tag{4.39}$$

By introducing the notation $\sigma^2(l) := \sigma(l)^2$ and using a standard geometric series representation, the *conditional* squared jump scales or jump variances derived in (4.37) can be written as

$$\sigma^2_{\mathbb{N}}(l) := 2\sum_{\lambda=0}^{l} \sigma^2_\lambda = 2\sum_{\lambda=0}^{l} \sigma_0^2 \, c^{2\lambda} = \frac{2\sigma_0^2}{c^2-1}\left(c^{2(l+1)} - 1\right) \qquad l \in \mathbb{N}. \tag{4.40}$$

In Section 4.2.2 a geometric level distribution $P(l)$ with a truncation at level L was proposed. Neglecting a proper interpretation in the context of the block model, any discrete distribution on $\mathbb{N}$ can be used. Let Λ denote the corresponding random variable.

In infinite domains an infinite number of block levels is possible, such that for every block there exists a parent block. From the perspective of the child with level l, the center location of the parent block is normally distributed with scale σ_{l+1}. The considerations and formalizations from Section 4.2.3 can be extended to $L = \infty$. This concerns in particular the jump scales (4.37) such that (4.40) and (4.38) are also valid for an infinite number of block levels. The according level distribution can for instance be a geometric distribution (without truncation) $\Lambda \sim \mathrm{Geom}(p)$ on $\mathbb{N}$. An interpretation was already presented in Section 4.2.2. The parameter p is the probability for intra-block interaction in a jump process. The complementary value $1 - p$ is the probability for increasing the interconnecting level by one.

The scaling of block dispersion (4.39) motivates the introduction of intermediate fractional block levels (e.g. by changing the scaling constant c and the level indexes l). In the limit, it is equivalent to observe real block levels $l \in \mathbb{R}$. The continuous

equivalent to the geometric distribution with parameter p is the exponential distribution $\Lambda \sim \mathrm{Exp}(\delta)$ with scale $\delta = -\ln(1-p)^{-1}$. The dispersion of fractional-level blocks requires integral representations for the conditional jump scales such as

$$\sigma^2_{\mathbb{R}0+}(l) := 2\int_0^l \sigma_0^2\, c^{2\lambda}\,\mathrm{d}\lambda = \frac{2\sigma_0^2}{\ln c^2}\big(c^{2l}-1\big) \qquad l \in \mathbb{R}_+ \tag{4.41}$$

$$\sigma^2_{\mathbb{R}1+}(l) := 2\int_0^{l+1} \sigma_0^2\, c^{2\lambda}\,\mathrm{d}\lambda = \frac{2\sigma_0^2}{\ln c^2}\big(c^{2(l+1)}-1\big) \qquad l \in \mathbb{R}_+. \tag{4.42}$$

Because $\ln c^2 \approx c^2 - 1$ for small $c > 1$, the latter formulation ($\mathbb{R}1+$) *with level offset* is similar to (4.40). The former ($\mathbb{R}0+$) *without level offset* allows to simulate blocks with infinitely small dispersion whereas blocks in the second formulation have a lower bound for their spatial extent,

$$\sigma^2_{\mathbb{R}0+} : l \mapsto s : [0,\infty) \to [0,\infty) \tag{4.43}$$

$$\sigma^2_{\mathbb{R}1+} : l \mapsto s : [0,\infty) \to \left[\frac{2\sigma_0^2}{\ln c^2}\big(c^2-1\big),\infty\right). \tag{4.44}$$

Analogous to infinitely high levels, also negative block levels can be introduced. In this case the level distribution must be extended to the whole real line $\mathbb{R}$ (or all integer numbers $\mathbb{Z}$). A possible model is for instance the Laplace (bilateral exponential) distribution $\Lambda \sim \mathrm{Laplace}(\delta)$. The corresponding conditional squared jump scales are

$$\sigma^2_{\mathbb{Z}}(l) := 2\sum_{\lambda=-\infty}^{l} \sigma_\lambda^2 = 2\sum_{\lambda=-\infty}^{l} \sigma_0^2\, c^{2\lambda} = \frac{2\sigma_0^2}{c^2-1}c^{2(l+1)} \qquad l \in \mathbb{Z} \tag{4.45}$$

$$\sigma^2_{\mathbb{R}0}(l) := 2\int_{-\infty}^{l} \sigma_0^2\, c^{2\lambda}\,\mathrm{d}\lambda = \frac{2\sigma_0^2}{\ln c^2}c^{2l} \qquad l \in \mathbb{R} \tag{4.46}$$

$$\sigma^2_{\mathbb{R}1}(l) := 2\int_{-\infty}^{l+1} \sigma_0^2\, c^{2\lambda}\,\mathrm{d}\lambda = \frac{2\sigma_0^2}{\ln c^2}c^{2(l+1)} \qquad l \in \mathbb{R}. \tag{4.47}$$

The inverted mappings $(\sigma^2)^{-1}(s)$ and their derivatives $D(\sigma^2)^{-1}(s)$, where $Df(x) = f'(x)$ is the usual differential operator, can be calculated as

$$(\sigma^2_{\mathbb{R}0+})^{-1}(s) = \frac{1}{\ln c^2} \ln\left(\frac{s \ln c^2 + 2\sigma_0^2}{2\sigma_0^2}\right) \qquad D(\sigma^2_{\mathbb{R}0+})^{-1}(s) = \frac{1}{s \ln c^2 + 2\sigma_0^2} \tag{4.48}$$

$$(\sigma^2_{\mathbb{R}1+})^{-1}(s) = \frac{1}{\ln c^2} \ln\left(\frac{s \ln c^2 + 2\sigma_0^2}{2\sigma_0^2 c^2}\right) \qquad D(\sigma^2_{\mathbb{R}1+})^{-1}(s) = \frac{1}{s \ln c^2 + 2\sigma_0^2} \tag{4.49}$$

$$(\sigma^2_{\mathbb{R}0})^{-1}(s) = \frac{1}{\ln c^2} \ln\left(\frac{s \ln c^2}{2\sigma_0^2}\right) \qquad D(\sigma^2_{\mathbb{R}0})^{-1}(s) = \frac{1}{s \ln c^2} \tag{4.50}$$

$$(\sigma^2_{\mathbb{R}1})^{-1}(s) = \frac{1}{\ln c^2} \ln\left(\frac{s \ln c^2}{2\sigma_0^2 c^2}\right) \qquad D(\sigma^2_{\mathbb{R}1})^{-1}(s) = \frac{1}{s \ln c^2}. \tag{4.51}$$

The introduction of real valued levels and the scaling of block sizes motivates the term *fractal block model* (FBM). The derived conditional jump scales $\sigma^2(l) = \sigma(l)^2$ can be used to transform random levels Λ into random jump scales $\sigma(\Lambda)$ and $\sigma^2(\Lambda)$. The corresponding densities satisfy

$$f_{\sigma(\Lambda)}(s) = 2s\, f_{\sigma^2(\Lambda)}(s^2), \tag{4.52}$$

$$f_{\sigma^2(\Lambda)}(s) = f_\Lambda\big((\sigma^2)^{-1}(s)\big)\, D(\sigma^2)^{-1}(s). \tag{4.53}$$

As an alternative to conditional jump scales, the jump scales could be formalized as random variables that are parameterized with a level parameter l such that we can write $\Sigma^2|\Lambda$. The densities of random jump scales are then integrals of the form $\int f_{\Sigma^2}(s|l)\, f_\Lambda(l)\, \mathrm{d}l$. An interpretation in the context of the block model is less intuitive.

4.3 Fractional diffusion

Following Section 3.2.2, to simulate strictly space fractional diffusion, it is sufficient that the jump distribution has a certain algebraic asymptotic decay (3.45) and satisfies a scaling property (3.48). These requirements are now imposed onto the fractal block model.

4.3.1 Asymptotic characterization of stable jumps

From Section 4.2.3 and Section 4.2.4 if follows that random jump scales $\sigma(\Lambda)$ can be used for simulating jumps in the fractal block model by $\mathbf{N}\,\sigma(\Lambda)$ where $\mathbf{N} \sim \text{Normal}_2(1)$, $\sigma(l)$ is one of the presented conditional jump scale functions and Λ is a corresponding random level.

Let $P(l) = f_\Lambda(l)$ be the density or probability mass function of the random level distribution. The density of the resulting isotropic jump distribution $P(\boldsymbol{x} \to \boldsymbol{y}) = P(\boldsymbol{y} - \boldsymbol{x})$ can be written as (compare (4.38))

$$P(\boldsymbol{x}) = \sum_l f_{\boldsymbol{N}}\big(\boldsymbol{x}|\sigma(l)\big)\, f_\Lambda(l) = \sum_l f_{\boldsymbol{N}}\big(\boldsymbol{x}\,\sigma(l)^{-1}\big)\,\sigma(l)^{-2}\, f_\Lambda(l) \tag{4.54}$$

$$P(\boldsymbol{x}) = \int f_{\boldsymbol{N}}\big(\boldsymbol{x}|\sigma(l)\big)\, f_\Lambda(l)\,\mathrm{d}l = \int f_{\boldsymbol{N}}\big(\boldsymbol{x}\,\sigma(l)^{-1}\big)\,\sigma(l)^{-2}\, f_\Lambda(l)\,\mathrm{d}l \tag{4.55}$$

$$= \int f_{\boldsymbol{N}}\big(\boldsymbol{x}s^{-1}\big)\, s^{-2}\, f_\Lambda\big(\sigma^{-1}(s)\big)\, D\big(\sigma^{-1}\big)(s)\,\mathrm{d}s \tag{4.56}$$

$$= \int f_{\boldsymbol{N}}\big(\boldsymbol{x}s^{-1}\big)\, s^{-2}\, f_{\sigma(\Lambda)}(s)\,\mathrm{d}s \tag{4.57}$$

for discrete and real valued levels. The reciprocal value $\sigma(l)^{-1}$ should not be confused with the inverted mapping $\sigma^{-1}(s)$. For readability the summation and integration limits (i.e. the domain of the level distribution) have been left out.

In Section 2.5.4 a similar formalization of bivariate isotropic stable random variables $\text{Stable}_2(\alpha, \gamma)$ with $\alpha < 2$ was presented. A bivariate isotropic stable random variable can be decomposed as the product $\boldsymbol{N}\sqrt{A}$ where A is an univariate skew stable random variable and $\boldsymbol{N}$ is again a standard bivariate normal random variable. The probability

density can be written as

$$f_{\alpha,\gamma}(\boldsymbol{x}) = \int_0^\infty f_{\boldsymbol{N}}(\boldsymbol{x}s^{-1})\, s^{-2}\, f_{\sqrt{A}}(s)\, \mathrm{d}s. \tag{4.58}$$

As a consequence, in order for the density $P(\boldsymbol{x})$ of fractal block model jumps to display the same asymptotic behavior as the bivariate stable density $f_{\alpha,\gamma}(\boldsymbol{x})$ – and ultimately to yield the desired fractional diffusion behavior – it is necessary that the jump scale distribution $f_{\sigma(\Lambda)}(s)$ has the same asymptotic behavior as $f_{\sqrt{A}}(s)$. This problem, in turn, can be reduced to identifying the asymptotic law of the squared jump scale distributions $f_{\sigma^2(\Lambda)}(s)$ with the asymptotic law of the skew univariate stable density $f_A(s)$.

The parameterization of A was already presented in (2.58)

$$A \sim \text{Stable}\left(\overline{\alpha} = \frac{\alpha}{2}, \overline{\beta} = 1, \overline{\gamma} = 2\gamma^2 \cos\left(\frac{\pi\alpha}{4}\right)^{2/\alpha}\right). \tag{4.59}$$

In combination with (2.55) the asymptotic behavior of $f_A(s)$ expands to

$$f_A(s) \sim (\overline{\gamma})^{\overline{\alpha}}\, 2\sin\left(\frac{\pi\overline{\alpha}}{2}\right) \frac{\Gamma(\overline{\alpha}+1)}{\pi}\, s^{-(1+\overline{\alpha})} \tag{4.60}$$

$$= \left(2\gamma^2 \cos\left(\frac{\pi\alpha}{4}\right)^{2/\alpha}\right)^{\alpha/2} 2\sin\left(\frac{\pi\alpha}{4}\right) \frac{\Gamma(\alpha/2+1)}{\pi}\, s^{-(1+\alpha/2)} \tag{4.61}$$

$$= \left(2\gamma^2\right)^{\alpha/2} 2\cos\left(\frac{\pi\alpha}{4}\right) \sin\left(\frac{\pi\alpha}{4}\right) \frac{\Gamma(\alpha/2+1)}{\pi}\, s^{-(1+\alpha/2)} \tag{4.62}$$

$$= \left(2\gamma^2\right)^{\alpha/2} \sin\left(\frac{\pi\alpha}{2}\right) \frac{\Gamma(\alpha/2+1)}{\pi}\, s^{-(1+\alpha/2)} \tag{4.63}$$

$$= \left(2\gamma^2\right)^{\alpha/2} \frac{\alpha}{2} \frac{1}{\Gamma(1-\alpha/2)}\, s^{-(1+\alpha/2)} \tag{4.64}$$

where the last two steps are a known trigonometric identity and a property of the Gamma function.

For $\alpha = 2$, we know that the bivariate stable distribution $\text{Stable}_2(\alpha, \gamma)$ is equal to $\text{Normal}_2(\sqrt{2}\gamma)$. From the discussion in Section 2.5.5 it follows that A converges to a

degenerate distribution $A \xrightarrow{d} 2\gamma^2$ for $\alpha \to 2$, but the decomposition $\boldsymbol{N}\sqrt{A}$ where A is a univariate skew stable random variable is not valid for $\alpha = 2$.

4.3.2 Exponential level distributions

With an exponential level distribution on $\mathbb{R}_+$ and the conditional jump scale without offset ($\mathbb{R}0+$), as constructed in Section 4.2.4, the squared jump scale distribution (mixing distribution) can be calculated as

$$f_{\sigma^2_{\mathbb{R}0+}(\Lambda)}(s) = f_{\mathrm{Exp}(\delta)}\big((\sigma^2_{\mathbb{R}0+})^{-1}(s)\big)\, D(\sigma^2_{\mathbb{R}0+})^{-1}(s) \tag{4.65}$$

$$= \frac{1}{\delta}\exp\left(-\frac{1}{\delta \ln c^2}\ln\left(\frac{s\ln c^2 + 2\sigma_0^2}{2\sigma_0^2}\right)\right)\frac{1}{s\ln c^2 + 2\sigma_0^2} \tag{4.66}$$

$$= \frac{1}{\delta}\left(\frac{s\ln c^2 + 2\sigma_0^2}{2\sigma_0^2}\right)^{-1/(\delta \ln c^2)}\frac{1}{s\ln c^2 + 2\sigma_0^2} \tag{4.67}$$

$$= \frac{1}{\delta \ln c^2}\left(\frac{2\sigma_0^2}{\ln c^2}\right)^{1/(\delta \ln c^2)}\left(s + \frac{2\sigma_0^2}{\ln c^2}\right)^{-\left(1+1/(\delta \ln c^2)\right)}. \tag{4.68}$$

The conditions $\delta > 0$ and $c > 1$ ensure the validity of the probability density function, which is a Lomax-type density with shape $1/(\delta \ln c^2)$ and scale $2\sigma_0^2/\ln c^2$. The asymptotic behavior for $s \to \infty$ is

$$f_{\sigma^2_{\mathbb{R}0+}(\Lambda)}(s) \sim \frac{1}{\delta \ln c^2}\left(\frac{2\sigma_0^2}{\ln c^2}\right)^{1/(\delta \ln c^2)} s^{-\left(1+1/(\delta \ln c^2)\right)}. \tag{4.69}$$

Introducing an offset in the jump scales ($\mathbb{R}1+$), a similar calculation yields

$$f_{\sigma^2_{\mathbb{R}1+}(\Lambda)}(s) = \frac{1}{\delta \ln c^2}\left(\frac{2\sigma_0^2 c^2}{\ln c^2}\right)^{1/(\delta \ln c^2)}\left(s + \frac{2\sigma_0^2}{\ln c^2}\right)^{-\left(1+1/(\delta \ln c^2)\right)} \tag{4.70}$$

$$\sim \frac{1}{\delta \ln c^2}\left(\frac{2\sigma_0^2 c^2}{\ln c^2}\right)^{1/(\delta \ln c^2)} s^{-\left(1+1/(\delta \ln c^2)\right)}, \tag{4.71}$$

where $s \geq \frac{2\sigma_0^2}{\ln c^2}\big(c^2 - 1\big)$.

For a Laplacian level distribution (with domain $\mathbb{R}$) $\Lambda \sim \text{Laplace}(\delta)$ and a conditional jump scale without offset ($\mathbb{R}0$), the squared jump scale probability density is

$$f_{\sigma^2_{\mathbb{R}0}(\Lambda)}(s) = f_{\text{Laplace}(\delta)}\left((\sigma^2_{\mathbb{R}0})^{-1}(s)\right) D(\sigma^2_{\mathbb{R}0})^{-1}(s) \tag{4.72}$$

$$= \frac{1}{2\delta} \exp\left(-\frac{1}{\delta}\left|(\sigma^2_{\mathbb{R}0})^{-1}(s)\right|\right) \frac{1}{s \ln c^2} \tag{4.73}$$

$$= \frac{s^{-1}}{2\delta \ln c^2} \exp\left(Q \frac{1}{\delta \ln c^2} \ln\left(\frac{s \ln c^2}{2\sigma_0^2}\right)\right) \tag{4.74}$$

$$= \frac{1}{2\delta \ln c^2} \left(\frac{\ln c^2}{2\sigma_0^2}\right)^{Q/(\delta \ln c^2)} s^{-1+Q/(\delta \ln c^2)} \tag{4.75}$$

where

$$Q = \begin{cases} 1 & s < \frac{2\sigma_0^2}{\ln c^2} \\ -1 & s \geq \frac{2\sigma_0^2}{\ln c^2} \end{cases}. \tag{4.76}$$

Again, the conditions $\delta > 0$ and $c > 1$ yield the required restrictions and the distribution is composed of two power laws with a sharp transition in $\frac{2\sigma_0^2}{\ln c^2}$. For $s \to \infty$ the asymptotic behavior is

$$f_{\sigma^2_{\mathbb{R}0}(\Lambda)}(s) \sim \frac{1}{2\delta \ln c^2} \left(\frac{2\sigma_0^2}{\ln c^2}\right)^{1/(\delta \ln c^2)} s^{-\left(1+1/(\delta \ln c^2)\right)}. \tag{4.77}$$

With a level offset ($\mathbb{R}1$), the asymptotic behavior is

$$f_{\sigma^2_{\mathbb{R}1}(\Lambda)}(s) \sim \frac{1}{2\delta \ln c^2} \left(\frac{2\sigma_0^2 c^2}{\ln c^2}\right)^{1/(\delta \ln c^2)} s^{-\left(1+1/(\delta \ln c^2)\right)}. \tag{4.78}$$

The formulation

$$f_{\sigma^2(\Lambda)}(s) \sim \frac{1}{2^{1-U}\delta \ln c^2} \left(\frac{2\sigma_0^2 V}{\ln c^2}\right)^{1/(\delta \ln c^2)} s^{-\left(1+1/(\delta \ln c^2)\right)}. \tag{4.79}$$

with

$$U := \begin{cases} 1 & \Lambda \sim \text{Exp}(\delta) \\ 0 & \Lambda \sim \text{Laplace}(\delta) \end{cases} \qquad V := \begin{cases} 1 & \text{without offset} \\ c^2 & \text{with offset} \end{cases} \tag{4.80}$$

combines the cases discussed above. The generalized conditional jump scales can be written as

$$\sigma^2(l) = \frac{2\sigma_0^2}{\ln c^2}\left(c^{2l}V - U\right). \tag{4.81}$$

However, different jump scale densities can have different domains.

4.3.3 Identification of the asymptotic behavior

An identification of the asymptotic behaviors of the squared jump scale distributions $f_{\sigma^2(\Lambda)}$ based on exponential-type level distributions (4.79) and the asymptotic behavior of A (4.64) yields the equations

$$\frac{\alpha}{2} = \frac{1}{\delta \ln c^2}, \tag{4.82}$$

$$\left(2\gamma^2\right)^{\alpha/2} \frac{\alpha}{2} \frac{1}{\Gamma(1-\alpha/2)} = \frac{1}{2^{1-U}\delta \ln c^2} \left(\frac{2\sigma_0^2 V}{\ln c^2}\right)^{1/(\delta \ln c^2)}, \tag{4.83}$$

which are solved by the following parameterization of the fractal block model,

$$c = \exp\left(\frac{1}{\alpha\delta}\right) \tag{4.84}$$

$$\sigma_0 = \gamma \sqrt{\frac{2}{\alpha\delta}}\, \Gamma(1-\alpha/2)^{-1/\alpha}\, 2^{(1-U)/\alpha}\, V^{-1/2}. \tag{4.85}$$

By the definition of U and V in (4.80),

$$2^{(1-U)/\alpha} = \begin{cases} 1 & \Lambda \sim \text{Exp}(\delta) \\ 2^{1/\alpha} & \Lambda \sim \text{Laplace}(\delta) \end{cases} \qquad V^{-1/2} = \begin{cases} 1 & \text{without offset} \\ c^{-1} & \text{with offset} \end{cases}. \tag{4.86}$$

Figure 15 compares the density of the random scale A with accordingly parameterized squared jump scale distribution $\sigma^2(\Lambda)$ for different choices of α, γ, Λ and level offset. Without loss of generality the scale δ of the level distribution can be set to 1. A different scale of the level distribution is compensated by a different scaling of the block dispersion.

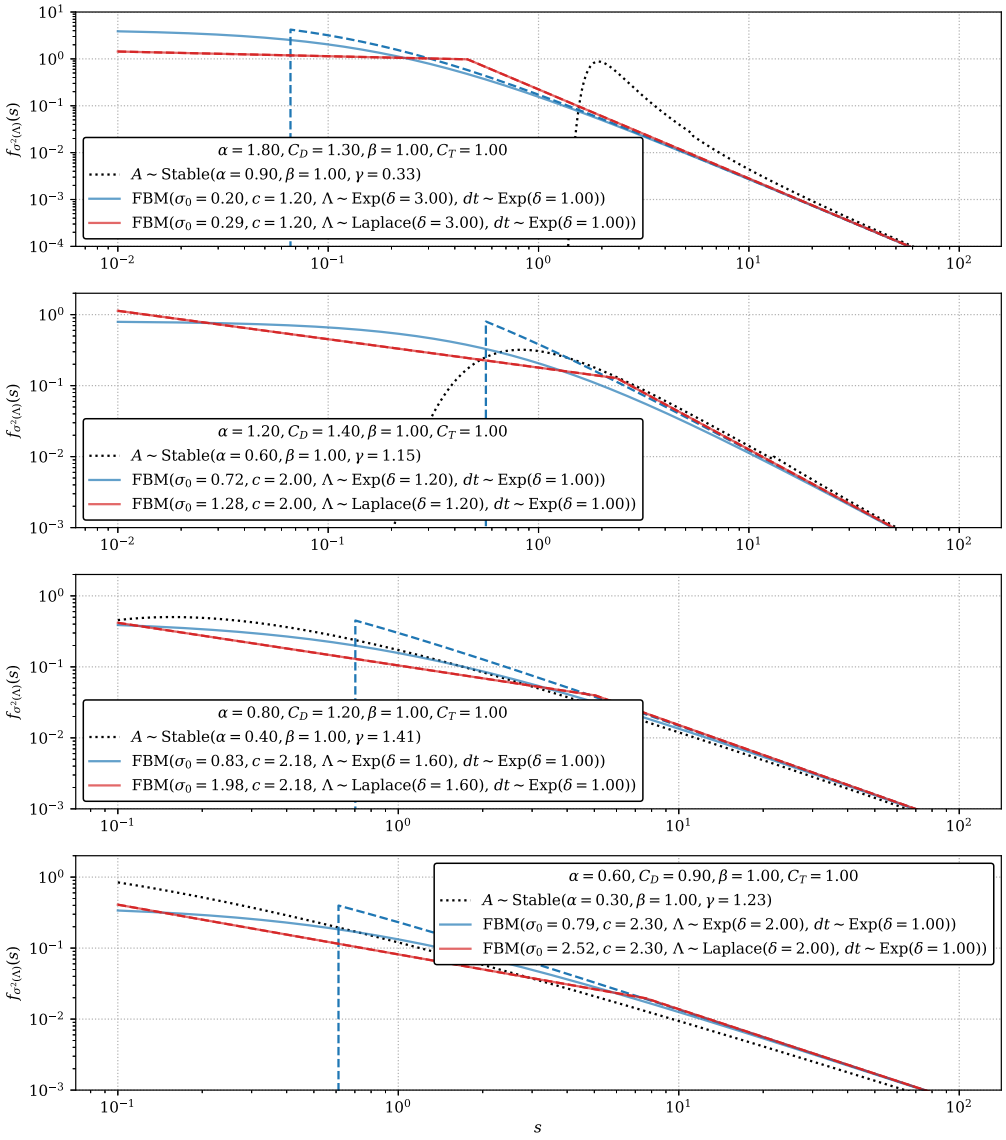

Figure 15: Comparison of different jump scale distributions parameterized according to a given continuous time random walk configuration. In all cases the dashed line shows the corresponding configuration with offset. Exponential level distributions with a level offset yield a minimum jump scale greater than 0. A level offset has no effect in the Laplacian model.

4.3.4 Scaling and limits

For a given stability $\alpha < 2$ and spatial scaling C_D, the presented identification allows to configure the fractal block model to generate random walks with the same characteristics as random walks driven by bivariate stable spatial increments with stability α and scale $\gamma = \sqrt{C_D}\,\Delta t^{1/\alpha}$. Because only the asymptotic behavior of the density of stable distributions is approximated, the fractal block model approaches standard continuous time random walks in the continuum limit $\Delta t \to 0$ (compare Section 3.2.2). This can be recognized in Figure 15 by the fact that the behavior of the univariate stable distribution of A is matched by the behavior of the distribution of $\sigma^2(\Lambda)$ only for larger values. For small α, however, we can assume that the approximation in the continuum limit is faster.

The required scaling relation (3.48) of the increment distribution is satisfied because the coefficients in the asymptotic laws were fitted exactly by solving the parameter equations. In combination with (3.41) this leads to the same coefficients in the asymptotic expansion of the characteristic functions, which in turn ensures convergence to the same generalized diffusion constant (continuum limit of the Montroll-Weiss equation (3.38)).

The presented identification is valid for $\alpha < 2$ and exponential-type level distributions. For the fractal block model to conform with the parameterization of continuous time random walks and the fractional diffusion equation, the transition $\boldsymbol{N}\sigma(\Lambda) \xrightarrow{d} \boldsymbol{N}\sqrt{2}\gamma$ for $\alpha \to 2$ must be stipulated. Analogous to the decomposition of bivariate isotropic random variables in Section 2.5.5, also here the original distribution model must be changed for $\alpha = 2$.

One way to obtain a constant jump scale value, is by modeling Λ as a degenerate distribution with the constant value 0. This can be interpreted as a discrete-level scenario and the according conditional jump scale function (4.40) evaluates to $\sigma_{\mathbb{N}}(0) = \sqrt{2}\sigma_0$. The block scaling parameter c has no effect because only 0-level jumps will be sampled. As a consequence, for $\alpha = 2$ the parameterization $(p = 1, \delta = 0), c = \infty, \sigma_0 = \gamma$ of the fractal block model with discrete levels is obtained (compare Section 4.4.1).

A way to tame the scaling properties of the fractal block model with real positive levels is by setting $c = 1$. This modification yields equally sized blocks, which actually makes no sense from a modeling perspective. Nevertheless, in this case the conditional jump scales take the forms

$$\sigma_{\mathbb{N}}(l) = \sqrt{2\sigma_0^2(l+1)} \tag{4.87}$$

$$\sigma_{\mathbb{R}0+}(l) = \sqrt{2\sigma_0^2(l)} \tag{4.88}$$

$$\sigma_{\mathbb{R}1+}(l) = \sqrt{2\sigma_0^2(l+1)}. \tag{4.89}$$

In the scenario with offset ($\mathbb{R}1+$) we have to ensure that

$$\boldsymbol{N}\sqrt{2}\gamma \stackrel{d}{=} \boldsymbol{N}\sqrt{2}\sigma_0\sqrt{\Lambda+1}. \tag{4.90}$$

For $\Lambda \sim \text{Exp}(\delta)$ or $\Lambda \sim \text{Laplace}(\delta)$ the convergence in distribution to the degenerate case with constant value 0 is obtained from $\delta \to 0$. This follows from an investigation of the respective distribution or characteristic functions. The resulting parameterization is $\delta = 0, c = 1, \sigma_0 = \gamma$. In the case without offset ($\mathbb{R}0+$), the required condition is

$$\boldsymbol{N}\sqrt{2}\gamma \stackrel{d}{=} \boldsymbol{N}\sqrt{2}\sigma_0\sqrt{\Lambda}. \tag{4.91}$$

The random variable Λ must take a constant value greater than 0, which cannot be obtained from a limit ($\delta \to 0$) of the exponential distribution (or of the centered Laplace distribution). Hence, the jump scale distributions with level offset seem more suitable in this regard.

Despite the conceptional transition of the fractal block model to a single layered model with the characteristics of usual diffusion is intuitive, a formal reconstruction is complicated by the limited range for which the presented parameterizations are valid ($\alpha < 0, \delta > 0, c > 1$). For instance, in the found parameterizations of the fractal block models for $\alpha < 2$ the relation $2/\alpha = \delta \ln c^2$ is required. This leads to contradictions in the analysis of the formal limits of the jump scale distributions (e.g.

$c = 1, \delta = 0$) and indicates that alternative parameterizations, stochastic models and scaling formulas should be be investigated. A further approach might be to replace the normal spatial increments in the usual scenario by more general increments with finite moments. In this case it is more likely that the limits of the presented jump scale distributions and parameterizations for $\alpha \to 2$ can be identified with the usual scenario. A thorough discussion of the formal transition to usual diffusion is out of the scope of this presentation.

4.4 Simulation results and model variants

With the previous calculations it follows that in the fractal block model stable spatial increments are constructed as normal random variables with stochastic scales, $\mathbf{N}\,\sigma(\Lambda)$. To obtain strictly space fractional random walks (compare Lévy flights), the time increments can either be constant or exponentially distributed. As usual, the combination of uncorrelated temporal and spatial increments yields the desired random walk trajectories $\boldsymbol{x}(t)$. Strictly space fractional random walks and trajectories generated from the parameterized fractal block model are compared in Figure 16 and Figure 17. Irrespective of the level offset and the choice for an exponential-type level distribution, the same quantitative congruence is obtained. However, larger scaling C_D and stability α must be compensated by smaller step sizes Δt in order to maintain correspondence.

Alternative models for the level distribution can for instance be the geometric, binomial or exponential power distribution. Whereas geometrically distributed levels yield a fractal block model with discrete levels and the same characteristics (Section 4.4.1), binomially distributed levels severely change the diffusion dynamics of simulated particles. The same is true if random levels are distributed with the exponential power distribution. In these cases the characteristics of the fractional diffusion equation, as defined in Section 3.1.2, are not met. The obtained dynamics are interesting as well, but beyond the scope of this thesis.

From the perspective of fractal block models with geometrically distributed levels, hierarchical block models can be interpreted as instantiation with persistent blocks and a limited number of levels. A statistical connection of hierarchical block model trajectories to fractional diffusion is discussed and reproduced in Section 4.4.2. Fractal block model random walks with power-law distributed temporal increments are linked to space-time fractional diffusion in Section 4.4.4.

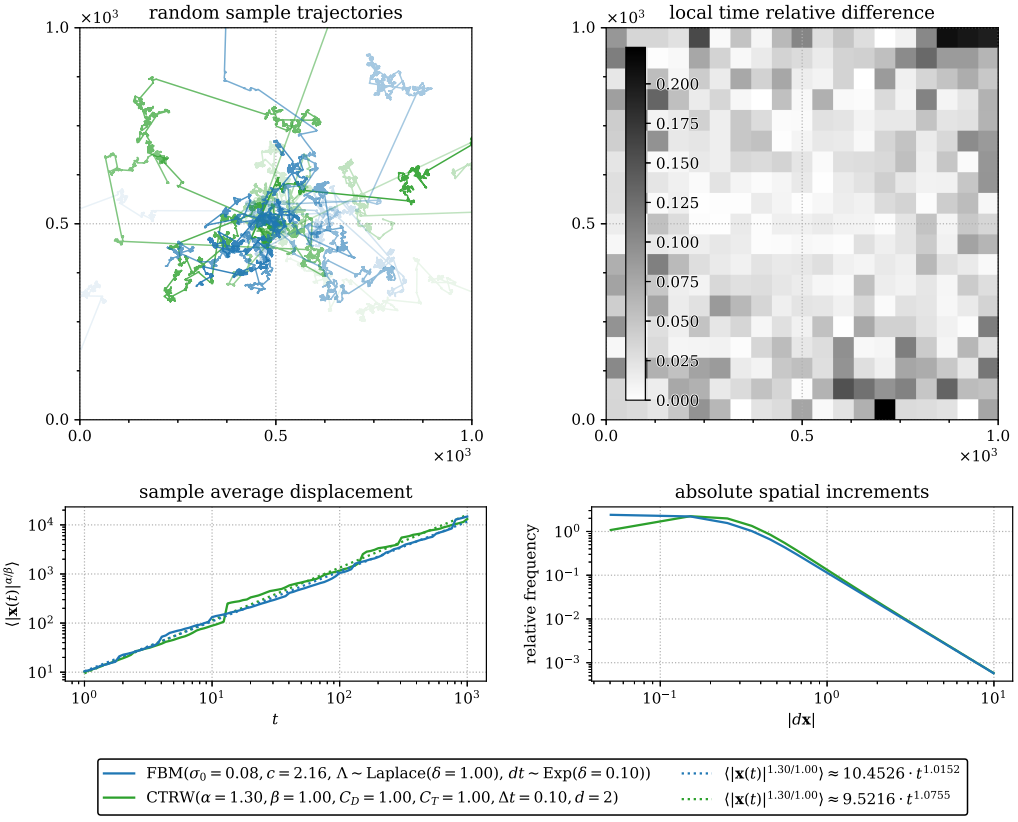

Figure 16: Comparison of space fractional continuous time random walks with random walks generated by the parameterized fractal block model with Laplacian level distribution (with level offset). The top left figure shows 10 random trajectories from each of the two samples, totaling 10^5 particles each. The difference of the spatial local time profiles of the two samples is displayed in the upper right. The bottom row displays the sample average displacement and the distribution of absolute spatial increments.

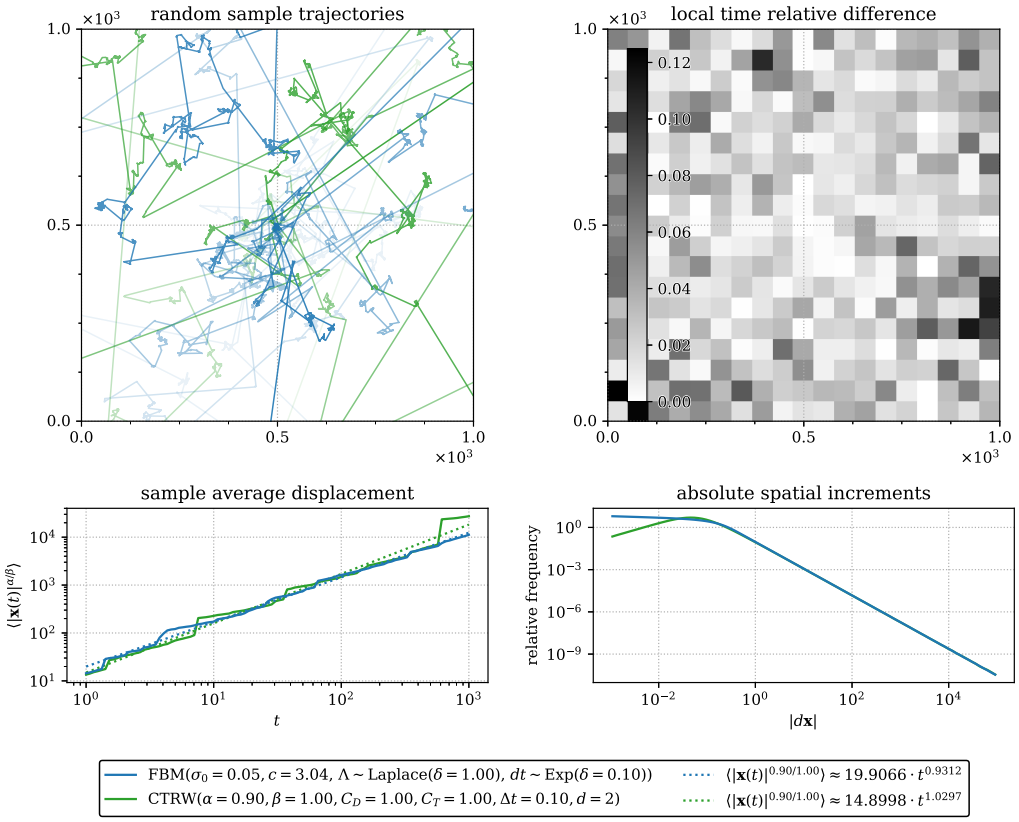

Figure 17: Comparison of space fractional continuous time random walks with random walks generated by the parameterized fractal block model with Laplacian level distribution (with level offset) and small α. The number of simulated trajectories is 10^5 in both models.

4.4.1 Discrete levels

In a scenario with quantized block levels, exponential level distributions $\Lambda \sim \mathrm{Exp}(\delta)$ transform into geometric distributions $\Lambda \sim \mathrm{Geom}(p)$. We call the scenario of geometrically distributed levels the *discrete-level fractal block model*. The aggregation of exponential probability densities into discrete points of mass was discussed in Section 2.3.3. The following equation identifies the asymptotic behavior for $l \to \infty$ of skew stable and jump scale distributions driven by geometric levels using the same principle,

$$f_{\sigma^2_{\mathbb{N}}(\Lambda)}\big(\sigma^2_{\mathbb{N}}(l)\big) \sim \int_{\sigma^2_{\mathbb{N}}(l)}^{\sigma^2_{\mathbb{N}}(l+1)} f_A(s)\,\mathrm{d}s \tag{4.92}$$

$$p\,(1-p)^l \sim \int_{\sigma^2_{\mathbb{N}}(l)}^{\sigma^2_{\mathbb{N}}(l+1)} \big(2\gamma^2\big)^{\alpha/2}\,\frac{\alpha}{2}\,\frac{1}{\Gamma(1-\alpha/2)}\,s^{-(1+\alpha/2)}\,\mathrm{d}s \tag{4.93}$$

$$\sim \big(2\gamma^2\big)^{\alpha/2}\,\frac{1}{\Gamma(1-\alpha/2)}\left(\frac{2\sigma_0^2}{c^2-1}\right)^{-\alpha/2}(1-c^{-\alpha})\,c^{-\alpha}\,c^{-\alpha l}. \tag{4.94}$$

In the second line the stable density was replaced by their asymptotic approximation (4.64). The conditional jump scale $\sigma^2_{\mathbb{N}}(l)$ was introduced in (4.40).

Above identification is solved by the following parameterization of the discrete-level fractal block model,

$$c = (1-p)^{-1/\alpha} \tag{4.95}$$

$$\sigma_0 = \gamma\,\frac{1}{c}\,\sqrt{c^2-1}\left(\frac{1-c^{-\alpha}}{p\,\Gamma(1-\alpha/2)}\right)^{1/\alpha}. \tag{4.96}$$

Note that the relation $\delta = -\ln(1-p)^{-1}$ holds for the parameter of the exponential level distribution in the fractal block model and the parameter of the geometric distribution in the discrete-level fractal block model. There, however, exist alternative identification approaches which deliver the same parameterization of the discrete-level model. Figure 18 compares the resulting jump scale probability mass function $f_{\sigma^2_{\mathbb{N}}(\Lambda)}(s)$ with continuous-level jump scale densities and the density of the stable distribution of A. Figure 19 shows a comparison of simulated topological trajectories from the discrete-

level fractal block model using above parameterization with classical continuous time random walks. As with the continuous-level fractal block model, a similar quantitative correspondence between topological transport and fractional diffusion is obtained. Without loss of generality we can set $p = 0.5$.

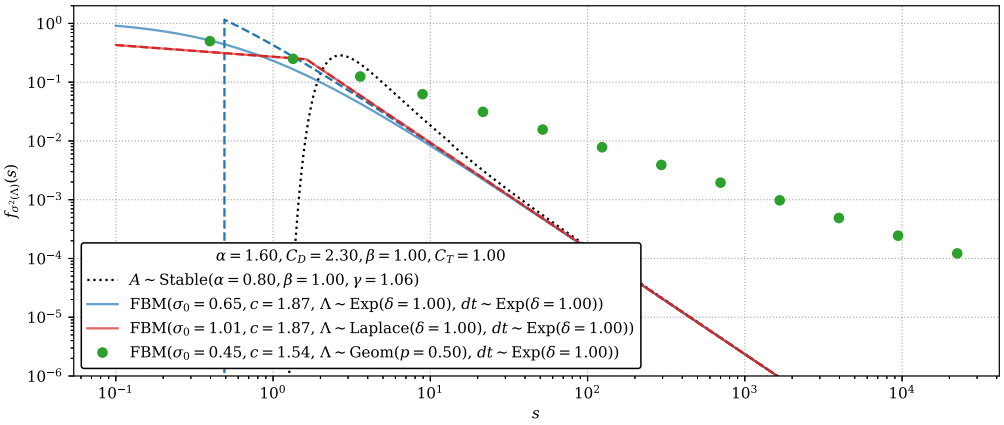

Figure 18: Comparison of discrete and continuous jump scale distributions.

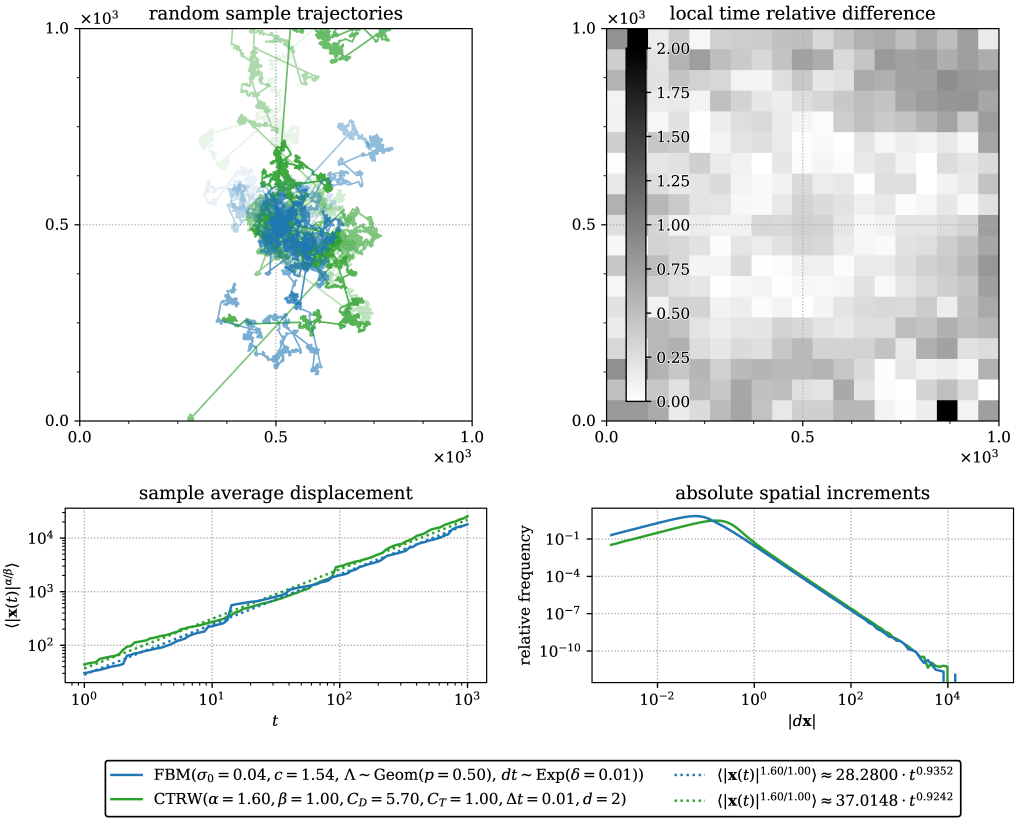

Figure 19: Comparison of space fractional continuous time random walks and fractal block model trajectories with discrete levels, $\Lambda \sim \text{Geom}(p)$. The data was collected from samples with $3 \cdot 10^3$ trajectories each.

4.4.2 The persistent topology hierarchical block model

Whereas the fractal block model describes a volatile topology by stochastic means, the hierarchical block model (Section 4.2.2) is characterized by persistent blocks. Furthermore, since the hierarchical block model is defined with a finite number of levels, a connection to the discrete-level fractal block model seems more intuitive. But the level distribution in the hierarchical model must be truncated at the maximum level L. Instead of using the re-weighted geometric distribution $\mathrm{Geom}(p, L)$ presented in (2.39), here all randomly generated levels exceeding L are clipped such that the total cropped mass is concentrated in the highest level L. Theoretically, to approximate the fractal block model with geometrically distributed levels, it should be sufficient to choose a large enough number of levels L and children per block N while leaving the remaining parameters σ_0, c and p identical.

In Figure 20 standard continuous time random walk trajectories are compared with trajectories generated from the hierarchical block model ($N = 3$, $L = 17$), parameterized according to the fractal block model with geometric level distribution (Section 4.4.1). The persistent topology consists of $N^L = 3^{17} \approx 130 \cdot 10^6$ 0-level blocks and $\sum_{l=0}^{L} N^l = (1 - N^{L+1})/(1 - N) \approx 190 \cdot 10^6$ blocks in total. However, for simulating topological trajectories, higher level blocks can be discarded from computer memory. The spatial increments are sampled correctly and reproduce the amplitude of the bivariate stable distribution. The sample average dispersion and the spatial profile, on the other hand, are strongly influenced by the particular (i.e. persistent) instantiation of the topological structure. The results in Figure 20 represent a case where the persistent topology model reproduced the characteristic displacement of fractional diffusion rather correctly. Nevertheless, from the inhomogeneous and persistent positioning of blocks (gray circles) it follows that the hierarchical block model cannot produce the symmetric spatial profiles of the fundamental solution and of local time.

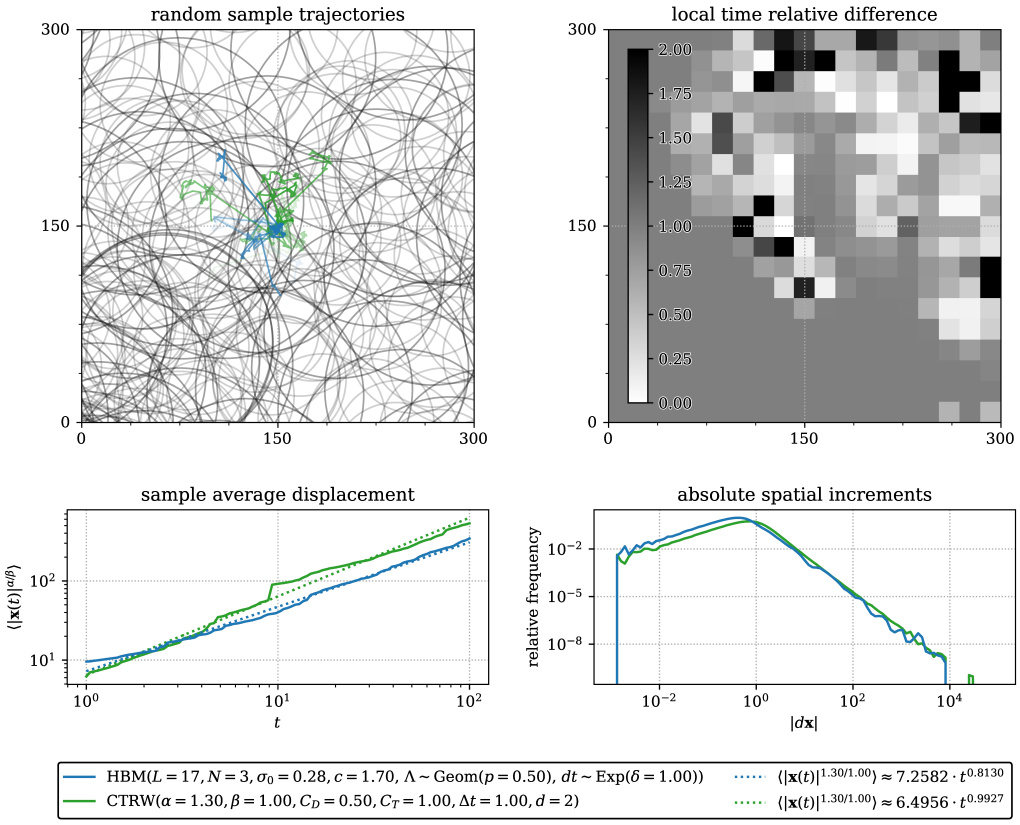

Figure 20: Comparison of hierarchical block model trajectories (persistent topology) and standard continuous time random walk trajectories. After random generation, the whole block structure was shifted such that the most central 0-level block is located in the center of the domain (also used as the initial position of simulated trajectories). This improves the visual display and allows to compare the spatial profiles of both simulation approaches. The blocks in the 8th and 9th level are visualized as gray circles with their radius corresponding to the 95% confidence interval of their spatial membership distributions. The data was collected from samples with $2 \cdot 10^4$ trajectories each.

To overcome the resulting artifacts, and to cover all possible instantiations of stochastic blocks in the fractal model, a larger number of sub-blocks N is required. This, however, explodes the amount of computer memory and computation time required. As an alternative approach, the fractal block model can be regarded as a mean field model for the hierarchical block model. This connection can be reproduced by rebuilding the hierarchical structure for every jump or for every simulated particle. The latter technique was used to generate the results in Figure 21 where $L = 17$ and $N = 2$. Also for the resampled hierarchical model, the correct reproduction of fractional diffusion depends on the parameterization and the discretization parameters L and N. In the following section, the parameterization of hierarchical block models and associated implications on numerical simulation and qualitative characteristics of trajectories are discussed.

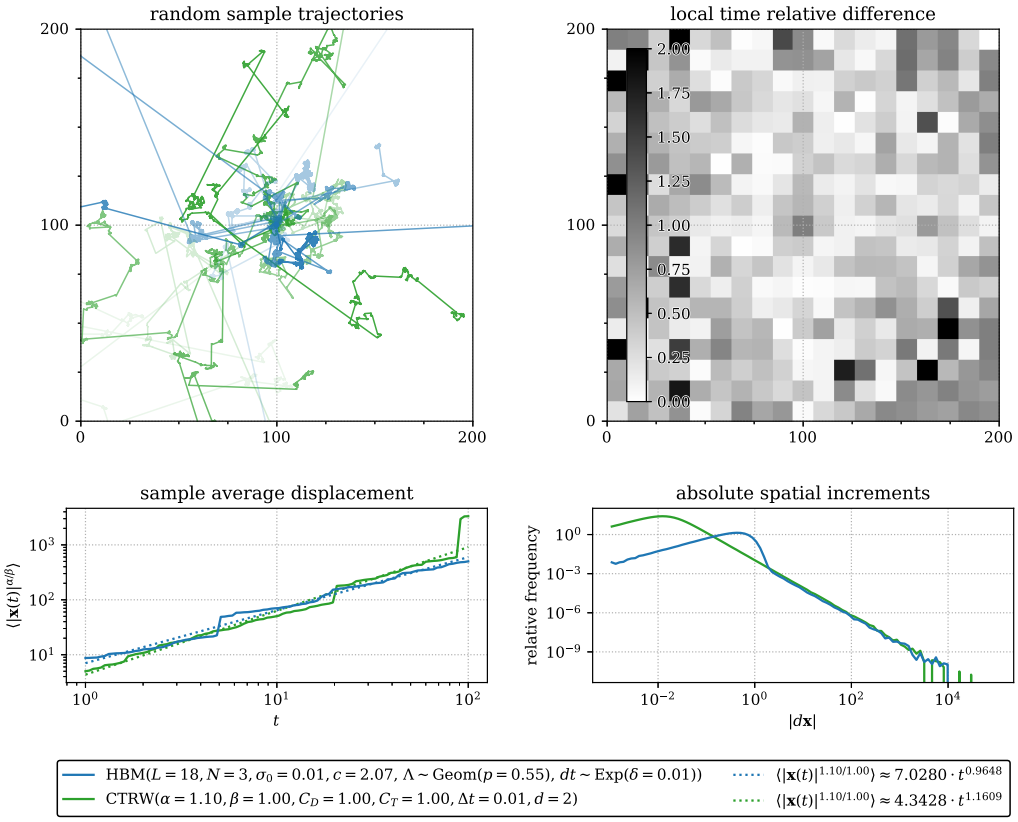

Figure 21: Comparison of hierarchical block model trajectories with individually sampled persistent block structures and standard continuous time random walks. Two times 10^3 trajectories were sampled.

4.4.3 Implications of the configuration of the hierarchical block model

Because all randomly generated levels exceeding L are clipped, the jumps in the hierarchical block model are limited to a maximum characteristic length, which is not the case for standard continuous time random walks and the fractal block model approach, which feature stable jumps with infinite moments. Hence, for small (finite) parameters L, an exponential cutoff in the distribution of spatial increments can be observed. This is owed to the fact that spatial jumps are a finite sum of normal increments (with varying but finite scales). In particular but not exclusively for the re-weighted geometric level distribution, also the over-representation of small spatial increments leads to a different linear slope in the sample average displacements and to smaller diffusion constants. These effects are amplified by longer observation periods and smaller α-values, because stable jumps are more likely to occur with larger magnitude and their block model analogues become more susceptible to the truncation.

In continuous time random walks with small α, we can observe greater distances between spatial clusters of consecutive particle locations. To reproduce these characteristics with trajectories in the hierarchical block model, a small number of sub-blocks N is sufficient. For large α, clustering effects vanish and a homogeneous distribution of resting locations can be observed. To obtain a homogeneous distribution of particle positions in the hierarchical block model, a larger number of sub-blocks N is required. This indicates that in a scenario with a homogeneous topological structure, the removal of blocks (i.e. smaller N) increases the anomalous characteristics of random walks and diffusion processes.

As noted before in connection with the fractal block model, the limit $\Delta t \to 0$ is required for approximating the fractional diffusion equation. With Δt also the scale of the stable increment distribution of continuous time random walks changes and, according to the parameter identification in Section 4.4.1, a different scaling of block dispersion in the (discrete level) block models is obtained. Smaller values increase the resolution of simulated trajectories but also increase the number of block levels required to avoid an early truncation in the empirical spatial increment distribution of the hi-

erarchical block model. In the hierarchical block model an additional discretization parameter is the intra-block interaction likelihood p (parameter of the geometric level distribution). Smaller values of p mean that larger levels are sampled more often, and hence an overall larger number of levels is necessary for approximating the same displacement characteristics. As a consequence, the parameter p controls the topological resolution of the hierarchical block model. Smaller values yield a better approximation of the increment distribution, but a larger number of levels also greatly increases the computational effort for sampling trajectories.

Despite the presented results on persistent topology models show that multiple quantitative characteristics (e.g. sample average displacement, the increment distribution) from fractional diffusion can be reproduced, qualitative differences can be recognized in the visual representation of sampled trajectories (compare Figure 20 and Figure 21). This concerns in particular the emergence of clusters in individual simulated trajectories. In this context the scale or dispersion of 0-level blocks plays an important role. If lower levels are removed (truncated) from the topological structure, or when the level distribution is modified accordingly, the distribution of small spatial increments becomes re-weighted whereas the distribution of large spatial increments remains identical. However, for small values the spatial increment distribution of the hierarchical block model differs anyways from the stable spatial increment distribution of continuous time random walks (both models coincide in the continuum limit). Hence, this modification can be used to improve the performance of simulations, because the discarded low-level layers contain a relatively large portion of the blocks. In simulated trajectories we can observe that a careful truncation of the geometric level distribution from below, yields larger volatile clusters whereas the displacement behavior is largely maintained (similar sample average displacement and spatial profiles).

4.4.4 Time fractional diffusion

Since a random level Λ must be sampled for every increment in block model trajectories, the notation $\Lambda(t)$ makes sense. For the strictly space fractional case, the time evolution of the interaction levels in the fractal block model corresponds to uncorrelated exponential or Laplacian noise. By demanding memory effects (for instance autocorrelated velocity) in the particle dynamics of the fractal block model, we can expect that the characteristics of $\Lambda(t)$ must change. It is however not sufficient that level changes and hence changes in the absolute value of velocity occur sporadic, also directional changes must only occur between waiting phases. In other words, it is not sufficient that the level process $\Lambda(t)$ is autocorrelated or stationary in order to introduce the desired memory effects. Revealing a more explicit form of the process $\Lambda(t)$ is beyond the scope of this thesis, the following is a qualitative characterization.

The intuitive method for introducing memory effects in the fractal block model is – analogous to continuous time random walks – by using Mittag-Leffler distributed waiting times. In Figure 22 different combinations of (uncoupled) waiting time and level distributions are shown. The resulting process $\Lambda(t)$ can be regarded as exponential or Laplacian noise subordinated to the operational time process t_* generated from Mittag-Leffler increments dt. A comparison of fractal block model trajectories with this configuration and standard continuous time random walk trajectories is displayed in Figure 23.

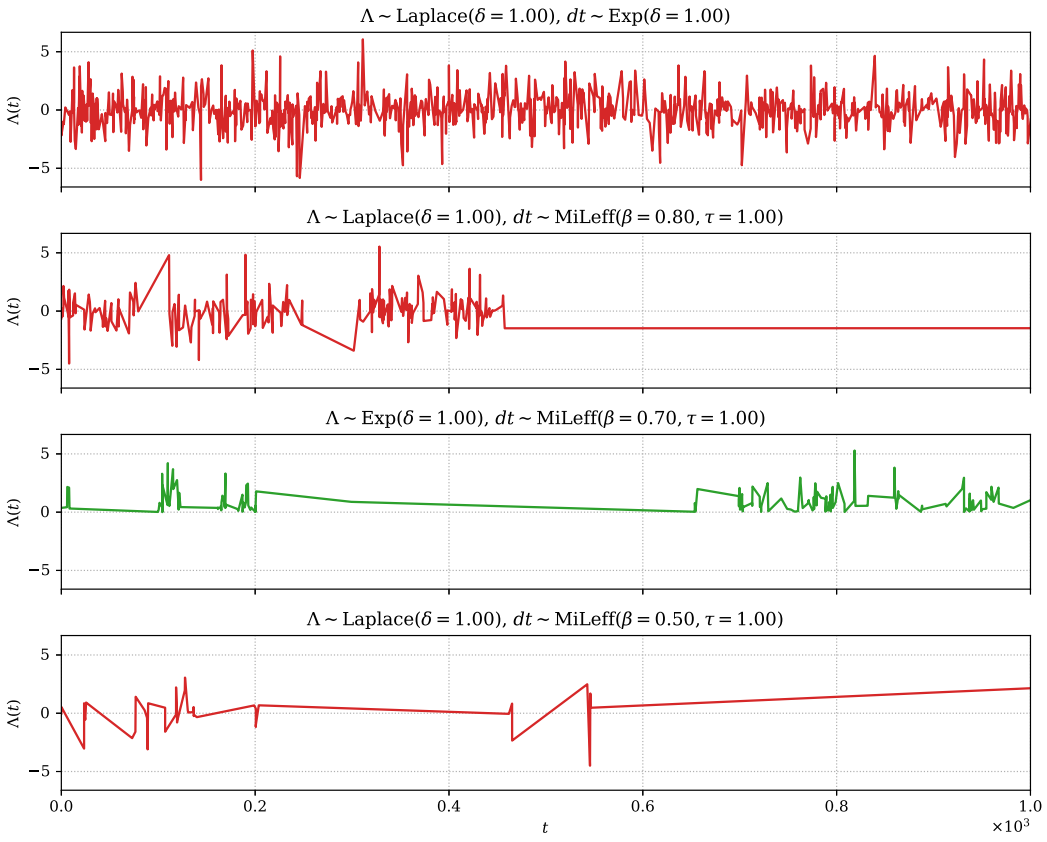

Figure 22: Random interaction levels displayed as a stochastic process with different configurations of the level distribution Λ and time increments dt.

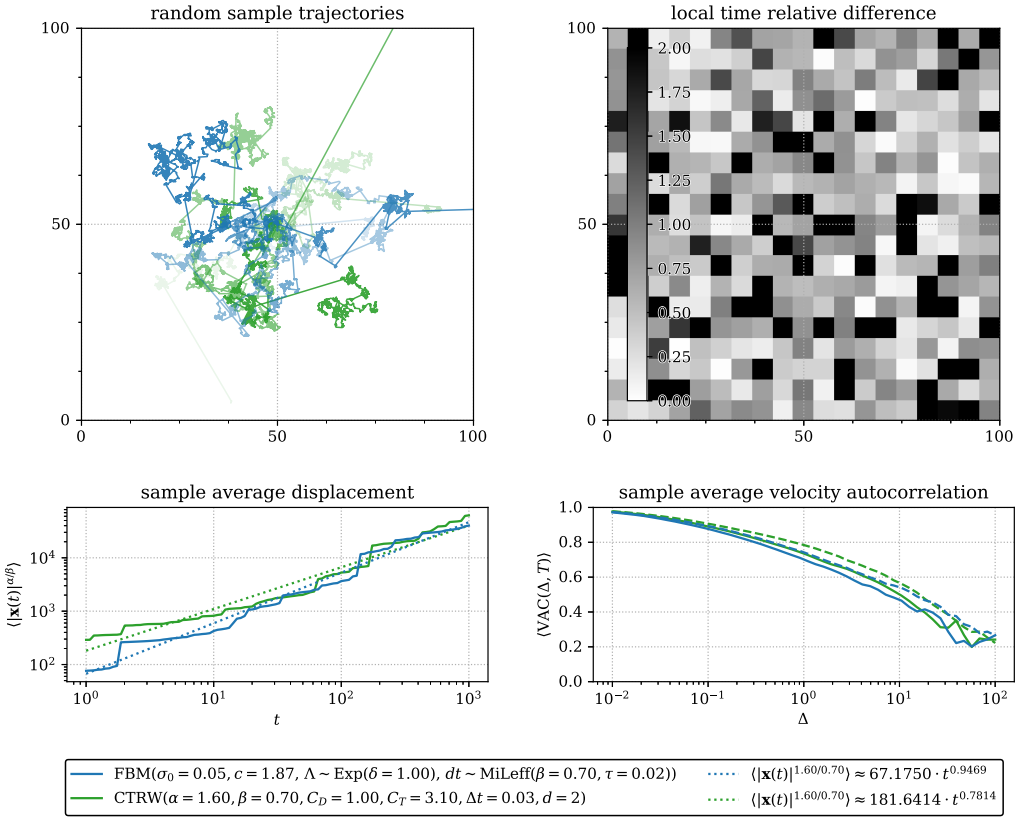

Figure 23: Comparison of standard space and time fractional random walks with random walks generated by the parameterized fractal block model with the level noise Λ subordinated to dt.

Technical approaches for simulating time fractional random walks with fixed step stochastic processes were presented in Section 3.2.4. One way is to separate spatial jumps by a random number – sampled from a discretization of the waiting time distribution – of consecutive time steps without jumps. If the velocity $\boldsymbol{v}(t)$ is replaced with time-averaged velocity $\boldsymbol{v}(t, \Delta)$, then the perceived velocity of a particle remains more or less constant even when additional 0-length jumps are inserted in between sampled event times. Carried over to the level process $\Lambda(t)$ this means that instances of high levels can be separated by instances of very low levels without changing the velocity profile of a trajectory. In terms of Figure 22 the gaps between intervals with high frequency high positive amplitude noise must be replaced with low or negative amplitude noise. Hence, in a fixed frequency version we can anticipate a low (negative) amplitude baseline signal interrupted by quasi-periodic bursts of high (positive) amplitude.

Besides by amplitude modulation, it might be possible to construct stochastic processes with skew increments and drift [53] that yield a dwelling time in the negative domain similar to subordinated Laplacian noise. It is however important to note that certain configurations of the level process can lead to coupled space and time increments in simulated trajectories.

5 Discussion

In this concluding chapter the developed technical approach is put in context with existing research (Section 5.1), an overview on open research questions and geometric observations is presented (Section 5.2) and the simulation of topological features of interacting populations in fractional differential equation models is discussed (Section 5.3).

5.1 Context

The presented result allows to reproduce fractional diffusion by random walks generated from topological block models.

5.1.1 Motivation and background

In networks often a clear distinction between intra- and inter-community links can be recognized. Particularly, in large interacting populations (compare Section 1.1 and Section 5.3) clustering properties and community structure are an important factor for the emergence of complex patterns in transport and interaction processes. Network models of structured populations and of systems with similar topological features have been researched in a vast range of scientific publications. Anomalous and complex patterns such as trapping, bursts, nonlinear diffusivity and spatial outliers have been found in many existing networks in all kinds of disciplines [21, 49, 55]. According models for the generation of networks and dynamic (spreading) processes with specific characteristics have been developed [39, 47, 79, 103]. In both, observed and artificially constructed systems, it is always the underlying topological structure, or the interplay of dynamic processes with the same, that is responsible for complex behavior. In particular, the hierarchical configuration of community structures has been linked to features like scaling invariance, power-law degree distributions and nonlinear dynamics [8, 20, 80, 98, 99].

In network theory the term *block model* refers to the segmentation of nodes into groups based on internal and external connectivity patterns [4, 71, 77]. Algorithms for

the detection of strongly interconnected clusters often work by stochastically assigning nodes to different blocks and by observing the effect on a certain quality measure (compare Gaussian mixture models). *Stochastic block models* are used to infer hierarchical and overlapping community structures by the means of Markov chain Monte Carlo methods [75, 76]. Other approaches exhaust the local diffusivity and percolation properties of networks when visited by random walkers to detect the separation of tightly connected clusters [97, 98].

Also in more general dynamical systems heterogeneous properties and dynamics can be responsible for complex behavior. Alike in networks, it is possible to identify and group together strongly interconnected components or parts of a system with similar features. For instance in spatial systems, different areas may be distinguishable based on proximity measures and local (parameter) configurations. In this work, block models are formalized on continuous domains by heterogeneous densities which are assembled from Gaussian membership likelihoods. In contrast to the representation of networks in terms of nodes and corresponding edges that are placed on a two-dimensional domain for visualization (graph layout), here, spatial proximity and interconnection are interrelated by construction.

5.1.2 Main result

A prerequisite for investigating fractional diffusion and continuous time random walks, is the discourse of the underlying theory (Section 3). To that end, the construction and definition of the fractional diffusion equation in the Caputo and Riesz-Feller sense in two dimensions was reviewed. Furthermore, the according formal connection between the fractional diffusion equation and continuous time random walks was presented. A programming library for simulating continuous time random walk trajectories in one and two dimensions was created [92]. Statistical measures for the quantification of simulated trajectories and approaches for the comparison of ensemble average spatial distributions with the fundamental solution of the fractional diffusion equation were prepared and implemented.

Block structures on two-dimensional domains in flat, hierarchical and fractal variants were introduced (Section 4). Thereby, blocks are formalized as Gaussian densities and model tightly interconnected spatial clusters. Topological interaction mechanisms based on the hierarchical and fractal arrangement of blocks were constructed. A stochastic formulation of topological interaction was finally identified with the Lévy-stable displacements in continuous time random walks. As a consequence, it is possible to parameterize the topological block models in order to display the characteristics of fractional diffusion in randomly generated topological trajectories. To verify the found mathematical connection and the corresponding parameterizations, sampled trajectories were compared with continuous time random walks by empirical means using the developed programming library. Hence, the theoretical and mathematical result of this work was reinforced by empirical and computational methods.

5.1.3 Model accuracy and convergence

The block models approximate continuous time random walks driven by Lévy-stable and Mittag-Leffler increments and the corresponding fractional diffusion equation in the Caputo and Riesz-Feller sense. A proper numerical analysis of the convergence and transition behavior of topological trajectories ($\Delta t \to 0$) – also with respect to parameterization – was not conducted. In Section 4.4 the effects and interrelations of the parameters $\Delta t, \alpha, p$ as well as L, N in connection with the approximation of continuous time random walks were discussed briefly from a qualitative perspective. For a complete analysis the following steps must be investigated:

$$\text{HBM} \longrightarrow \text{FBM} \longrightarrow \text{CTRW} \longrightarrow \text{fractional diffusion equation}$$

Also the last step, which is the convergence behavior of continuous time random walks to the fractional diffusion equation is not completely solved [10, 52, 63]. The convergence behavior in the anomalous setting depends heavily on the applied quantification metrics and special effects have to be taken into account (Section 3.3).

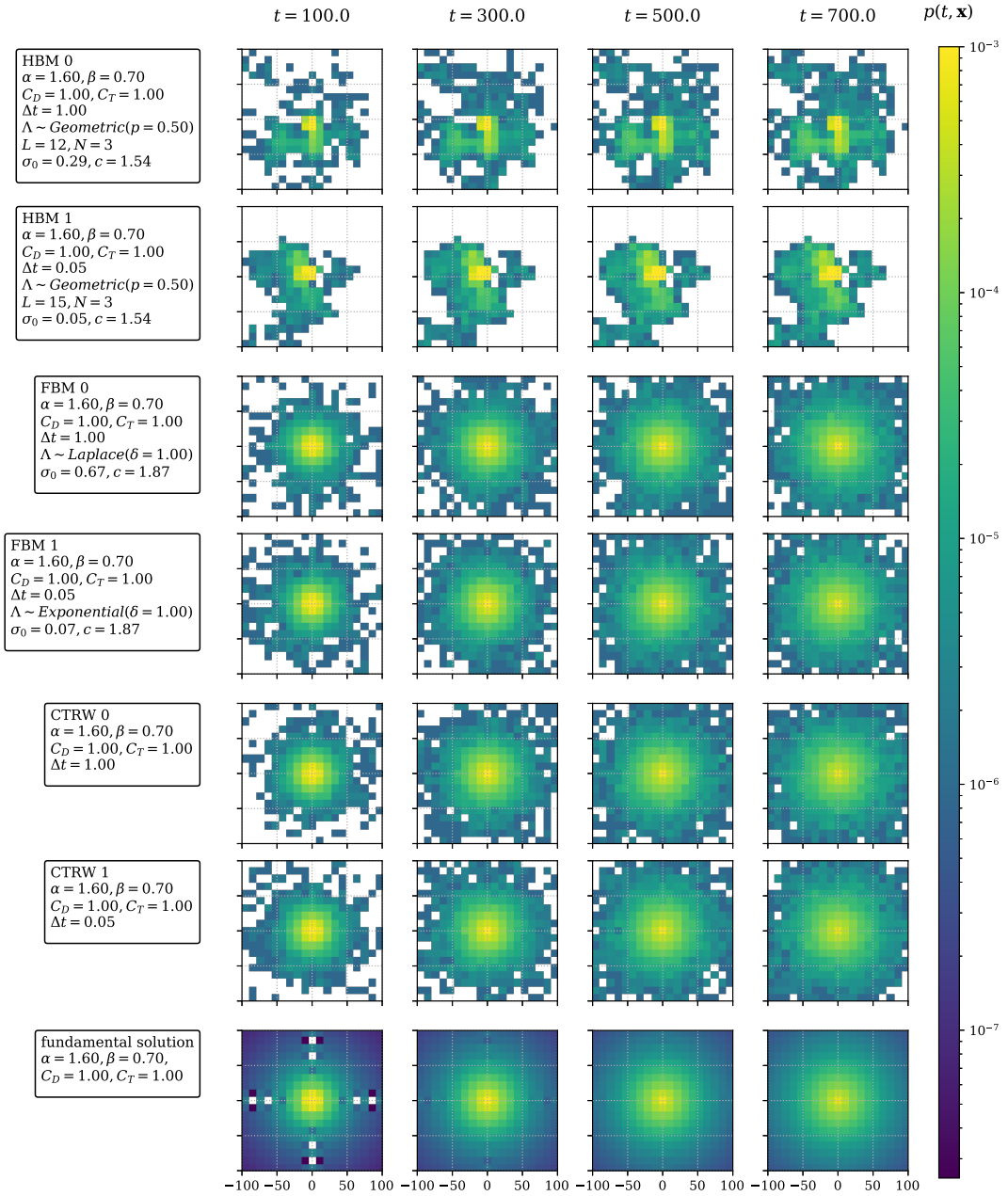

Figure 24: Comparison of empirical distributions calculated from 10^4 simulated trajectories with different models and parameterizations as well as the fundamental solution. The density profiles were calculated on a spatial lattice of 20×20 nodes on the bounded domain $[-100, 100]^2$ and the local density is encoded in a logarithmic color scale. The persistent topological structures in the hierarchical block model are clearly recognizable. Artifacts that result from the FFT-based evaluation of the fundamental solution are visible for small times (Section 3.4).

Figure 24 is a juxtaposition of empirical densities $p(t, \boldsymbol{x})$ calculated from ensembles of simulated trajectories in different models and the fundamental solution of the fractional diffusion equation $G(t, \boldsymbol{x})$. A basic error measure for quantifying the difference to the fundamental solution was applied on the same ensembles in Figure 25. Effects such as the power-law survival probability at the initial location (compare Section 3.3.1) and the heavy tails of the densities were not explicitly taken into account. Nevertheless, both figures indicate that the fractal block model is capable of approximating the fractional diffusion equation in the same order as the standard continuous time random walk model. The hierarchical block model is limited in this capability by the persistence of the underlying topological structure and accompanying computational challenges (Section 4.4.3).

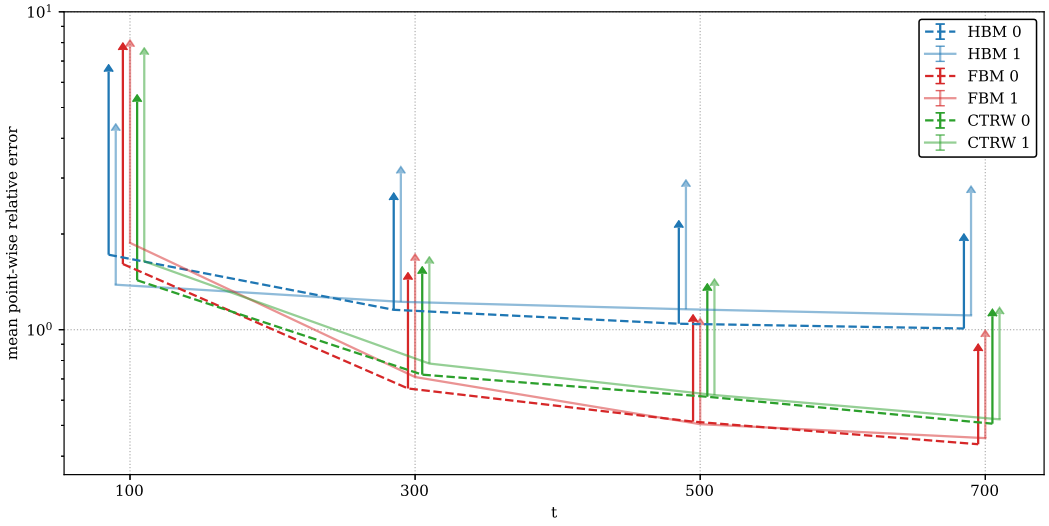

Figure 25: Crude quantitative comparison of the empirical distributions in Figure 24 with the fundamental solution of the fractional diffusion equation. The vertical axis displays the spatial mean and standard deviation of the pointwise relative error $|p(t, \boldsymbol{x}) - G(t, \boldsymbol{x})|/G(t, \boldsymbol{x})$. Note that the empirical particle distributions and the fundamental solution were calculated on a spatial lattice of 20×20 nodes on the bounded domain $[-100, 100]^2$. The presented values serve to support Figure 24 and do not qualify for a numerical convergence analysis. Because of the heavy tails of the observed densities, a complete numerical analysis requires more elaborate measures. The difference of the hierarchical block model to the fractional diffusion equation stems from the persistence and sparsity of the sampled topological structure. The improved accuracy in the fractal block model and in continuous time random walks for larger times results – at least partially – form the equilibration of the initial conditions (Section 3.3.1). For all models the difference to the fundamental solution can be further reduced by adapting the respective parameterization $(\Delta t, L, N, \dots)$ and increasing the number of sampled trajectories.

5.1.4 Related geometric approaches to anomalous diffusion

It is known that random walks on fractal geometries can lead to anomalous diffusion. Stochastic forms of geometric fractals such as Sierpinski gaskets, Menger sponges, Cantor sets, fractal combs etc. were investigated as the spatial domain of random walk particles [6, 13, 50, 61, 81, 86, 87]. Measures such as mean squared displacement, time averaged mean squared displacement and percolation properties were used to quantify the resulting diffusion processes. In [86, 87] a space-time fractional diffusion equation in the Caputo and Riesz sense was constructed from basic lattice equations. Corresponding analytical representations of the probability density were formulated in terms of Fox-H functions. The super-diffusive scenario could be obtained by using memory kernels to compensate trapping effects in particle trajectories.

Stochastic forms of the fractal geometries facilitate the derivation of the macroscopic equations. Analogously, fractal block models were used as an intermediary to identify persistent topology hierarchical block models with continuous time random walks and the Caputo and Riesz-Feller fractional diffusion equation in this work. The geometric fractals discussed in literature are rectangular structures and usually reproduce the sub-diffusive scenario. The topological interpretation of fractional dynamics on continuous domains provides a new perspective. To the knowledge of the author, the investigation of continuous time random walks and fractional diffusion on fractal topological or geometric structures on continuous domains is new. However, the reproduction of spatial increments as a (fractal) mixing of normal distributions aligns with the standard mathematical construction of bivariate Lévy-stable distributions [73, 101].

Mathematical connections between the fractal geometry of media and resulting scaling exponents (compare α and β) and diffusion constants in associated random walks were established [24, 33, 62, 107]. A proper discussion of the fractal dimension in hierarchical and fractal block models is left to future research. Furthermore, also a direct reconstruction of the fractional diffusion or Fokker-Planck equation from the stochastic description of fractal block models is not included here.

5.2 Outlook

The presented topological perspective on anomalous diffusion could provide new insight in the topic. Here, some unanswered questions and a discussion of geometric observations in this approach are presented.

5.2.1 Open questions

A great number of questions, that were raised during the development and the discussion of the main result, cannot be fully pursued here. Foremost, this concerns the numerical convergence of the topological approximation of continuous time random walks and the fractional diffusion equation (compare Section 5.1.3). This problem, in turn, is not independent from the applied exponential-type level distributions and topological scaling formulas. The uniqueness or optimality of the used stochastic models and of the found identification was not investigated. Furthermore, the numerical quantification of the convergence of continuous time random walks (to the fractional diffusion equation) poses an additional problem.

A formal statement about the convergence of the topological jump distributions to the usual normal distribution for $\alpha \to 2$ could not be derived (Section 4.3.4), despite the simulation of usual diffusion in terms of single layered block models is intuitive.

Alternative models for the level distribution such as exponential power distributions or other distributions with finite moments were not investigated further. The choice for a level distribution and topological scaling, however, depends on the natural system under investigation and in different application scenarios different configurations and different fractional diffusion equations can make sense.

The analytical reconstruction of the macroscopic diffusion equation from the topological configuration of block models was not considered in this work. Also, the fractal dimension of the topological structures and resulting random walks and possible connections to the scaling parameters were not discussed.

In order to simulate space-time fractional diffusion in topological models, in Section 4.4.4 topological increments were subordinated to power-law waiting times. Quali-

tative characteristics of the resulting level process $\Lambda(t)$ were discussed, but more explicit methods for the construction of such processes that in turn yield the desired uncoupled configuration were not investigated.

In the following sections geometric patterns and observations in simulated topological trajectories are discussed in more detail. Also in this case a proper mathematical investigation is out of the scope of this thesis.

5.2.2 Persistence of topological structure

The fractal block model is designed to reproduce the characteristics of continuous time random walks and of fractional diffusion by stochastic topological structures and derived interaction mechanisms. The hierarchical block model instantiates stochastic blocks and features discretized persistent neighborhoods, which again induce interaction and transport likelihoods. Hence, in certain anomalous transport and interaction processes, the existence or emergence of a latent topological structure can be anticipated. Table 1 compares the persistence and volatility of topological structures and the relation to spatial interaction in the presented models.

model	topology		non-local transport
continuous time random walk	latent	$\Longleftarrow$	bivariate isotropic stable distribution
fractal block model	volatile stochastic	$\Longrightarrow$	normal increments with distributed scales
hierarchical block model	persistent	$\Longrightarrow$	topological jumps

Table 1: Relation between topological structure and spatial transport in different models. In the setting of continuous time random walks a latent and volatile topological structure is the result of microscopic particle dynamics. In the block models explicit formalizations of topological structures are the drivers of microscopic (and resulting macroscopic) dynamics.

In visualizations of trajectories of continuous time random walks, the predicted latent topological structure can be recognized as confined areas of consecutive particle

locations. Trapping and long-range interaction phenomena of fractional diffusion are the cause of such volatile spatial clusters. An empirical characterization can for instance be in terms of distributed local time (Section 3.3.5) or based on the fractal dimension of simulated trajectories. The blocks in the fractal and hierarchical models, which are based on Gaussian densities, can be understood to explicitly reproduce these clustering patterns. Especially in the fractal block model, blocks stochastically exist in all orders of magnitude and in all spatial locations.

5.2.3 Trapping and infinitesimal increments

As discussed in connection with the persistent topology hierarchical block model (Section 4.4.3), the truncation of lower layers of the hierarchy has a limited effect on the anomalous characteristics of simulated trajectories. However, different clustering properties can be observed, which can be attributed to the altered shape of the jump scale and spatial increment distributions for small values. A modification of lower level blocks, that is related to truncation, consists is changing their spatial dispersion or concentrating the weight in the center location. In simulated trajectories, this has the effect that jumps sampled with a low random level do generate infinitesimal or no spatial displacements and represent absolute resting.

In Section 4.4.4, 0-length jumps were already used to discretize power-law distributed waiting periods in continuous time random walks simulating time fractional diffusion. This indicates that a geometric interpretation of particle resting could provide a mathematical approach for better interrelating heavy-tailed waiting times with stable spatial increments in coupled and uncoupled scenarios. In particular the stochastic level process $\Lambda(t)$ and the scaling function $\sigma(l)$ could play an important role in such investigations.

In the context of spatially interacting populations, dwelling time in local communities can be a crucial factor for transport and interaction. During the trapping period of a particle, information can be transmitted only to the local surrounding. But the longer a particle remains in a certain community, the greater is the accumulated intra-block

interaction. In persistent-structure block models, we can clearly distinguish between local intra- and non-local inter-block transport. This is reflected by the parameter of the geometric level distribution (intra-block interaction likelihood). As a consequence, the concept of waiting times can be understood to additionally modulate the local interaction strength.

5.2.4 Discrete block layers in application

The presented result provides a geometric and more accessible perspective on the topological characteristics of fractional diffusion. This can be useful in many application scenarios because hierarchical and fractal structures can be encountered in many natural systems. However, with the persistent topology hierarchical block model it is difficult to exactly reproduce the dynamics of the fractional diffusion equation, because the required number of layers and blocks can render simulations unfeasible. There might exist different parameterizations or constructions of discrete-level hierarchical block models that perform better, but it was shown that the basic and typical characteristics of fractional diffusion can be reproduced by this model. Furthermore, natural systems need not have the exact standard fractional diffusion dynamics. This can be recognized in many occasions in applied research, where different fractional dynamics and variants are introduced or discussed.

In the hierarchical block model the existence of a smallest level and a smallest block scale is implied. The characteristic size of 0-level blocks can be prescribed by the underlying natural system, or in other words, the truncation of lower levels can make sense from an application perspective. When a limited number of levels is used, exponential cutoff in spatial increments can be compensated by sampling long-range spatial jumps according to some heavy-tailed distribution, which is independent from the block structure. For instance, if the maximum level is exceeded in the random level process, topological interaction can be replaced by interaction kernels. This can be understood as the introduction of an interaction likelihood for sampling infrequent long-range interactions in addition to frequent topological interaction.

5.3 Scenario

Because this work is focused on the mathematical connection between topological block models and continuous time random walks simulating a fractional diffusion equation, investigation of particular dynamical systems and the simulation of dynamic diffusion-reaction processes are not included. A short outline on the numerical solution of fractional diffusion equations and on the application of fractional diffusion equations for modeling and simulating large structured populations with complex interaction patterns are presented.

5.3.1 Numerical solution of fractional differential equations

There exist a broad range of fractional differential operators and in literature an even greater number of notations, terminologies and fractional differential equations are applied. Coherent discussions of the space-time fractional diffusion equation in connection with continuous time random walks in higher dimensions are less frequent.

Fractional diffusion or Fokker-Planck equations have been applied in many occasions, but usually certain restrictions are made in these models. For instance, space-time fractional differential equations are often discussed in the one dimensional setting; in higher dimensions, usually the strictly time fractional case is discussed; in space fractional scenarios, boundary conditions are implied (to evade problems resulting from non-locality).

For the numerical solution of fractional differential equations, a large number of different schemes and methods have been developed [2, 7, 16, 17, 28, 38, 104, 109]. Most of the references above also present and make available implementations of numerical algorithms. Numerical methods for solving fractional differential equations are distinguished not only by their underlying technical approach, but also by the fractional differential operators they encompass as well as the dimensionality of space and the boundary conditions.

Stochastic approximation of the solution of certain fractional diffusion equations based on continuous time random walks (and random walks generated from topological block models) could be an alternative approach (compare Section 5.1.3).

5.3.2 Structured interacting populations

In models of a heterogeneous population, densities on a multidimensional domain can represent the statistical distribution of individual attributes. For instance, age, gender, wealth, location of residence, etc. If pairwise interaction patterns align with the locations of sampled individuals on this domain, a system with local interaction is obtained. Otherwise, interaction is only local along certain dimensions and non-local in other dimensions. In models that investigate the transmission of information or infectious diseases, spatial proximity is often a fundamental prerequisite for interaction and should therefore be represented in the multidimensional alignment. Furthermore, it is known that the occurrence of (face-to-face) contacts is reflected in the membership of persons in social communities (like households and workplaces). These types of communities partially reproduce the spatial alignment of individuals and result in hierarchal structuring (in combination with spatial embedding). This conceptual model leads to a heterogeneous population that can be structured in multiple layers of overlapping spatially confined blocks. Close proximity interaction happens predominantly within these blocks, but infrequent and non-periodic contacts can occur independently from the community structure and with arbitrary spatial distance.

Variants of this model have been investigated in a broad range of scientific publications. In the following, an overview is presented on network models and macroscopic approaches that focus on anomalous and complex patterns in such systems.

Data-driven approaches for the reconstruction of contact networks and for the simulation of epidemic spread based on individual contact patterns were discussed in [22, 32, 94]. In [21, 49] air travel data was used to infer long-range effects in global epidemic outbreaks. The hidden geographical hierarchy in online social networks was discussed in [55]. A hierarchical population model with spatial alignment and topological interac-

tion simulating disease transmission was proposed in [103]. General scaling properties of hierarchically structured networks were discussed in [8, 20, 80, 99]. Periodic patterns in close proximity networks were investigated in [19]. Dynamic effects of delayed interaction processes in connection with structural alignment were analyzed in [47, 79]. Both papers discuss bursts and fluctuations in the spread of infectious diseases which result from a social structuring and should be related to sub-diffusive behavior. Diffusion processes on hierarchically structured networks were investigated in [98]. Different diffusion time scales were found to result from the hierarchical configuration of networks.

Recently fractional calculus has been increasingly applied in the formulation and simulation of epidemic spread. A space fractional differential equation for the spread of an infectious disease in one dimension was discussed in [41] and a space fractional diffusion equation in two dimensions was formulated in [40]. Time fractional differential equations in aggregated models for infectious spread were presented in [1, 3, 11, 43, 57, 78, 105]. Topological structuring in macroscopic models was investigated in [56, 102].

5.3.3 Topological structuring in macroscopic models

The results presented in this work could be useful for simulating topological features of structured interacting populations in macroscopic models formalized by fractional diffusion and transport equations. Foremost, these topological features include hierarchical structuring, long-range interaction and trapping. To a certain extent this is accomplished by the fractional differential equation models for the spread of infectious diseases referenced in the previous section.

Obviously, the hierarchical configuration and scaling of the community structure as well as the occurrence of long-range interaction is related to the space fractional derivative in corresponding macroscopic models. The sojourn times of individuals in tightly connected communities (compare trapping) are linked to the time fractional derivative.

Further topological phenomena and observations in structured interacting populations that were discussed in the referenced literature on networks were also encountered in the topological models presented in this work. Hence, an extended discussion of microscopic structures and dynamics in the context of topological block models could provide additional insight in the construction of macroscopic models in this domain.

In particular, adapted fractional differential operators, analogous to specially crafted waiting time and jump distributions, provide further potential to translate topological observations to the macroscopic setting. Exponential cutoff in the interaction distances can be obtained from tempered fractional derivatives. Specific temporal multiscale dynamics can be obtained from mixed order fractional derivatives. Time-space coupled configurations could be useful for reproducing a correlation between dwelling times in communities and the spatial extent thereof.

In the end, individual-based or network models with certain topological configurations should produce the same macroscopic dynamics as accordingly constructed fractional diffusion interaction equations. Simulation results of topologically structured network models should match with the numerical solution of macroscopic fractional differential equations.

List of Figures

Bibliography

[1] S. Abuasad, A. Yildirim, I. Hashim, S. A. Karim, and J. Gómez-Aguilar. "Fractional Multi-Step Differential Transformed Method for Approximating a Fractional Stochastic SIS Epidemic Model with Imperfect Vaccination". In: *International Journal of Environmental Research and Public Health* 16.6 (2019), p. 973. DOI: 10.3390/ijerph16060973.

[2] G. Acosta, F. M. Bersetche, and J. P. Borthagaray. "A short FE implementation for a 2d homogeneous Dirichlet problem of a fractional Laplacian". In: *Computers & Mathematics with Applications* 74.4 (2017), pp. 784–816. DOI: 10.1016/j.camwa.2017.05.026.

[3] E. Ahmed and A. Elgazzar. "On fractional order differential equations model for nonlocal epidemics". In: *Physica A: Statistical Mechanics and its Applications* 379.2 (2007), pp. 607–614. DOI: 10.1016/j.physa.2007.01.010.

[4] E. Airoldi, D. Blei, S. Fienberg, and E. Xing. "Mixed Membership Stochastic Blockmodels". In: *Journal of Machine Learning Research* 9 (2008), pp. 1981–2014.

[5] S. Ament and M. O'Neil. "Accurate and efficient numerical calculation of stable densities via optimized quadrature and asymptotics". In: *Statistics and Computing* 28.1 (2017), pp. 171–185. DOI: 10.1007/s11222-017-9725-y.

[6] D. H. N. Anh, P. Blaudeck, K. H. Hoffmann, J. Prehl, and S. Tarafdar. "Anomalous diffusion on random fractal composites". In: *Journal of Physics A: Mathematical and Theoretical* 40.38 (2007), pp. 11453–11465. DOI: 10.1088/1751-8113/40/38/002.

[7] L. Banjai, J. M. Melenk, R. H. Nochetto, E. Otarola, A. J. Salgado, and C. Schwab. "Tensor FEM for spectral fractional diffusion". In: (2017). arXiv: http://arxiv.org/abs/1707.07367v1.

[8] A.-L. Barabási and R. Albert. "Emergence of Scaling in Random Networks". In: *Science* 286.5439 (1999), pp. 509–512. DOI: 10.1126/science.286.5439.509.

[9] E. Barkai, R. Metzler, and J. Klafter. "From continuous time random walks to the fractional Fokker-Planck equation". In: *Physical Review E* 61.1 (2000), pp. 132–138. DOI: 10.1103/physreve.61.132.

[10] E. Barkai. "CTRW pathways to the fractional diffusion equation". In: *Chemical Physics* 284.1-2 (2002), pp. 13–27. DOI: 10.1016/s0301-0104(02)00533-5.

[11] A. Bashir, M. Mushtaq, Z. U. A. Zafar, K. Rehan, and R. M. A. Muntazir. "Comparison of fractional order techniques for measles dynamics". In: *Advances in Difference Equations* 2019.1 (2019). DOI: 10.1186/s13662-019-2272-4.

[12] G. Bel and E. Barkai. "Weak Ergodicity Breaking in the Continuous-Time Random Walk". In: *Physical Review Letters* 94.24 (2005). DOI: 10.1103/physrevlett.94.240602.

[13] D. ben-Avraham and S. Havlin. *Diffusion and Reactions in Fractals and Disordered Systems*. Cambridge University Press, 2000. DOI: 10.1017/cbo9780511605826.

[14] D. Bickson. *Linear Characteristic Graphical Models*. 2010. URL: http://www.cs.cmu.edu/~bickson/stable/.

[15] D. Bickson and C. Guestrin. "Inference with Multivariate Heavy-Tails in Linear Models". In: (2010). arXiv: 1008.5325.

[16] A. Bonito, J. P. Borthagaray, R. H. Nochetto, E. Otárola, and A. J. Salgado. "Numerical methods for fractional diffusion". In: *Computing and Visualization in Science* (2018). DOI: 10.1007/s00791-018-0289-y.

[17] A. Bueno-Orovio, D. Kay, and K. Burrage. "Fourier spectral methods for fractional-in-space reaction-diffusion equations". In: *BIT Numerical Mathematics* 54.4 (2014), pp. 937–954. DOI: 10.1007/s10543-014-0484-2.

[18] J. M. Chambers, C. L. Mallows, and B. W. Stuck. "A Method for Simulating Stable Random Variables". In: *Journal of the American Statistical Association* 71.354 (1976), pp. 340–344. DOI: 10.1080/01621459.1976.10480344.

[19] A. Clauset and N. Eagle. "Persistence and periodicity in a dynamic proximity network". In: (2012). arXiv: 1211.7343v1.

[20] A. Clauset, C. Moore, and M. E. J. Newman. "Hierarchical structure and the prediction of missing links in networks". In: *Nature* 453.7191 (2008), pp. 98–101. DOI: 10.1038/nature06830.

[21] V. Colizza, A. Barrat, M. Barthélemy, and A. Vespignani. "The role of the airline transportation network in the prediction and predictability of global epidemics". In: *Proceedings of the National Academy of Sciences* 103.7 (2006), pp. 2015–2020. DOI: 10.1073/pnas.0510525103.

[22] L. Danon, T. A. House, J. M. Read, and M. J. Keeling. "Social encounter networks: collective properties and disease transmission". In: *Journal of The Royal Society Interface* 9.76 (2012), pp. 2826–2833. DOI: 10.1098/rsif.2012.0357.

[23] S. Denisov, V. Zaburdaev, and P. Hänggi. "Lévy walks with velocity fluctuations". In: *Physical Review E* 85.3 (2012). DOI: 10.1103/physreve.85.031148.

[24] J.-R. de Dreuzy, P. Davy, J. Erhel, and J. de Brémond d'Ars. "Anomalous diffusion exponents in continuous two-dimensional multifractal media". In: *Physical Review E* 70.1 (2004). DOI: 10.1103/physreve.70.016306.

[25] B. Dyda, A. Kuznetsov, and M. Kwaśnicki. "Fractional Laplace operator and Meijer G-function". In: (2015). arXiv: 1509.08529.

[26] L. R. Evangelista and E. K. Lenzi. *Fractional Diffusion Equations and Anomalous Diffusion*. Cambridge University Press, 2018. DOI: 10.1017/9781316534649.

[27] D. Fulger, E. Scalas, and G. Germano. "Monte Carlo simulation of uncoupled continuous-time random walks yielding a stochastic solution of the space-time fractional diffusion equation". In: *Physical Review E* 77.2 (2008). DOI: 10.1103/physreve.77.021122.

[28] M. Garg and P. Manohar. "Matrix method for numerical solution of space-time fractional diffusion-wave equations with three space variables". In: *Afrika Matematika* 25.1 (2012), pp. 161–181. DOI: 10.1007/s13370-012-0101-y.

[29] R. Garrappa. *Evaluation of the Mittag-Leffler function with 1, 2 or 3 parameters*. 2015. URL: https://se.mathworks.com/matlabcentral/fileexchange/48154-the-mittag-leffler-function.

[30] R. Garrappa. "Numerical Evaluation of Two and Three Parameter Mittag-Leffler Functions". In: *SIAM Journal on Numerical Analysis* 53.3 (2015), pp. 1350–1369. DOI: 10.1137/140971191.

[31] R. Garrappa and M. Popolizio. "Computing the Matrix Mittag-Leffler Function with Applications to Fractional Calculus". In: *Journal of Scientific Computing* 77.1 (2018), pp. 129–153. DOI: 10.1007/s10915-018-0699-5.

[32] M. Génois, C. L. Vestergaard, C. Cattuto, and A. Barrat. "Compensating for population sampling in simulations of epidemic spread on temporal contact networks". In: *Nature Communications* 6.1 (2015). DOI: 10.1038/ncomms9860.

[33] L. Gmachowski. "Fractal model of anomalous diffusion". In: *European Biophysics Journal* 44.8 (2015), pp. 613–621. DOI: 10.1007/s00249-015-1054-5.

[34] R. Gorenflo, J. Loutchko, and Y. Luchko. "Computation of the Mittag-Leffler function and its derivatives". In: *Fractional Calculus & Applied Analysis (FCAA)* 5 (2002).

[35] R. Gorenflo and F. Mainardi. "Fractional diffusion Processes: Probability Distributions and Continuous Time Random Walk". In: *Processes with Long-Range Correlations*. Springer Berlin Heidelberg, 2003, pp. 148–166. DOI: 10.1007/3-540-44832-2_8.

[36] R. Gorenflo, F. Mainardi, D. Moretti, G. Pagnini, and P. Paradisi. "Discrete random walk models for space-time fractional diffusion". In: *Chemical Physics* 284.1-2 (2002), pp. 521–541. DOI: 10.1016/s0301-0104(02)00714-0.

[37] R. Gorenflo, F. Mainardi, and A. Vivoli. "Continuous-time random walk and parametric subordination in fractional diffusion". In: *Chaos, Solitons & Fractals* 34.1 (2007), pp. 87–103. DOI: 10.1016/j.chaos.2007.01.052.

[38] L. Guo, F. Zeng, I. Turner, K. Burrage, and G. E. Karniadakis. "Efficient Multistep Methods for Tempered Fractional Calculus: Algorithms and Simulations". In: *SIAM Journal on Scientific Computing* 41.4 (2019), A2510–A2535. DOI: 10.1137/18m1230153.

[39] Q. Guo, E. Cozzo, Z. Zheng, and Y. Moreno. "Lévy random walks on multiplex networks". In: *Scientific Reports* 6.1 (2016). DOI: 10.1038/srep37641.

[40] K. B. Gustafson, B. S. Bayati, and P. A. Eckhoff. "Fractional Diffusion Emulates a Human Mobility Network during a Simulated Disease Outbreak". In: *Frontiers in Ecology and Evolution* 5 (2017). DOI: 10.3389/fevo.2017.00035.

[41] E. Hanert, E. Schumacher, and E. Deleersnijder. "Front dynamics in fractional-order epidemic models". In: *Journal of Theoretical Biology* 279.1 (2011), pp. 9–16. DOI: 10.1016/j.jtbi.2011.03.012.

[42] H. J. Haubold, A. M. Mathai, and R. K. Saxena. "Mittag-Leffler Functions and Their Applications". In: *Journal of Applied Mathematics* 2011 (2011), pp. 1–51. DOI: 10.1155/2011/298628.

[43] S. He and S. Banerjee. "Epidemic outbreaks and its control using a fractional order model with seasonality and stochastic infection". In: *Physica A: Statistical Mechanics and its Applications* 501 (2018), pp. 408–417. DOI: 10.1016/j.physa.2018.02.045.

[44] Y. He, S. Burov, R. Metzler, and E. Barkai. "Random Time-Scale Invariant Diffusion and Transport Coefficients". In: *Physical Review Letters* 101.5 (2008). DOI: 10.1103/physrevlett.101.058101.

[45] R. Hilfer. "On fractional diffusion and continuous time random walks". In: *Physica A: Statistical Mechanics and its Applications* 329.1-2 (2003), pp. 35–40. DOI: 10.1016/s0378-4371(03)00583-1.

[46] K. Hinsen. *The Mittag-Leffler function in Python*. 2017. URL: https://github.com/khinsen/mittag-leffler.

[47] D. X. Horváth and J. Kertész. "Spreading dynamics on networks: the role of burstiness, topology and non-stationarity". In: *New Journal of Physics* 16.7 (2014), p. 073037. DOI: 10.1088/1367-2630/16/7/073037.

[48] F. Huang and F. Liu. "The fundamental solution of the space-time fractional advection-dispersion equation". In: *Journal of Applied Mathematics and Computing* 18.1-2 (2005), pp. 339–350. DOI: 10.1007/bf02936577.

[49] L. Hufnagel, D. Brockmann, and T. Geisel. "Forecast and control of epidemics in a globalized world". In: *Proceedings of the National Academy of Sciences* 101.42 (2004), pp. 15124–15129. DOI: 10.1073/pnas.0308344101.

[50] A. Iomin. "Subdiffusion on a fractal comb". In: *Physical Review E* 83.5 (2011). DOI: 10.1103/physreve.83.052106.

[51] K.-H. Kim and S. Lim. "Asymptotic behaviors of fundamental solution and its derivatives related to space-time fractional differential equations". In: (2015). arXiv: 1504.07386.

[52] M. Kotulski. "Asymptotic distributions of continuous-time random walks: A probabilistic approach". In: *Journal of Statistical Physics* 81.3-4 (1995), pp. 777–792. DOI: 10.1007/bf02179257.

[53] T. Kozubowski and K. Podgorski. "Laplace probability distributions and related stochastic processes". In: *Probability: Interpretation, Theory and Applications*. 2011, pp. 105–145.

[54] R. Kutner and J. Masoliver. "The continuous time random walk, still trendy: fifty-year history, state of art and outlook". In: *The European Physical Journal B* 90.3 (2017). DOI: 10.1140/epjb/e2016-70578-3.

[55] B. Lengyel, A. Varga, B. Ságvári, Á. Jakobi, and J. Kertész. *Data from: Geographies of an online social network*. en. 2016. DOI: 10.5061/DRYAD.33PS4.

[56] J. Li and X. Zou. "Dynamics of an epidemic model with non-local infections for diseases with latency over a patchy environment". In: *Journal of Mathematical Biology* 60.5 (2009), pp. 645–686. DOI: 10.1007/s00285-009-0280-9.

[57] T. Li, Y. Wang, F. Liu, and I. Turner. "Novel parameter estimation techniques for a multi-term fractional dynamical epidemic model of dengue fever". In: *Numerical Algorithms* 82.4 (2019), pp. 1467–1495. DOI: 10.1007/s11075-019-00665-2.

[58] F. Mainardi, Y. Luchko, and G. Pagnini. "The fundamental solution of the space-time fractional diffusion equation". In: *Fractional Calculus and Applied Analysis* 4.2 (2001), pp. 153–192. arXiv: cond-mat/0702419.

[59] F. Mainardi, G. Pagnini, and R. Saxena. "Fox H functions in fractional diffusion". In: *Journal of Computational and Applied Mathematics* 178.1-2 (2005), pp. 321–331. DOI: 10.1016/j.cam.2004.08.006.

[60] F. Mainardi, M. Raberto, R. Gorenflo, and E. Scalas. "Fractional calculus and continuous-time finance II: the waiting-time distribution". In: *Physica A: Statistical Mechanics and its Applications* 287.3-4 (2000), pp. 468–481. DOI: 10.1016/s0378-4371(00)00386-1.

[61] Y. Mardoukhi, J.-H. Jeon, and R. Metzler. "Geometry controlled anomalous diffusion in random fractal geometries: looking beyond the infinite cluster". In: *Physical Chemistry Chemical Physics* 17.44 (2015), pp. 30134–30147. DOI: 10.1039/c5cp03548a.

[62] M. M. Meerschaert, E. Nane, and Y. Xiao. "Fractal dimension results for continuous time random walks". In: *Statistics & Probability Letters* 83.4 (2013), pp. 1083–1093. DOI: 10.1016/j.spl.2013.01.001.

[63] M. M. Meerschaert and H.-P. Scheffler. "Limit theorems for continuous-time random walks with infinite mean waiting times". In: *Journal of Applied Probability* 41.3 (2004), pp. 623–638. DOI: 10.1239/jap/1091543414.

[64] M. M. Meerschaert and P. Straka. "Semi-Markov approach to continuous time random walk limit processes". In: *The Annals of Probability* 42.4 (2014), pp. 1699–1723. DOI: 10.1214/13-aop905.

[65] R. Metzler. "Weak ergodicity breaking and ageing in anomalous diffusion". In: *International Journal of Modern Physics: Conference Series* 36 (2015), p. 1560007. DOI: 10.1142/s2010194515600071.

[66] R. Metzler and J. Klafter. "The random walk's guide to anomalous diffusion: a fractional dynamics approach". In: *Physics Reports* 339.1 (2000), pp. 1–77. DOI: 10.1016/s0370-1573(00)00070-3.

[67] C. Milici, G. Drăgănescu, and J. T. Machado. *Introduction to Fractional Differential Equations*. Springer International Publishing, 2019. DOI: 10.1007/978-3-030-00895-6.

[68] J. M. Miotto and P. Harrison. *PyLevy – Lévy distributions for Python*. 2016-2018. URL: https://github.com/josemiotto/pylevy.

[69] *Mpmath – a Python library for arbitrary-precision floating-point arithmetic*. 2018. URL: http://mpmath.org.

[70] S. Murray. *hankel – Perform simple and accurate Hankel transformations using the method of Ogata*. 2019. URL: https://hankel.readthedocs.io.

[71] M. E. J. Newman. "Modularity and community structure in networks". In: *Proceedings of the National Academy of Sciences* 103.23 (2006), pp. 8577–8582. DOI: 10.1073/pnas.0601602103. eprint: http://www.pnas.org/content/103/23/8577.full.pdf+html.

[72] J. P. Nolan. *Stable Distributions - Models for Heavy Tailed Data (in preparation)*. Boston: Birkhauser, 2018.

[73] J. P. Nolan. "Multivariate elliptically contoured stable distributions: theory and estimation". In: *Computational Statistics* 28.5 (2013), pp. 2067–2089. DOI: 10.1007/s00180-013-0396-7.

[74] J. P. Nolan. "Numerical calculation of stable densities and distribution functions". In: *Communications in Statistics. Stochastic Models* 13.4 (1997), pp. 759–774. DOI: 10.1080/15326349708807450.

[75] T. P. Peixoto. "Efficient Monte Carlo and greedy heuristic for the inference of stochastic block models". In: *Phys. Rev. E* 89.1 (2014), p. 012804. DOI: 10.1103/PhysRevE.89.012804.

[76] T. P. Peixoto. "Hierarchical Block Structures and High-Resolution Model Selection in Large Networks". In: *Physical Review X* 4.1 (2014). DOI: 10.1103/physrevx.4.011047.

[77] T. P. Peixoto. "Nonparametric Bayesian inference of the microcanonical stochastic block model". In: *Physical Review E* 95.1 (2017). DOI: 10.1103/physreve.95.012317.

[78] C. M. Pinto and J. T. Machado. "Fractional model for malaria transmission under control strategies". In: *Computers & Mathematics with Applications* 66.5 (2013), pp. 908–916. DOI: 10.1016/j.camwa.2012.11.017.

[79] C. Poletto, M. Tizzoni, and V. Colizza. "Heterogeneous length of stay of hosts' movements and spatial epidemic spread". In: *Scientific Reports* 2.1 (2012). DOI: 10.1038/srep00476.

[80] E. Ravasz and A.-L. Barabási. "Hierarchical Organization in Complex Networks". In: *Physical Review E* 67.2 (2003), p. 026112. DOI: 10.1103/physreve.67.026112.

[81] F. D. A. A. Reis. "Scaling relations in the diffusive infiltration in fractals". In: *Physical Review E* 94.5 (2016). DOI: 10.1103/physreve.94.052124.

[82] J. Royuela-del-Val, F. Simmross-Wattenberg, and C. Alberola-López. "libstable: Fast, Parallel, and High-Precision Computation of α-Stable Distributions in R, C/C++, and MATLAB". In: *Journal of Statistical Software* 78.1 (2017). DOI: 10.18637/jss.v078.i01.

[83] S. G. Samko, A. A. Kilbas, and O. I. Marichev. *Fractional integrals and derivatives: Theory and applications*. Gordon and Breach Science Publishers, 1993.

[84] S. Samko. "A new approach to the inversion of the Riesz potential operator". In: *Fract. Calc. and Appl. Anal.* 1.3 (1998), pp. 225–245.

[85] T. Sandev, A. V. Chechkin, N. Korabel, H. Kantz, I. M. Sokolov, and R. Metzler. "Distributed-order diffusion equations and multifractality: Models and solutions". In: *Physical Review E* 92.4 (2015). DOI: 10.1103/physreve.92.042117.

[86] T. Sandev, A. Iomin, and H. Kantz. "Anomalous diffusion on a fractal mesh". In: *Physical Review E* 95.5 (2017). DOI: 10.1103/physreve.95.052107.

[87] T. Sandev, A. Iomin, and V. Méndez. "Lévy processes on a generalized fractal comb". In: *Journal of Physics A: Mathematical and Theoretical* 49.35 (2016), p. 355001. DOI: 10.1088/1751-8113/49/35/355001.

[88] T. Sandev, R. Metzler, and A. Chechkin. "From continuous time random walks to the generalized diffusion equation". In: *Fractional Calculus and Applied Analysis* 21.1 (2018), pp. 10–28. DOI: 10.1515/fca-2018-0002.

[89] G. Schneckenreither. "Developing Mathematical Formalisms for Cellular Automata in Modelling and Simulation". MA thesis. Vienna University of Technology, 2014.

[90] G. Schneckenreither, N. Popper, and F. Breitenecker. "Methods for Cellular Automata and Evolution Systems in Modelling and Simulation". In: *IFAC-PapersOnLine* 48.1 (2015), pp. 141–146. DOI: 10.1016/j.ifacol.2015.05.151.

[91] G. Schneckenreither, N. Popper, and F. Breitenecker. "Modelling SIR-type epidemics by ODEs, PDEs, difference equations and cellular automata – A comparative study". In: *Simulation Modelling Practice and Theory* 16.8 (2008), pp. 1014–1023. DOI: doi:10.1016/j.simpat.2008.05.015.

[92] G. Schneckenreither. *ctrw - a Python library for continuous time random walks*. 2019. URL: https://github.com/xgschneck/ctrw.

[93] G. Schneckenreither. "Probabilistic Drift Formulation of SIRS Models based on SPDEs and the Kolmogorov Equation". In: *SNE Simulation Notes Europe* 25.3-4 (2015). DOI: 10.11128/sne.25.tn.10317.

[94] G. Schneckenreither and N. Popper. "Dynamic multiplex social network models on multiple time scales for simulating contact formation and patterns in epidemic spread". In: *2017 Winter Simulation Conference (WSC)*. IEEE, 2017, pp. 4324–4335. DOI: 10.1109/wsc.2017.8248138.

[95] G. Schneckenreither, P. Tschandl, C. Rippinger, C. Sinz, D. Brunmeier, N. Popper, and H. Kittler. "Reproduction of patterns of melanocytic proliferations by agent-based simulation and geometric modeling (prel.)" in preparation, 2019.

[96] *SciPy – a Python-based ecosystem of open-source software for mathematics, science, and engineering*. URL: https://scipy.org.

[97] K. Shen, L. Song, X. Yang, and W. Zhang. "A Hierarchical Diffusion Algorithm for Community Detection in Social Networks". In: *2010 International Conference on Cyber-Enabled Distributed Computing and Knowledge Discovery*. IEEE, 2010. DOI: 10.1109/cyberc.2010.57.

[98] G. Siudem and J. A. Hołyst. "Diffusion on hierarchical systems of weakly-coupled networks". In: *Physica A: Statistical Mechanics and its Applications* 513 (2019), pp. 675–686. DOI: 10.1016/j.physa.2018.08.078.

[99] C. Stegehuis, R. van der Hofstad, and J. S. H. van Leeuwaarden. "Power-law relations in random networks with communities". In: *Physical Review E* 94.1 (2016). DOI: 10.1103/physreve.94.012302.

[100] A. A. Tateishi, H. V. Ribeiro, and E. K. Lenzi. "The Role of Fractional Time-Derivative Operators on Anomalous Diffusion". In: *Frontiers in Physics* 5 (2017). DOI: 10.3389/fphy.2017.00052.

[101] V. V. Uchaikin and V. M. Zolotarev. *Chance and Stability*. Walter de Gruyter GmbH, 1999. 598 pp. DOI: 10.1515/9783110935974.

[102] A. Vazquez. "Epidemic outbreaks on structured populations". In: *Journal of Theoretical Biology* 245.1 (2007), pp. 125–129. DOI: 10.1016/j.jtbi.2006.09.018.

[103] D. J. Watts, R. Muhamad, D. C. Medina, and P. S. Dodds. "Multiscale, resurgent epidemics in a hierarchical metapopulation model". In: *Proceedings of the National Academy of Sciences* 102.32 (2005), pp. 11157–11162. DOI: 10.1073/pnas.0501226102.

[104] Q. Yang, I. Turner, F. Liu, and M. Ilić. "Novel Numerical Methods for Solving the Time-Space Fractional Diffusion Equation in Two Dimensions". In: *SIAM Journal on Scientific Computing* 33.3 (2011), pp. 1159–1180. DOI: 10.1137/100800634.

[105] D. Yaro, W. O. Apeanti, S. W. Akuamoah, and D. Lu. "Analysis and Optimal Control of Fractional-Order Transmission of a Respiratory Epidemic Model". In: *International Journal of Applied and Computational Mathematics* 5.4 (2019). DOI: 10.1007/s40819-019-0699-7.

[106] V. Zaburdaev, S. Denisov, and P. Hänggi. "Space-Time Velocity Correlation Function for Random Walks". In: *Physical Review Letters* 110.17 (2013). DOI: 10.1103/physrevlett.110.170604.

[107] A. Zhokh, A. Trypolskyi, and P. Strizhak. "Relationship between the anomalous diffusion and the fractal dimension of the environment". In: *Chemical Physics* 503 (2018), pp. 71–76. DOI: 10.1016/j.chemphys.2018.02.015.

[108] Y. Zhou, J. Wang, and L. Zhang. *Basic Theory of Fractional Differential Equations*. World Scientific Pub Co Inc, 2016. 380 pp. DOI: 10.1142/10238.

[109] P. Zhuang and F. Liu. "Implicit difference approximation for the two-dimensional space-time fractional diffusion equation". In: *Journal of Applied Mathematics and Computing* 25.1-2 (2007), pp. 269–282. DOI: 10.1007/bf02832352.

[110] V. M. Zolotarev. "Integral Transformations of Distributions and Estimates of Parameters of Multidimensional Spherically Symmetric Stable Laws". In: *Contributions to Probability*. Elsevier, 1981, pp. 283–305. DOI: 10.1016/b978-0-12-274460-0.50029-1.